A quantitative investigation of the relation between deepwater flow and density difference within the thermohaline circulation of a marginal basin for use in lower complexity box models

MSc Thesis
Keijzer, R.M.A. (4066901)
Supervisors: Meijer, P.T. & Slomp, C.P.

Faculty of Geosciences
Utrecht University
01-06-2020

Abstract: A study of the effect of a number of forcing factors on a marginal basin is conducted using a 3D oceanic circulation model, the Princeton Ocean Model. These factors include relaxation to an air temperature, net evaporation, geometry and the amount of in and outflow within the system. The objective is to further the understanding of how these factors affect the deep-water flux from a marginal basin to a deep basin. Furthermore, it will be attempted to find a quantitative correlation between the deepwater flux and the corresponding density difference between the main and marginal basin. This relation will then be compared to comparable Mediterranean box models. It was found that the implementation of a net evaporation in the system was sufficient to produce a basis for a Mediterranean-like circulation. It was shown that it is necessary to implement both a net evaporation and temperature forcing to produce a realistic Mediterranean-like thermohaline circulation system. Any additional forcing factors only worked to increase or dampen the intensity of the circulation cells. When the variation in density difference between the marginal and deep basin was compared to the deep water flux no conclusive formulation was found based on the current data range. A power law relation was considered the most likely option based on the data present. Finally, it was concluded that a possible underestimation of the deepwater flux exists in comparable Mediterranean box models.

1. Introduction

The present-day Mediterranean Sea exhibits a complex flow pattern which is a product of a variety of interlocking factors that all contribute to the overall buoyancy variation of the seawater, and with it, the thermohaline circulation of the Mediterranean Sea. These factors include seawater temperature and salinity, net evaporation, geometry and the amount of in and outflow within the system. To study these factors more thoroughly a 3D oceanic circulation model is used, the Princeton Ocean Model (Blumberg & Mellor, 1987). The objective is to further the understanding of how these factors affect the deep-water flux from a marginal basin to a deep basin. Attention will be focussed on producing a Mediterranean like overturning circulation within the basin and examining which forcing factors are essential to produce such a circulation. The present-day Mediterranean thermohaline circulation is characterized by two distinct types of circulation cells. The first is located in the upper 500 to 800 m of the Mediterranean Sea and starts with a 100 to 200 m deep surface inflow of relatively fresh, warm water coming in through the strait of Gibraltar and originating from the Atlantic Ocean. When flowing into the Mediterranean Sea the water becomes saltier and warmer through a combination of atmospheric temperature forcing and mixing with the saltier, warmer water of the Mediterranean. The incoming water flows towards the east side of the basin were winter cooling occurs. This causes a high-density water mass to form in the east. This water mass then sinks and flows back westward to the Strait of Gibraltar at a depth of 200 to 800 m (Haines and Wu, 1995) (Roether et al., 1996). The second circulation cell type within the Mediterranean Sea concerns the formation of high-density water masses in the northern parts of the western and eastern basins. Due to higher latitudes causing more intense cooling, combined with above-average net evaporation, a dense water mass forms. When this water mass sinks to the bottom layers of the basin due to its high density, it spreads southwards and

then westwards towards the strait of Gibraltar. It then joins the outflowing water of the east-west flowing circulation cell and flows into the Atlantic Ocean through the deeper part of the strait of Gibraltar (Marshall and Schott., 1999). To examine such a circulation, atmospheric temperature and net evaporation will be closely examined on an annual basis to determine their effect on the thermohaline circulation within the basin. Seasonal temperature variations, and the corresponding density variations, will also be examined to observe their general effects, and to examine the quantitative correlation between the deepwater flux and the corresponding density difference between the main and marginal basin. Using the 3D model a basis for the most appropriate formulation can be found, leading to a parameterization of the deepwater flux which in turn can be used in, and compared to lower complexity box models like the ones of Karami (Karami et al., 2011) or Dirksen & Meijer (Dirksen & Meijer, 2019). In these box models, the different parts of the complete modelled system are represented by separate boxes. Each box is assumed to be well mixed and has a uniform salinity and temperature, both of which are used to calculate an average density. The boxes representing oceans like the Atlantic and the Indian ocean are prescribed a constant salinity and temperature while the boxes representing basins are not. A high-density deep flow and a low-density surface flow is allowed between each of the boxes. The density difference between the boxes is multiplied with a constant factor which relates the density to the deep-water flow. A constant background value is added, and the resulting total represents the deep water flux (Karami et al., 2011) (Dirksen & Meijer, 2019). The goal is to assert if the comprehensive model supports the assumptions made in these comparable box models.

2. Model description

2.1 The Princeton Ocean Model

The Princeton Ocean Model (POM) is a three-dimensional, free surface, hydrostatic, bottom-following vertical sigma coordinate, primitive equation model created by Blumberg and Mellor (Blumberg & Mellor, 1987) (Alhammoud et al., 2010). It uses a staggered grid and, in order to achieve computational efficiency, a 2D external (barotropic) time step in combination with a 3D internal (baroclinic) time step. The model numerically solves the momentum equations, the continuity equation and the temperature and salinity equations in a finite difference form. The temperature and salinity fields are coupled to the velocity field using a nonlinear equation of state $\rho = \rho(\theta,S,P)$ (Mellor, 1991).

The sigma coordinate system used is based on the system devised by N. A. Philips in his paper "A coordinate system having some special advantages for numerical forecasting" (Phillips, 1957). The coordinate system is based on the following transformation:

$$x^* = x, \ y^* = y, \ t^* = t, \ \sigma = \frac{z - \eta}{H + \eta} \qquad (eq. \ 1)$$

In this transformation x,y and z are the conventional cartesian coordinates. H(x,y) is the bottom topography and η(x,y,t) is the surface elevation (Mellor, 2002). A total of 16 sigma levels were used for the vertical grid of the model.

2.2 Model setup

2.2.1 Model region
To simulate a marginal basin a basic basin setup is used which is then adjusted to fit the specific region and topography. The GEBCO elevation dataset of the present-day Mediterranean with a resolution of 30 arc seconds is used as depth input. The chosen region is then cut out and the resolution is scaled down to fit the chosen resolution of the Princeton Ocean Model, which is 15 arc minutes or 0.25 degree. The maximum height of the region was capped at 1 m and a smoothing filter was applied to account for disproportionate transitions in-depth within the elevation map (fig. 1). To achieve an idealized basin with a single gateway the Tyrrhenian Sea was converted to land and an open boundary was created in the most western part of the region to simulate a gateway to an outside ocean which properties will be discussed in 2.2.3. No buffer zone was imposed between the open boundary and the model region, instead the open boundary connects directly to the
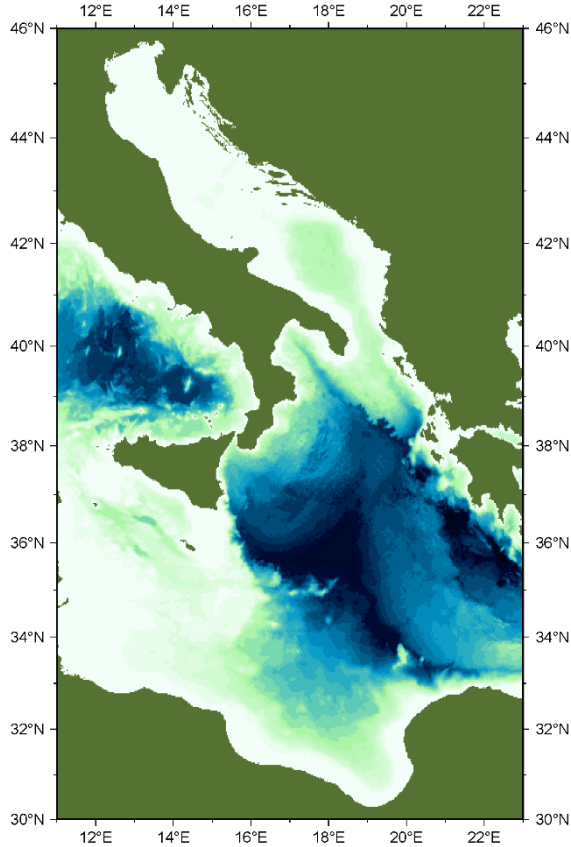
Figure 1: A 90 arc second GEBCO elevation dataset of the Ionian and Adriatic Sea with the elevation capped to 1 m.

model region. The gateway created has a width of 22 grid cells or about 610 km. For simplicity, the depth of the gateway was set to a constant 100 m. A grid size of 48 by 64 cells was used to best fit the chosen region and resolution (Fig. 2).

2.2.2 Model conditions

An external and internal timestep were used in the setup of the Princeton Ocean Model. The external time step (dte) of the model was determined using the CFL condition (Courant et al.,1928) and was set to an approximate maximum value of 40 seconds. The internal timestep (dti) was determined by setting the value of isplit where isplit = dti / dte. A value of 80 is used for isplit based on the 2002 paper by Ezer et al. (Ezer et al., 2002) which discusses POM stability. A depth smoothing value (slmax) of 0.1 is applied where slmax represents the difference in depths between two cells divided by the sum of the depths. The model was set to produce output every ten days throughout its entire runtime.

2.2.3 Forcing conditions

A number of forcing factors were applied to the model to simulate the conditions of the Mediterranean Sea region. The initial conditions of the marginal basin were set to a temperature of 20°C and a salinity of 35 psu based on the values used by Alhammoud et al. (2010). These values were chosen to approximate the values observed for the Atlantic Ocean. The outer ocean was given the same initial conditions, as were the waters flowing through the open boundary into the model. The temperature boundary condition consist of a relaxation of sea surface temperature to a constant atmospheric temperature field which varies only with latitude. The temperature field is based on the present-day annual mean temperature of the region. A zonal average is taken per degree latitude and a line is fitted through these data points to achieve a realistic temperature field. The relaxation coefficient between the temperature of the atmosphere and the sea surface is set to 1 m/day (Drakopoulos & Lascaratos, 1999). An exception was made for the region ranging from the open boundary to the eleventh vertical grid column. This region acts as a temperature ramp going from zero coupling at the open boundary to 1 m/day at the eleventh column. For simplicity, wind stress was not considered as a forcing factor. Previous papers by Myers et al. (1998) and Winton & Sarachik
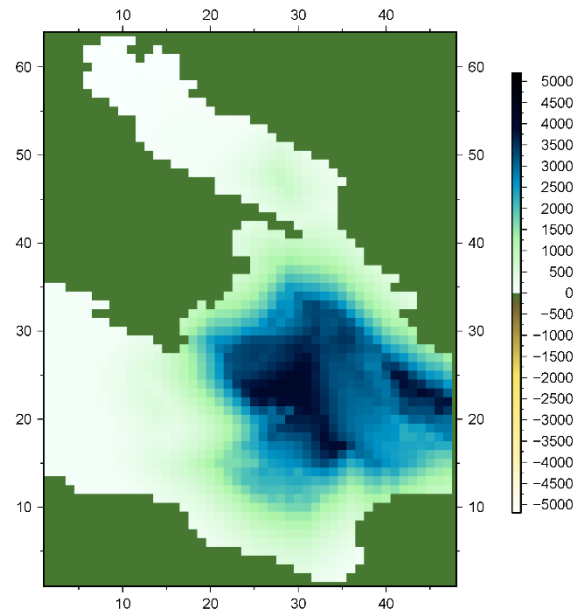

Figure 2: A 48 by 64 node map of the Ionian and Adriatic Sea, with the Tyrrhenian Sea converted to land.

Experiment #	Net evaporation	Temperature forcing	Uabw inflow	Uabw outflow	Max Seasonal T variation	Corresponding figures
2060	N/A	N/A	0 Sv	N/A	N/A	-
2020	1-2 m/year	N/A	evap.	N/A	N/A	6 to 12
2041	1-2 m/year	1 m/day	evap.	N/A	0 °C	13 to 15
2042	1-2 m/year	1 m/day	1 Sv + evap.	1 Sv	0 °C	16, 17
2031	1-2 m/year	1 m/day	evap.	N/A	5-8 °C	18, 19
2044	1-2 m/year	1 m/day	1 Sv + evap.	1 Sv	5-8 °C	20, 21

Table 1: Experiment characteristics.

(1993) showed that its effect on the thermohaline circulation pattern is minimal, only intensifying the upper overturning cell of the system. Based on a range of present-day estimates of the Mediterranean region a net evaporation was applied to the system. A constant value of 1 m/yr is taken based on the rough approximation used by Alhammoud et al. (2010). An exception is made for the northern part of the region where a net evaporation of 2 m/yr is applied. This was done in each experiment to account for higher net evaporation values generally found in the north caused by strong Bora winds (Paklar et al., 2001). A zone was created between the north and the south where an average net evaporation of 1.5 m/yr is applied to act as a buffer zone. This zone ranges from the 40th horizontal grid row to the 45th horizontal grid row. A second zone was created from the open boundary to the fifth vertical grid column to act as a ramp going from a zero net evaporation at the open boundary to 1 m/year at the fifth column. To compensate for the net evaporation removing water from the system a horizontal depth-averaged velocity (uabw) was imposed at the open boundary to the west. Each grid cell was given an equally small value of uabw in such a way that when combined they exactly compensate for the water lost due to net evaporation. The baroclinic velocity at the open boundary was left unconstrained to allow for free flow between the model region and the open boundary. The salinity and temperature of the inflowing water is set to be equal to the initial values of the outer ocean, namely 35 psu and 20°C respectively. In subsequent experiments, a two-way

barotropic flow was implemented at the open boundary to simulate the in- and outflow occurring at the Strait of Sicily. For simplicity, outflow only occurs in the south and inflow only occurs in the west. A sinusoidal horizontal depth-averaged velocity profile was created at the open boundary to govern the amount of flow in and out of the system (fig. 3). Special care was taken to preserve the water volume of the system by imposing an inflow equal to outflow plus net evaporation. A value of 1 Sv was chosen as a baseline value for the in and outflow of the system to approximate the in and outflow of the Strait of Sicily, which is generally found to lie in the 0.6 to 1.4 Sv range (Manzella et al, 1988). To study the effect of a
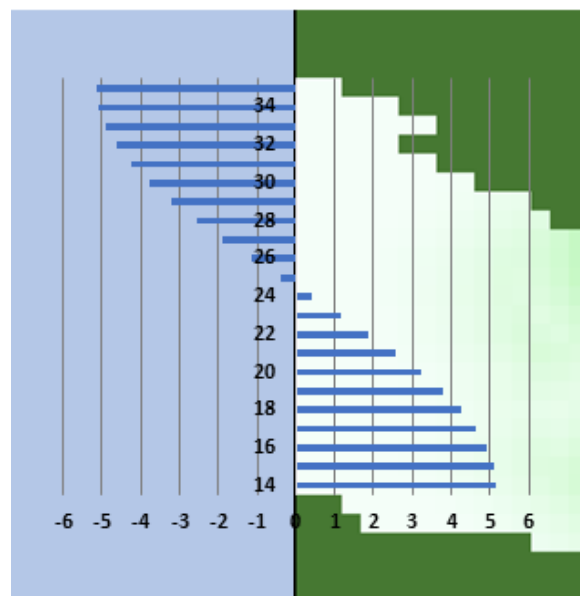

Figure 3: The horizontal depth-averaged velocity profile in m/s (x-axis) implemented at the open boundary for each j-node (y-axis).
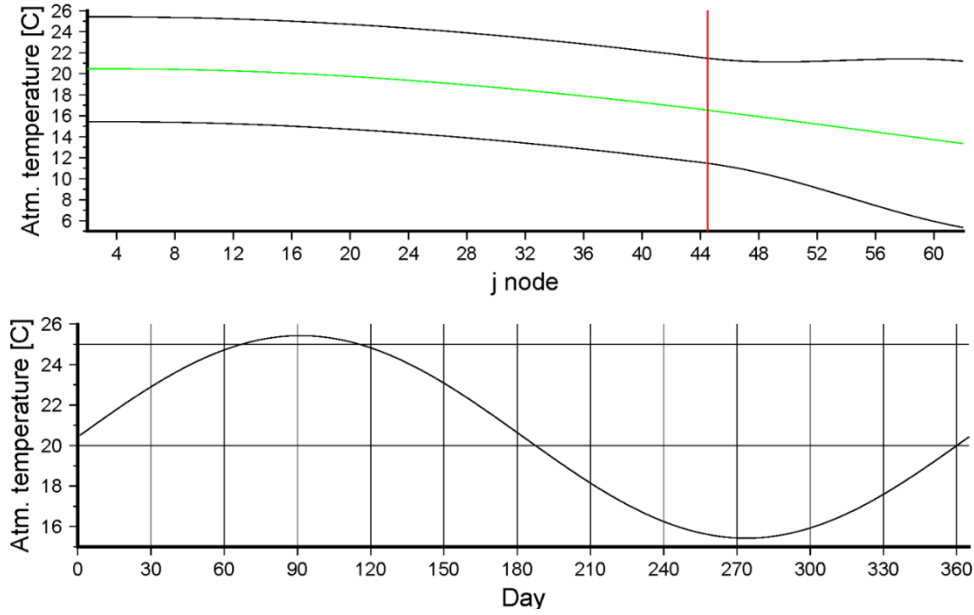
Figure 4: (Top) The atmospheric temperature over the j (vertical) nodes. (Top line: peak summer conditions, bottom line: peak winter conditions, green line: average conditions, red line: starting point increase from 5 to 8 °C .) (Bottom) Annual atmospheric temperature variation in the 2 to 45 j node region over time.

seasonal variation on the system a sinusoidal temperature variation over a yearly period was introduced in a selection of runs. The maximum temperature variation is based on monthly mean temperature measurement data of the Mediterranean region provided by the National Centers for Environmental Information (NCEI, 2019) and available through the "Fundació de la Comunitat Valenciana Centro d'Estudis Ambientals del Mediterrani" or CEAM (CEAM, 2019). The southern part of the Mediterranean near Libya shows a seasonal variation of about 5 °C while the northern part of the Adriatic Sea shows a variation of up to 8 °C. This was taken into account in the model by gradually increasing the maximum amplitude of the sinusoid in the north from 5 °C to 8 °C (fig. 4). An overview of the most relevant experiments is given in table 1.

3. Model results

A range of experiments was performed under varying conditions and timescales. The most relevant results will be discussed here. A reference experiment, experiment 2060, was performed to serve as a baseline for future experiments (panel A1.1). In this experiment, no net evaporation or temperature forcing was imposed, as well as a mean depth-averaged velocity of zero at the open boundary. The baroclinic velocity at the open boundary was left unconstrained allowing ocean water to flow freely through the open boundary. This reference experiment was subsequently built upon by imposing
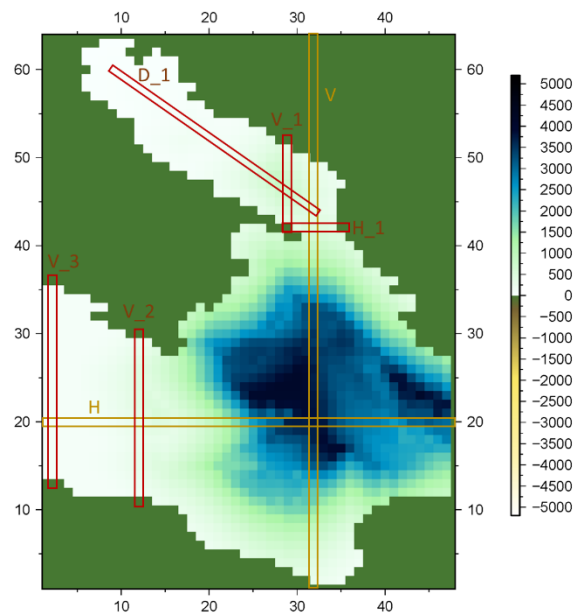
Figure 5: Sections within the model region. (red: local sections, orange: regional sections)
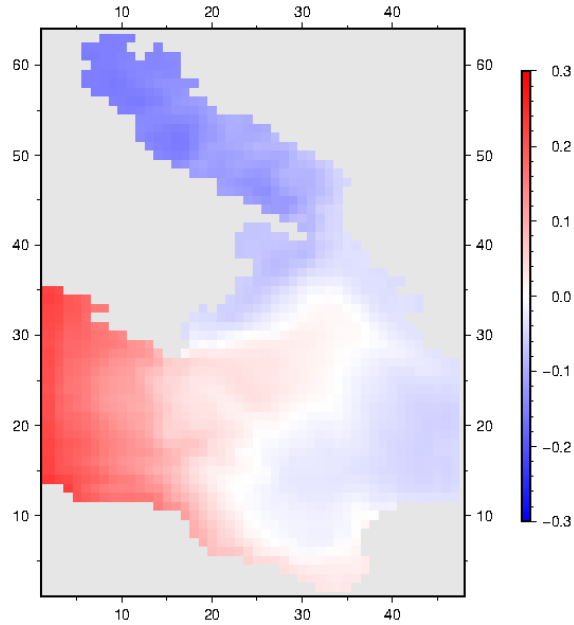
F*igure 6: Surface elevation map of exp. 2020. (red: above average, blue: below average)*

net evaporation, temperature and a two-way flow at the open boundary. Time-dependent results were averaged over a dynamically stable 990 to 1000 year range to account for small scale variations and recurring patterns within the system. The dynamically stable timescale used was checked by comparison to a 900 to 1000 year range, and by close inspection of the averaged data over time (see below). No significant differences were found in the results as to warrant further extension of the 990 to 1000 year averaged timescale chosen.

3.1 net evaporation forcing

In the most basic experiment, experiment 2020, only net evaporation is imposed as a forcing on the system. To compensate for water loss due to net evaporation an inflow of ocean water is imposed at the open boundary in the west as to maintain a constant water volume within the system over time.

A number of variables were recorded over the runtime of the experiment to check its validity and provide insight into the evolution of the model over time (panel A1.2). These include basin averaged temperature, salinity, density and surface elevation; in, out and net flow of the two main straits; and mean kinetic energy (a measure of kinetic energy divided by

the density). The corresponding panels for each experiment are presented in appendix A1. In the case of experiment 2020 the in- and outflow at the strait of Otranto and the strait of Sicily stabilize around 2.7 Sv and 1.1 Sv respectfully. After the in- and outflow reaches a steady state a constant oscillating pattern remains showing a constant maximum and minimum amplitude. After closer inspection, no obvious repeating pattern is found within this oscillation. The steady state nature of each oscillation was checked with a 2000 year run and was found to remain stable for the entire run period after the 500 year mark (panel A1.7). The volume average salinity increases until it reaches a steady state of 39.5 ppt while the volume average temperature remains constant since there is no temperature forcing present. The mean kinetic energy slowly stabilizes while the average surface elevation shows a slow increase over time. This increase reaches a maximum 0f 5 mm after a 1000 years and is attributed to an accumulation of small model imperfections. In each of these cases, it takes about 200 to 500 years to reach a steady state.

3.1.1 map regions

A surface temperature, salinity and density map were made for each of the experiments (figure 7, 8 & appendix B), as well as a surface particle trace map
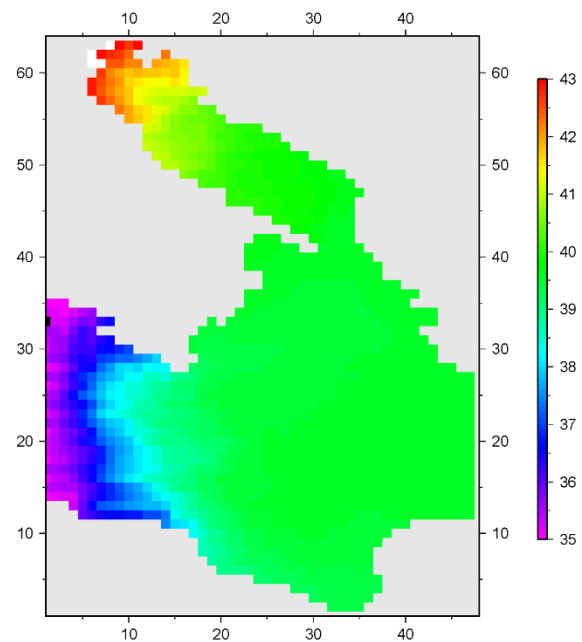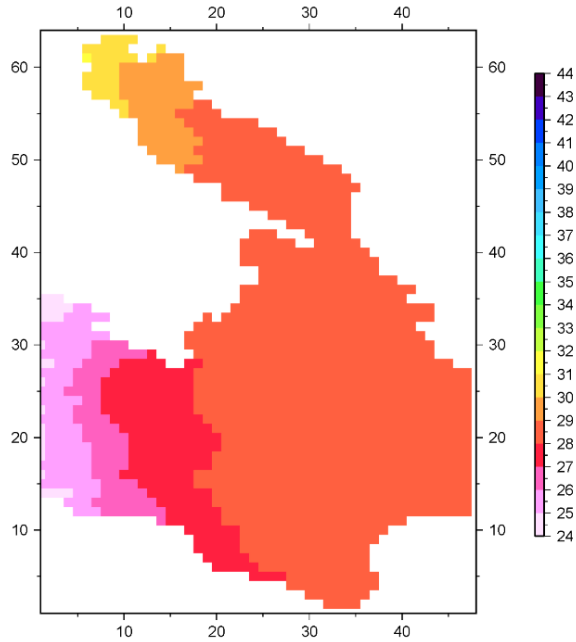

Figure 7: Surface salinity in psu of exp. 2020.

6

Figure 8: Surface density (ρ-1000) in kg/m3 of exp. 2020.

(figure 9, appendix C), a map of the barotropic stream function (figure 10, appendix D) and a surface elevation map (figure 6, appendix C). Experiment 2020 shows a constant sea surface temperature of 20 °C throughout the whole region since no temperature forcing is yet applied. The sea surface salinity shows a low value where relatively fresh water enters the region through the open boundary and a high value in the north where a higher net evaporation value is imposed compared to the south. The sea surface density shows a similar picture since, in this case, its value is dependent on the salinity only. The surface particle trace map shows the existence of multiple surface circulation cells despite the fact that net evaporation is the only forcing factor imposed on the model system. The surface circulation system consists of one major cell, occupying most of the Ionian Sea, and a number of smaller cells, one of which occupies the strait of Otranto and parts of both the Ionian and the Adriatic Sea. A similar circulation system can be observed in the map of the barotropic stream function. It should be noted that the barotropic stream function represents the entire depth range of the model system and not just the sea surface as is the case with the surface particle trace map. Finally, the surface elevation map shows a high positive deviation at the open boundary, where water flows

into the system to compensate for net evaporation, and a high negative deviation in the north, where the highest net evaporation value is imposed. A positive deviation can be observed in the northwest of the Ionian Sea and a negative deviation in the southeast. The deviation pattern shows resemblance with the pattern observed in the surface particle trace map and the barotropic stream function. More specifically, similarities can be observed in the upper north-western part of the Ionian Sea and in the rough outlines of the smaller surface circulation cells in the south and east of the model region.

3.1.2 The zonal and meridional overturning stream function

The zonal and meridional overturning stream function were examined in each experiment to gain further insight into the circulation within the system (figure 11, 12 & Appendix E, F). The meridional overturning stream function is horizontally integrated from East to West over the model region and the zonal overturning stream function from North to South. They both represent the entire circulation over
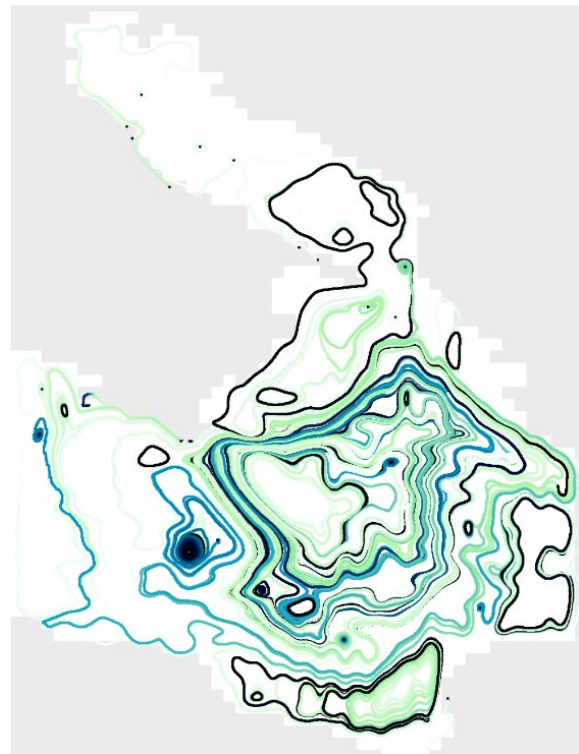

Figure 9: The traces of a selection of equally spaced surface particle through time of exp. 2020. The tail of each particle becomes lighter as the trace of the particle becomes longer.
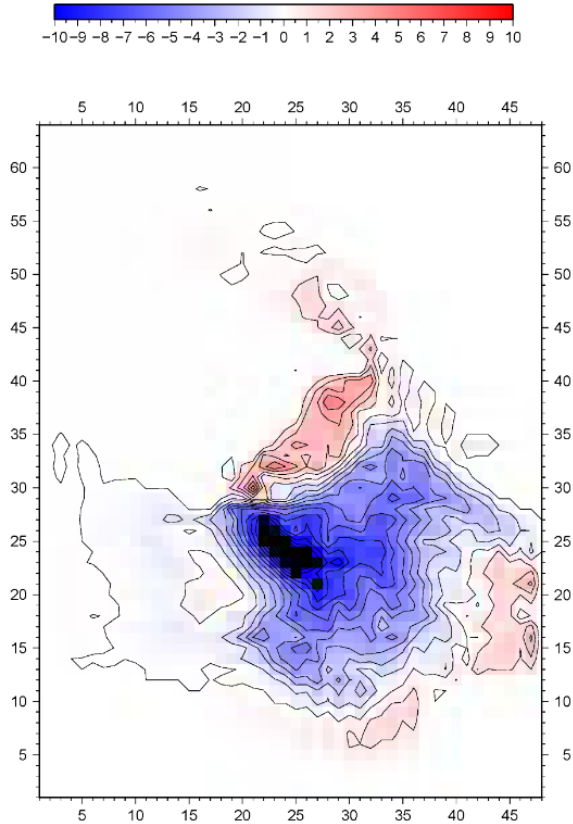
Figure 10: The depth integrated potential of flow in Sv of exp. 2020. (red=counter-clockwise, blue=clockwise)

this range, where the meridional stream function shows a westward point of view and the zonal stream function a northward point of view. In the case of the zonal stream function, the North-South horizontal integration amounts to the overturning circulation within the Adriatic and Ionian Sea to both be represented as one circulation system while they are clearly two separate systems. However, since the Adriatic Sea is extremely shallow compared to the Ionian Sea its representation in the horizontally integrated image is minimal. This amounts to the zonal overturning stream function being mostly a representation of the Ionian Sea, rather than the Adriatic Sea. In the zonal overturning circulation figure of experiment 2020 a single large cell with a clockwise circulation can be observed. This circulation cell represents the streamlines tangent to the flow velocity vector. The cell occupies the whole basin with the exception of parts of the lower basin region, where two low intensity counter-clockwise circulation cells exist. In the meridional overturning

circulation figure of experiment 2020 a high intensity counter-clockwise circulation can be observed in the south of the region and a lower intensity clockwise circulation cell in the north of the region which extends into the Adriatic Sea. In the lower regions of the basin two very low intensity clockwise circulation cells can be noted, just as was the case for the zonal stream function.

3.1.3 Cross sections

To further examine the underlying processes within the model a number of cross sections through the model region were created (fig. 5). Special attention was focussed on the two straits in the model region, the strait of Otranto, which connects the Adriatic with the Ionian Sea, and the strait of Sicily, which connects the model region with the outer ocean through the open boundary. Three cross sections were made in the strait of Otranto region (appendix G, H) and two in the strait of Sicily region (appendix J). Furthermore, two regional cross sections were made through the centre of the basin, one horizontal cross section (Panel J8, J9) and one vertical cross section (Panel H1, H3, H5, H6). Temperature, salinity, density and flow velocity were considered in each of these cross sections.

Strait of Otranto

To get a clear picture of the strait of Otranto region in experiment 2020 the observations of the three cross sections through the region, as well as the regional vertical cross section, were combined. When examining the velocity field of the zonal cross section across the strait (H_1 in fig. 5) a clear picture of the in- and outflow through the strait can be observed (panel G4). Combined with the observations of the salinity and density a clear southward flowing outflow region of the Adriatic Sea can be identified in the west. The salinity cross section show that the outflowing water has a high salinity, which is expected for deep outflowing water. The density cross section shows a more moderate picture since density is not only a product of salinity and temperature, but also of depth, which acts as a dampening factor. A northward flowing region of
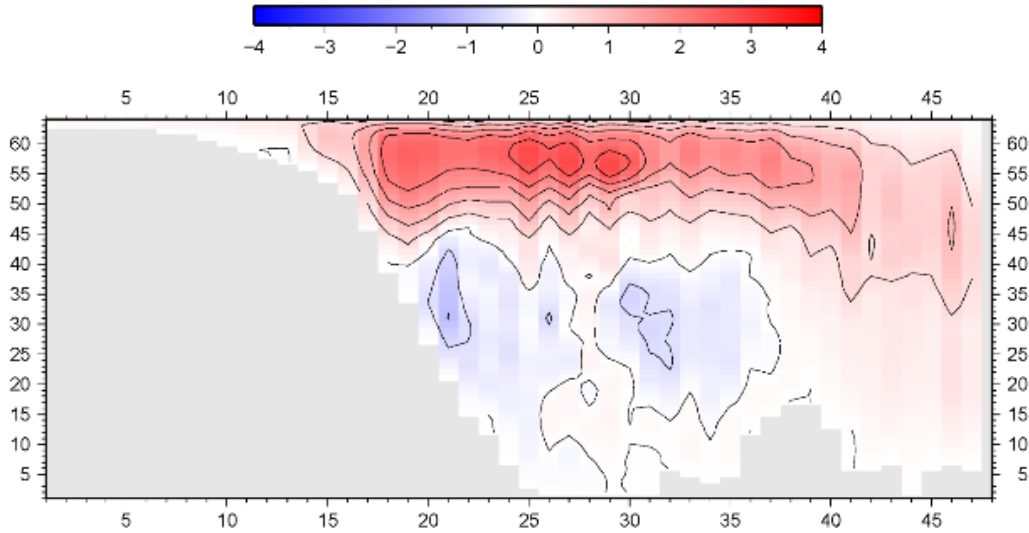
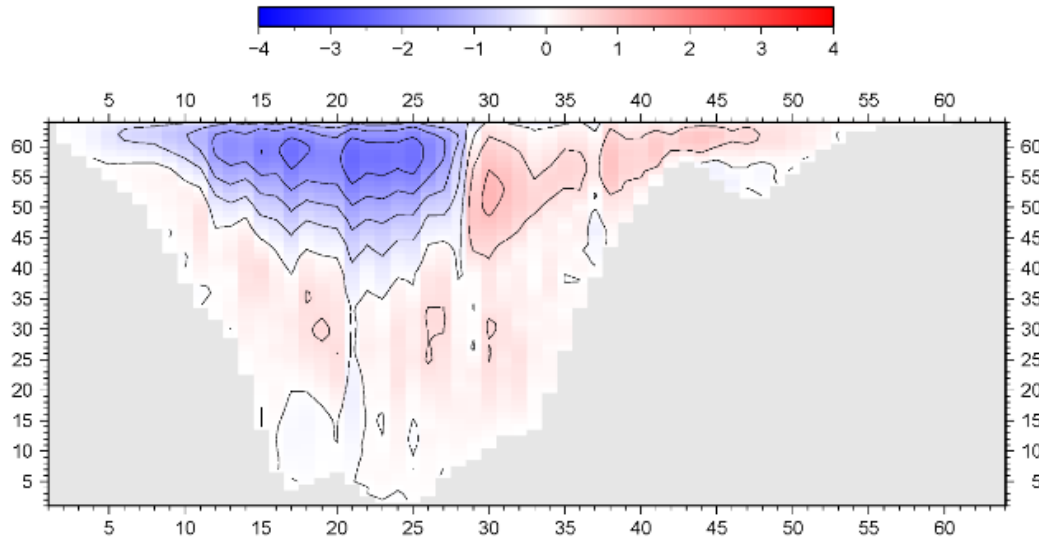*Figure 11: The zonal overturning stream function in Sv representing streamlines tangent to the flow velocity vector of exp. 2020 (red=clockwise, blue=counter clockwise). Depth [m] is represented on the y axis through the following formulation: depth = 65*(64-y).*

inflow can also be distinguished in the top left of the cross section and in the middle of the section. The region of inflow occupies a larger area and shows higher salinity compared to the region of outflow. Finally, a low intensity southward flowing region and a low intensity northward flowing region are present in the eastern part of the cross section. Since no clear temperature and salinity correlation can be found it is presumed that these regions are not part of the main circulation cell within the Adriatic Sea but instead represent smaller scale circulations existing in the region. Another point to note is the difference in position between the centre of outflow intensity in panel G4 and the centre of salinity intensity in panel G2. This is caused by the fact that the path of the water flowing through the 30th horizontal grid cell in the cross section is obstructed moving further to the south causing a strong reduction in flow velocity at this grid cell. Two further examine the properties of the water flowing through the strait the average salinity and temperature of the in- and outfling water was recorded (Appendix I). Since there is no temperature forcing present a constant average temperature is found for the in- and outflow. In the case of the salinity both the in- and outflow show a higher average salinity then the volume average of the entire model region. The difference between the average salinity of the in- and outflow is minimal, with

only a 0.11 ppt difference between them. In each experiment that follows the average salinity of the outflowing water is consistently higher and the average temperature lower, which is consistent with the higher net evaporation and the lower atmospheric temperature imposed on the Adriatic Sea.

Strait of Sicily

In the case of the strait of Sicily region of experiment 2020 the two cross sections present in the region were combined with observations of the horizontal regional cross section to study the area in further detail. The salinity cross section at the open boundary shows a relatively high salinity at the bottom and the centre of the section, and a relatively low salinity at the top and sides of the section (panel J2). When moving further away from the open boundary in section V_3 a more homogenous higher intensity salinity profile can be observed. Regions of lower salinity still exist in the top corners of the profile but are more concentrated in the corner areas. When examining the salinity profile of the regional horizontal cross section similar results can be found (panel J9). Salinity slowly increases from 35 ppt at the open boundary to about 39 ppt in the main basin. When moving away from the open boundary the salinity remains lower at the surface compared to the
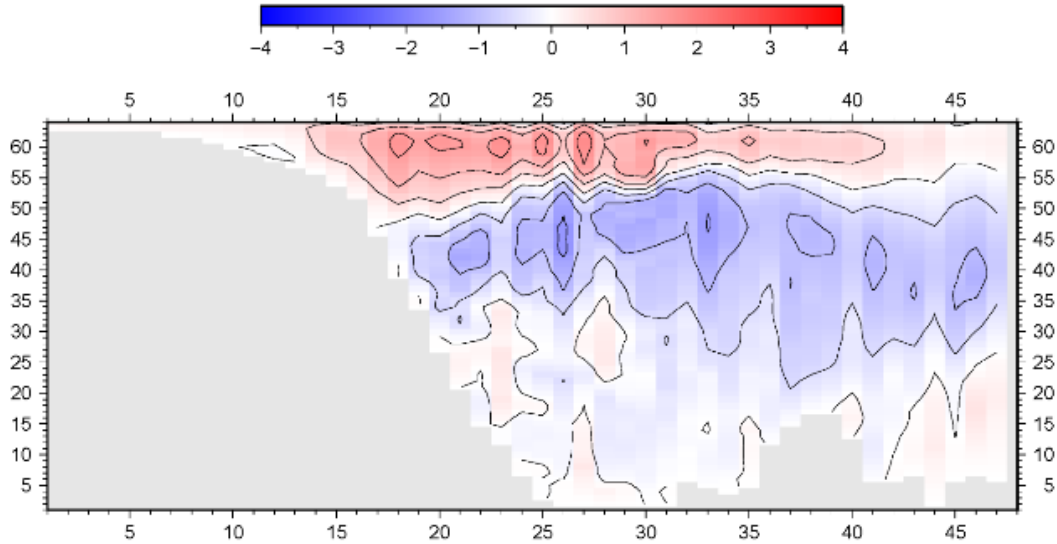
Figure 12: The meridional overturning stream function in Sv representing streamlines tangent to the flow velocity vector of exp. 2020 (red=clockwise, blue=counter clockwise). Depth [m] is represented on the y axis through the following formulation: depth = 65*(64-y).

bottom creating a diagonal salinity gradient. This gradient disappears further into the main basin where the salinity becomes homogenous. No clear flow pattern can be observed in the velocity cross sections of the Sicily region (V_2, V_3). This is consistent with what was observed in the zonal depth integrated potential of flow (Appendix E).

3.2 Atmospheric temperature forcing

In experiment 2041, a temperature boundary condition was imposed on the model system. The temperature boundary condition consists of a relaxation of sea surface temperature to a constant atmospheric temperature field which varies only with latitude. Except for the addition of temperature forcing all other variables were kept the same. Panel A1.3 shows the basin averaged temperature, salinity, density and surface elevation; in, out and net flow of the two main straits; and mean kinetic energy. Compared to experiment 2020 volume averaged temperature and salinity have both decreased while mean kinetic energy and volume averaged density have increased. The net-, in- and outflow through the strait of Sicily has remained approximately equal. The in- and outflow through the strait of Otranto, however, has significantly increased, going from an approximate average value of 2.7 Sv to a value of 4.0

Sv. Furthermore, the maximum and minimum amplitude of both the in- and outflow and the net flow has increased.

3.2.1 map regions

The surface temperature map shows the effect of the atmospheric temperature field on the sea surface (Appendix B). The sea surface temperature ranges from about 13 °C in the most northern part of the region to about 20 °C in the most southern part of the region. A relatively high sea surface temperature can be observed at the open boundary in the west compared to a similar latitude in the east. The sea surface salinity map shows an overall decrease in surface salinity compared to experiment 2020, especially in the north of the model region. This decrease is in line with the volume averaged salinity decrease observed in panel A1.3. The sea surface density map shows an increase in density in the Adriatic Sea and a slight decrease in the west of the Ionian Sea. This change corresponds to the surface temperature and salinity changes observed for this experiment. The surface particle trace map shows a clear change in the surface circulation cells present in the model system (appendix C). The main cell that was present in experiment 2020 is broken up into three smaller circulation cells which together occupy
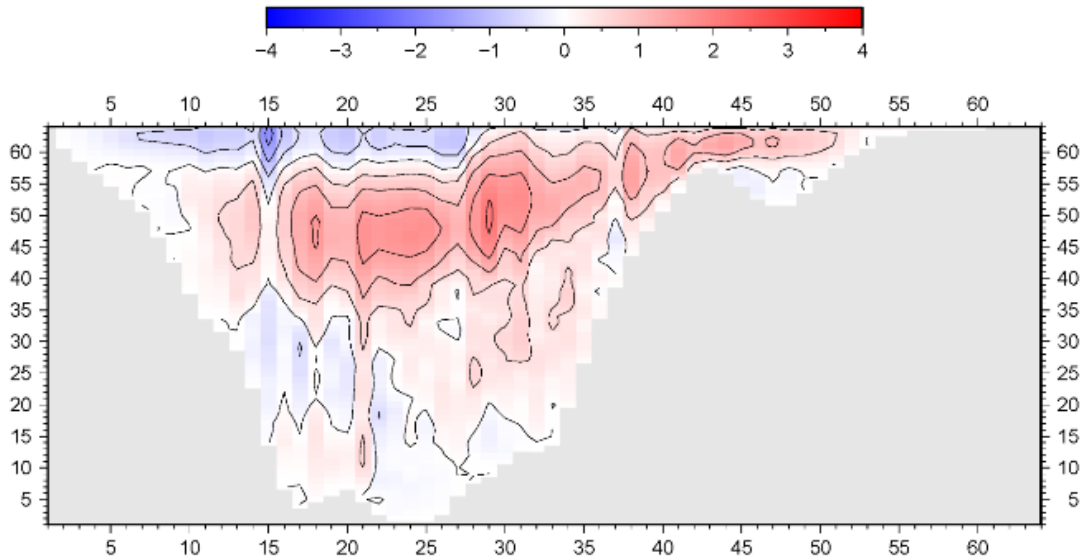
Figure 13: The zonal overturning stream function in Sv representing streamlines tangent to the flow velocity vector of exp. 2041 (red=clockwise, blue=counter clockwise). Depth [m] is represented on the y axis through the following formulation: depth = 65*(64-y).

the entire basin. The smaller circulation cell that formed a connection between the Adriatic and Ionian Sea is no longer present in the system. The barotropic stream function shows a similar change, with the exception of a somewhat more developed circulation in the Adriatic Sea (appendix D). Finally, the surface elevation map shows a similar picture as in experiment 2020 with some important differences (appendix C). The negative deviation in the Adriatic Sea has increased while the positive deviation at the open boundary has slightly decreased. The negative deviation previously present in the southeast of the Ionian Sea has disappeared and has been replaced by a less clearly divined negative deviation. The rough outlines of the circulation cells of the surface particle trace map can be somewhat distinguished in the surface particle trace map when it is overlain by the surface elevation map (fig. 14, fig. C6) .

3.2.2 The zonal and meridional overturning stream function

In the zonal overturning circulation figure of experiment 2041 (figure 13, appendix E) two clearly distinct clockwise and counter-clockwise circulation cells can be observed. The single large clockwise circulation cell that was present in experiment 2020 has progressed to shallower depths while a clear counter-clockwise circulation cell is now present at

greater depths. In the case of the meridional overturning circulation (figure 15, appendix F) a shift has taken place of the two main cells in the system. The clockwise circulation cell that was present in the north has expanded into the main basin, thereby forming a circulation system than ranges from the south of the Ionian Sea to the north of the Adriatic Sea. The counter-clockwise circulation cell that was
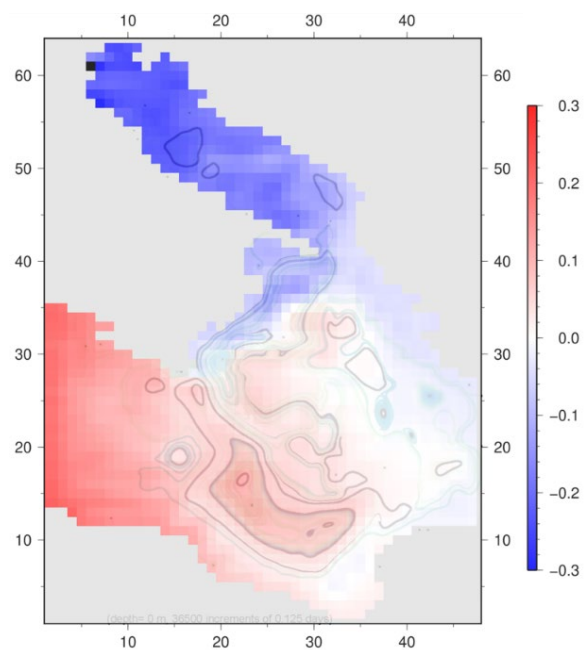
Figure 14: The particle trace map of exp. 2041 overlain by the surface elevation map of exp. 2041.
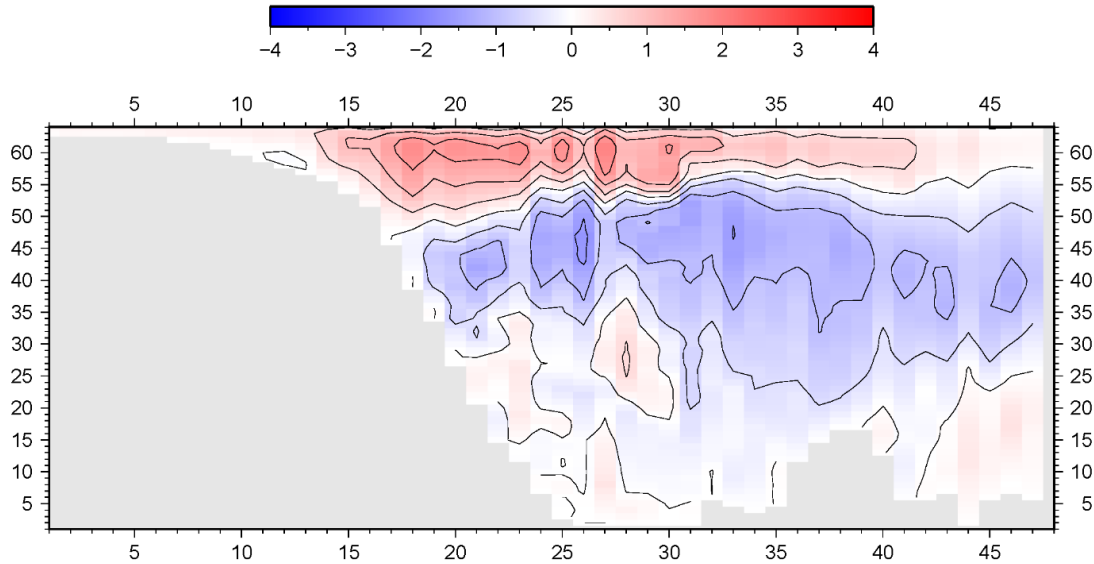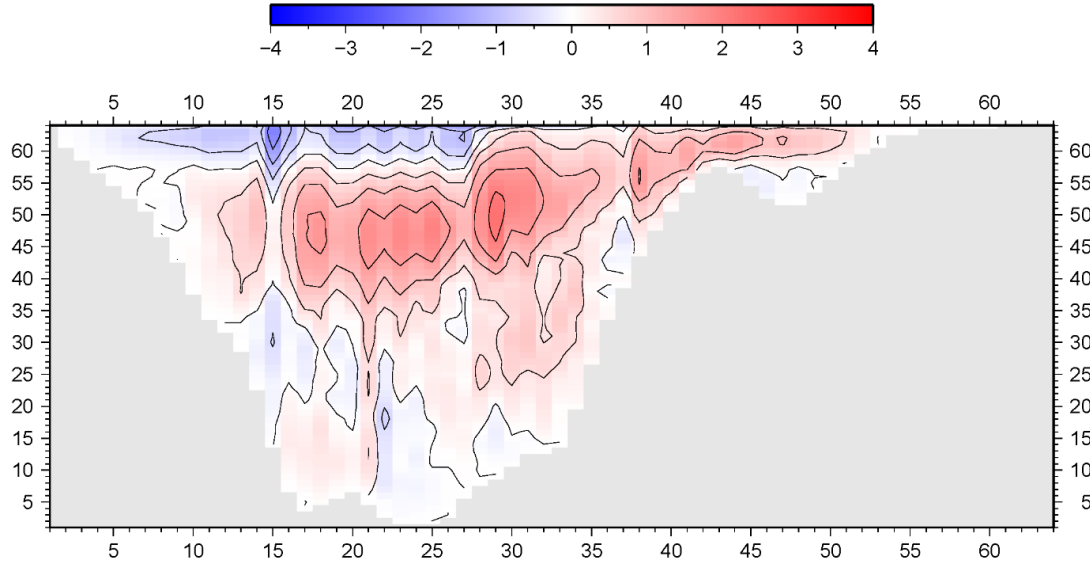
Figure 15: The meridional overturning stream function in Sv representing streamlines tangent to the flow velocity vector of exp. 2041 (red=clockwise, blue=counter clockwise). Depth [m] is represented on the y axis through the following formulation: depth = 65*(64-y).

present in the south still occupies the same latitudinal range of the Ionian Sea but at a shallower depth range then was previously the case. It should be noted that in both the meridional and the zonal case the deeper region of the Ionian Sea shows little to no circulation compared to the shallower parts of the model system.

3.2.3 Cross sections

Strait of Otranto
The velocity field of experiment 2041 at the strait of Otranto (H_1 in fig. 5) is similar to the velocity field of experiment 2020 (appendix G). The only difference being the velocity intensity of the flow. The salinity profile shows a similar picture. The profile is very much the same but an overall decrease in salinity can be observed, which is consistent with what was observed in the sea surface salinity map of experiment 2041. The temperature profile of the experiment is consistent with the salinity profile. A clear centre of cold, outflowing water can be observed at the bottom-west of the section with the water becoming warmer in the east and at shallower depth. In the case of the density profile only a moderate variation between the two experiments is observed, becoming somewhat higher, which is in line with what was observed in the barotropic regional overview. Similar observations can be made

regarding the cross sections of temperature, salinity and density through the Adriatic Sea (D_1 in fig. 5) and the Ionian Sea (V in fig. 5) (appendix H). When examining the average salinity and temperature of the in- and outfling water (appendix I) of experiment 2041 an overall salinity and temperature decrease is present, as is expected based on previous results. Notably, the difference between the average salinity of the in- and outflow has also decreased from an average value of about 0.104 ppt to an average value of about 0.065. Furthermore, the maximum and minimum amplitude of the salinity difference between the in- and outflow has increased.

Strait of Sicily
The difference between the salinity profiles (V_2, V_3 in fig. 5) of experiment 2041 and 2020 is minimal, showing only a small decrease in overall salinity in experiment 2041 (appendix J). The velocity profiles of these two cross sections are very similar as well, showing only a somewhat higher velocity intensity in experiment 2041 (appendix J). Just as was the case at the strait of Otranto, the temperature profile at the V_3 cross section corresponds to what is observed in the salinity profile. However, the range is much smaller, ranging from 19.6 to 19.9 °C. In the case of
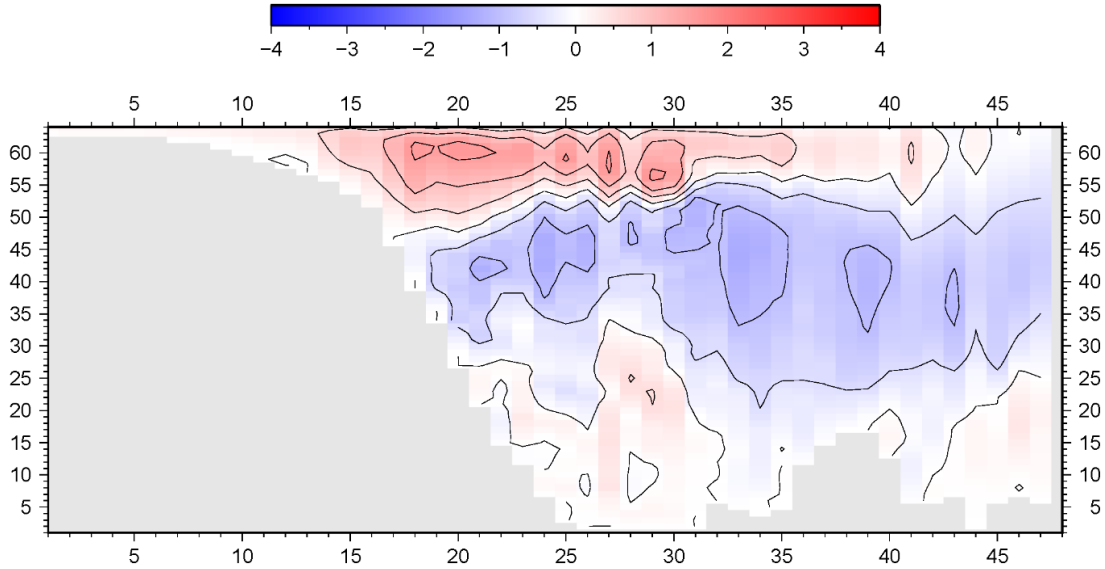
Figure 16: The zonal overturning stream function in Sv representing streamlines tangent to the flow velocity vector of exp. 2042 (red=clockwise, blue=counter clockwise). Depth [m] is represented on the y axis through the following formulation: depth = 65*(64-y).

the V_2 cross section the salinity and temperature profile do not correspond since the temperature profile in this cross section is not just affected by flow but also by atmospheric temperature forcing. To examine the larger picture concerning temperature and salinity in the strait of Sicily the horizontal regional cross section was used. A decrease in temperature can be observed when moving further away from the open boundary, as was observed in the map view of the sea surface temperature. A decrease can be also be observed when moving towards greater depths. The salinity profile of the horizontal regional cross section shows a similar picture as the salinity profile of experiment 2020, with the exception of an overall salinity decrease.

3.3 two way flow

In experiment 2042, a two-way barotropic flow was implemented at the open boundary. All other variables were kept the same. Compared to experiment 2031 volume averaged salinity and density have both decreased while mean kinetic energy and volume averaged temperature have remained equal (Appendix A1). The net-, in- and outflow through the strait of Otranto has remained approximately equal. The in- and outflow through the strait of Sicily, however, has slightly increased, going

from an approximate average value of 1.15 Sv to a value of 1.20 Sv. Furthermore, the maximum and minimum amplitude of the in- and outflow has decreased.

3.3.1 map regions

The surface temperature map of experiment 2042 shows little to no change compared to experiment 2041 while the sea surface salinity map shows an overall decrease in surface salinity. Furthermore, the effect of two way flow on the surface salinity at the open boundary can also be observed. The sea surface density map shows a decrease in overall density throughout the region. Once again, the effect of two way flow can be clearly observed at the open boundary. The surface particle trace map and the barotropic stream function show some small changes but the larger patterns seen in experiment 2041 remain (appendix C, D). Finally, the surface elevation map shows little to no change with the exception of a decrease in positive deviation at the open boundary.

3.3.2 The zonal and meridional overturning stream function

The addition of a two way flow at the open boundary has little to no effect on the zonal and meridional overturning circulation. Figure 16 and 17 & 13 and 15 show only a minimal difference between experiment
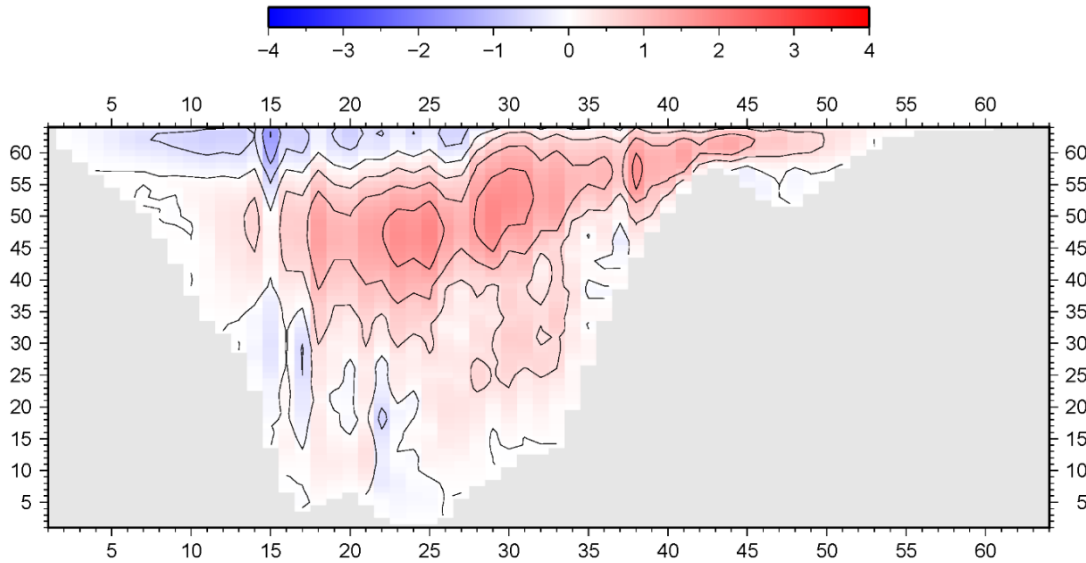
Figure 17: The meridional overturning stream function in Sv representing streamlines tangent to the flow velocity vector of exp. 2042 (red=clockwise, blue=counter clockwise). Depth [m] is represented on the y axis through the following formulation:
depth = 65*(64-y)

2042 and 2041 for both overturning circulations.

3.3.3 Cross sections

Strait of Otranto

The velocity and temperature field of experiment 2042 at the strait of Otranto (H_1 in fig. 5) show little to no difference from the velocity and temperature field of experiment 2041. The salinity and density profile do show a change, but only in overall salinity and overall density (appendix G). Similar observations can be made regarding the cross sections of temperature, salinity and density through the Adriatic Sea (D_1 in fig. 5) and the Ionian Sea (V in fig. 5) (appendix H). The average salinity and temperature of the in- and outfling water (appendix I) of experiment 2042 show similar results. There is no change in average temperature while a decrease in average salinity of about 0.025 ppt is present in the in- and outflow. No change occurs in the difference between the average salinity of the in- and outflow.

Strait of Sicily

The velocity profile of cross section V_3 shows a clear change when a two way flow is implemented. In the north of the section a region of westward flow is present and in the south a region of eastward flow is present (appendix J). This difference between

experiment 2041 and 2042 disappears in the velocity profile of section V_2. In this section the velocity profiles remain similar, the only change being a small decrease in overall velocity intensity. The salinity profiles of section V_2 and V_3 show a similar pattern (appendix J). In section V_3 a clear difference can be observed between the north and the south of the profile, with the eastward flowing water in the south havening a lower salinity and the westward flowing water in the north having a higher salinity. This difference between experiments then disappears in section V_2 where a similar salinity profile as in experiment 2041 can be observed, with the difference being a decrease in overall salinity. The temperature profile at the V_3 cross section corresponds to what is observed in the salinity profile with the difference being the small temperature range. It ranges from 19.6 to 19.9 °C, just as was the case in experiment 2041. The temperature profile at V_2 shows a slight increase but otherwise remains unchanged. In the case of the horizontal cross section H the temperature profile shows little to no difference while the salinity profile shows an overall decrease in salinity.

3.4 Seasonal temperature variation

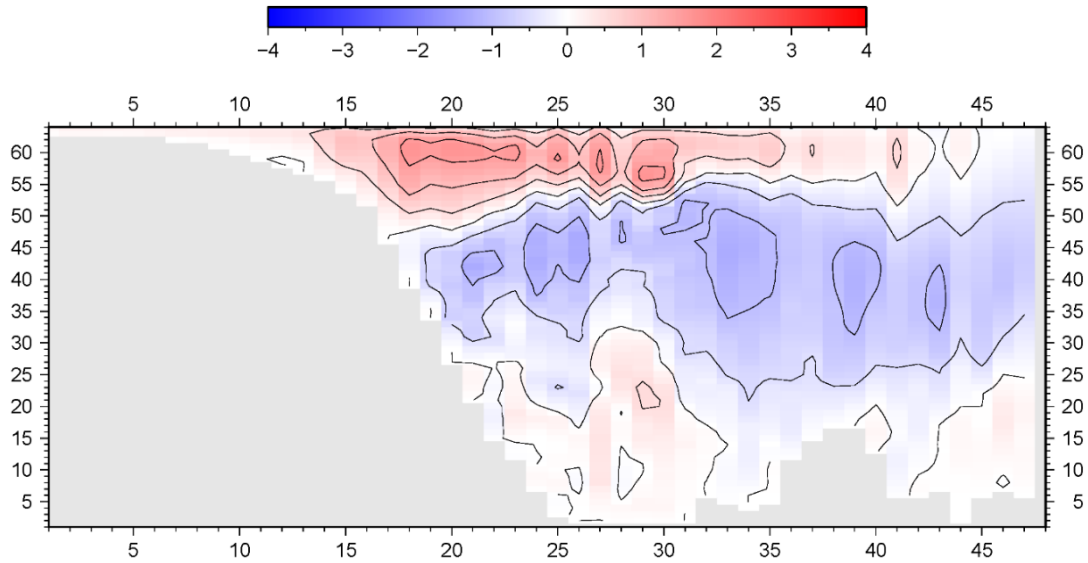In experiment 2031, a sinusoidal temperature

Figure 18: The zonal overturning stream function in Sv representing streamlines tangent to the flow velocity vector of exp. 2031 (red=clockwise, blue=counter clockwise). Depth [m] is represented on the y axis through the following formulation:
depth = 65*(64-y).

variation over a yearly period was introduced. No two way flow was implemented at the open boundary. Compared to experiment 2041 volume averaged temperature and salinity have both decreased while mean kinetic energy and volume averaged density have increased. Due to the yearly temperature variation the maximum and minimum amplitude of both the volume averaged temperature and the volume averaged density have increased accordingly. This annual pattern caused by constant seasonal temperature variation can be observed in panel A2.1. It should be noted that the net flow of the two main straits in the model show a comparable pattern, even when temperature forcing is absent. This pattern can be clearly distinguished in panel A2.2. Based on surface elevation maps through time, the pattern is likely caused by wave action within the model. The maximum and minimum amplitude of the mean kinetic energy has also greatly increased ranging from about 1.5 to 3.5 x 10-3 m2s-2 with an average of about 2.4, compared to a previous average of about 2.1. The net-, in- and outflow through the strait of Sicily has remained approximately equal. The in- and outflow through the strait of Otranto, however, has increased, going from an approximate average value

of 4.0 Sv to a value of 4.1 Sv. Furthermore, the maximum and minimum amplitude of both the in- and outflow and the net flow has significantly increased.

3.4.1 map regions

The surface salinity map of experiment 2031 shows little to no change compared to experiment 2041 while the sea surface temperature map shows an overall increase in surface temperature. This increase is mostly present in the south of the Ionian Sea and the south of the Adriatic Sea. Since the volume average temperature of the model region decreases in experiment 2031 when compared to 2041 a decrease in temperature at greater depth must be present to compensate for the increase observed at the sea surface. The sea surface density map shows a moderate decrease in overall density throughout the region. Logically, these regions of decreased density correspond to the regions of increased sea surface temperature. The surface particle trace map shows a clear similarity with experiment 2041 but also shows some differences (appendix C). The larger cell that occupied the north-west and centre of the Ionian Sea
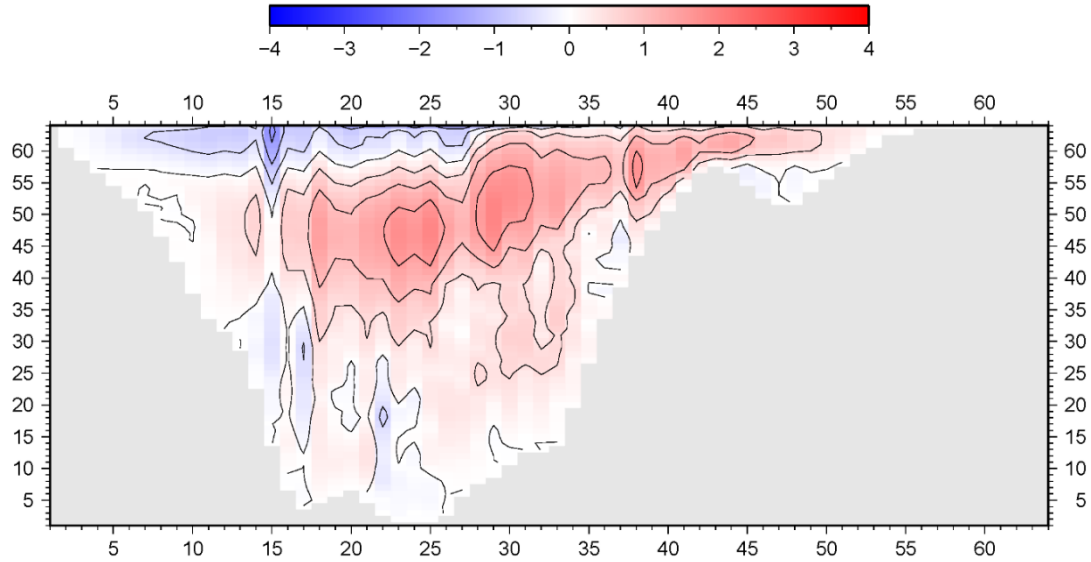
Figure 19: The meridional overturning stream function in Sv representing streamlines tangent to the flow velocity vector of exp. 2031 (red=clockwise, blue=counter clockwise). Depth [m] is represented on the y axis through the following formulation: depth = 65*(64-y).

has been somewhat broken up in the centre, thereby partly forming a new cell in this region. The cell that was present in the south and south-west of the Ionian Sea has increased in intensity and expanded to the west towards the open boundary. Lastly, the cell that was present in the east of the Ionian Sea has somewhat expanded in size towards the west. Little to no change has occurred in the Adriatic Sea. The change observed in the barotropic stream function correspond to the change observed in the surface particle trace map (appendix D). The exception is the expansion of the south-western cell of the particle trace map towards the open boundary. This expansion is not present on the barotropic stream function. Conversely, the barotropic stream function does show some circulation in the Adriatic were the surface particle trace map does not.

3.4.2 The zonal and meridional overturning stream function

The addition of a sinusoidal temperature variation only has a moderate effect on the zonal and meridional overturning circulation. The main difference between experiment 2031 and 2041 is a decrease in the overall circulation intensity.

3.4.3 Cross sections

Strait of Otranto

The salinity field of experiment 2031 at the strait of Otranto (H_1 in fig. 5) shows little to no difference from the salinity and density field of experiment 2041. The velocity and density profiles do show a change, but only in an increase of the overall intensity (appendix G). The temperature profile shows an overall decrease in temperature combined with a change in the temperature gradients. This change in temperature gradients can best be observed in cross section V to examine the change at a basin scale (appendix H). While the surface temperature has increased the temperature at greater depth has decreased, shifting to a temperature field that is less dependent on latitude and more dependent on depth (panel H1). The same process can be observed within the density field. While the density at the surfaces slightly decreases, the density at larger depth slightly increases (panel H6). The average salinity of the in- and outfling water (appendix I) of experiment 2031 shows little to no change compared to 2041 while the average temperature shows a moderate decrease of about 0.2 °C. Furthermore, the maximum and minimum amplitude of the average temperature of the in- and outflow, as well as the temperature difference between the in- and outflow, has increased.

16

Figure 20: The zonal overturning stream function in Sv representing streamlines tangent to the flow velocity vector of exp. 2044 (red=clockwise, blue=counter clockwise). Depth [m] is represented on the y axis through the following formulation: depth = 65*(64-y).

Strait of Sicily

The velocity profile of experiment 2031 at the V_3 cross section and the V_2 cross section show a similar picture as in experiment 2041. The only difference is a decrease in flow intensity at the V_3 cross section. The salinity profiles of experiment 2031 and 2041 at cross section V_2 and V_3 show little to no difference. The temperature profile at the V_3 cross section closely corresponds to what was observed in experiment 2041 with the difference being a larger range in temperature, going from 19.1 to 19.9 °C. The temperature profile at the V_2 cross section shows a temperature field that is less dependent on latitude and more dependent on depth, just as was in the case for the strait of Otranto. A warmer region still exists in the north of the cross section caused by the influence of the atmospheric temperature. In the case of the horizontal cross section H the salinity profile shows little to no difference while the temperature profile shows a higher temperature decrease with depth than was previously the case.

3.5 Two way flow combined with temperature variation

In experiment 2044, a two-way barotropic flow was implemented at the open boundary. All other variables were kept the same. Compared to experiment 2031 volume averaged salinity and density have both decreased while mean kinetic energy and volume averaged temperature have remained equal (Appendix A1). The net-, in- and outflow through the strait of Otranto and the strait of Sicily have remained approximately equal. However, the maximum and minimum amplitude of the in- and outflow through the strait of Sicily has decreased.

3.5.1 map regions

The surface temperature map of experiment 2044 shows little to no change compared to experiment 2031 while the sea surface salinity and density maps shows an overall decrease (appendix B). The surface particle trace map shows a similar flow pattern as in experiment 2031 with some small differences (appendix C). The cell that is present in the south and south-west of the Ionian Sea has decreased in intensity while the cell that is present in the east of the Ionian Sea has increased in intensity. Furthermore, the circulation present in the Adriatic Sea has somewhat increased. Interestingly, little to no change is present between the barotropic stream function map of experiment 2031 and experiment 2044 (appendix D). Finally, the surface elevation map shows little to no change with the exception of a decrease in positive deviation at the open boundary.

17

Figure 21: The meridional overturning stream function in Sv representing streamlines tangent to the flow velocity vector of exp. 2044 (red=clockwise, blue=counter clockwise). Depth [m] is represented on the y axis through the following formulation: depth = 65*(64-y).

3.5.2 The zonal and meridional overturning stream function

The addition of a two way flow at the open boundary has little to no effect on the zonal and meridional overturning circulation. Figure 18 and 19 & 20 and 21 show only a minimal difference between experiment 2031 and 2044 for both overturning circulations.

3.5.3 Cross sections

Strait of Otranto

The temperature field of experiment 2042 at the strait of Otranto (H_1 in fig. 5) shows little to no difference from the temperature field of experiment 2041. The salinity, velocity and density profile do show a change, but only in overall salinity, flow intensity and overall density (appendix G). Similar observations can be made regarding the cross sections of temperature, salinity and density through the Adriatic Sea (D_1 in fig. 5) and the Ionian Sea (V in fig. 5) (appendix H). The average salinity and temperature of the in- and outfling water (appendix I) of experiment 2042 show similar results. There is no change in average temperature while a decrease in average salinity of about 0.028 ppt is present in the in- and outflow. No change occurs in the difference between the average salinity of the in- and outflow.

Strait of Sicily

The velocity profile of cross section V_3 shows a clear change when a two way flow is implemented (appendix J). This difference between experiment 2031 and 2044 disappears in the velocity profile of section V_2. In this section the velocity profiles shows little to no change between experiments. The salinity profiles of section V_2 and V_3 show a similar pattern
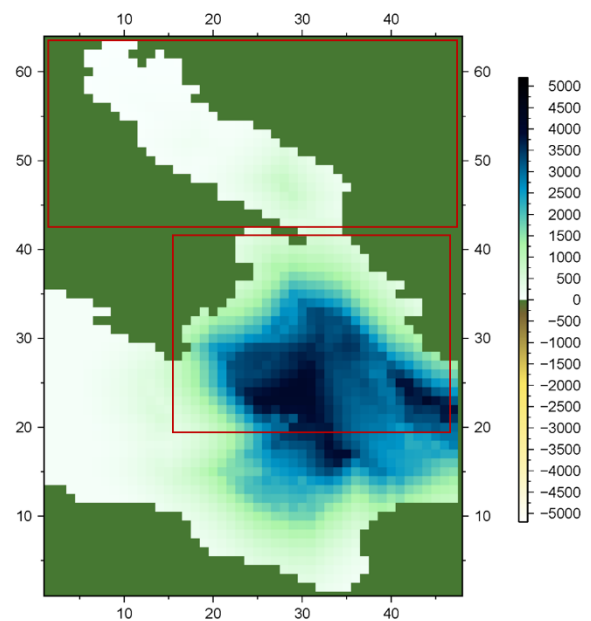
Figure 22: The Adriatic sea region (top box) and the Ionian sea box (bottom box)

(appendix J). In section V_3 a clear difference can be observed between the north and the south of the profile, with the eastward flowing water in the south having a lower salinity and the westward flowing water in the north having a higher salinity. This difference between experiments then disappears in section V_2 where a similar salinity profile as in experiment 2031 can be observed, with the difference being a decrease in overall salinity. The temperature profile at the V_3 cross section corresponds to what is observed in the salinity profile. It ranges from 19.1 to 19.9 °C, just as was the case in experiment 2031. The temperature profile at V_2 shows a slight increase but otherwise remains unchanged. In the case of the horizontal cross section H the temperature profile shows little to no difference while the salinity profile shows an overall decrease in salinity.

3.6 Density vs. deep water flux

To examine the relationship between the density difference between the Adriatic Sea and the Ionian Sea and the deepwater flux, the average density of both regions needs to be calculated. Because density is a function of depth the average density in a deep basin is mostly affected by the depth of such a basin and less by the salinity and temperature of the water. Since the thermohaline circulation is driven by temperature and salinity differences this is a problem. To solve this problem depth is fully ignored and a linear equation of state is used to calculate the density from the average temperature and salinity of the water. This way only temperature and salinity are taken into account and the influence of depth on the density is fully ignored. This was deemed acceptable since the effect of depth induced density variations is not present at the boundary between the two regions as the boundary lies at the same depth for both regions. The two regions can be compared to two directly juxtaposed water masses with calculated average properties. Two regions in experiment 2044 were chosen to calculate the average temperature, salinity and density (Fig. 7). The first consists of the entire Adriatic Sea and the second consists of an Ionian box which represents the region of potential deepwater outflow flowing southward through the strait of Otranto. In the Ionian box no depth limits are set, instead all the grid cells in the region with a northward water velocity component were excluded since only the grid cells with a southward velocity component are relevant for the outflow. This method was checked against an experiment where a depth limit is set for the Ionian box. This depth limit was based on the approximate depth of the border of the southward flowing water which can be determined from the meridional overturning stream function of experiment 2044. The top three sigma layers of the Ionian box were then excluded from the temperature and salinity calculations as to represent this depth limit. The resulting volume average salinity of this Ionian box shows no change compared to the previously defined Ionian box. The volume average temperature shows a slight decline from 18 to 17.8 °C. Finally, the density difference between the Ionian and Adriatic box decreases by about 0.03 kg m^{-3}. Based on these results the Ionian box where grid cells are excluded was deemed appropriate to calculate the density from. Any further mentions of an Ionian box will refer to this type of Ionian box.

The average temperature and salinity and the calculated average density of the two regions over time are displayed in panel K1. For comparison, the average density when depth is taken into account is displayed in figure K2.

To compare the density difference variation with the deepwater flux they were plotted against each other. To remove the high-frequency fluctuations in the deepwater flux the average of a ten year period window was taken. As previously stated, the last 500 years of each experiment can be considered dynamically stable. In practice, this means that 50 ten-year period samples were taken using a moving window to calculate a ten-year average. The resulting deepwater flux graph can be observed in figure L1a. The resulting density overlay can be observed in figure L1b. To better compare the deepwater flux and the density difference the latter was shifted somewhat over time to compensate for the lag between the density fluctuation and the fluctuation of the deepwater flux (Fig. L1c). This difference between the density and the deepwater flux is about

3 months and is believed to be caused by a slower adaption of the deepwater flow to a change in forcing compared to the model density. This data was used to produce a graph which shows the density difference fluctuation versus the deepwater flux fluctuation (Fig. L2). Two trendlines were plotted to approach the most appropriate formulation (Fig. L3a, L3b).

4. Discussion

4.1 Essential forcing factors

From the modelling results, a picture forms of the role each of the forcing factors has on the overturning circulation within the model. When no forcing factors are imposed on a basin with an open boundary through which free flow is allowed within the constraints of a zero horizontal depth-averaged velocity, no significant flow will occur in the system or at the open boundary. However, once net evaporation is imposed onto the system and the horizontal depth-averaged velocity at the open boundary is adjusted to account for water loss due to the net evaporation, a significant overturning circulation develops based on salinity induced density differences in the system. While this system does not yet represent a Mediterranean like circulation, it does produce a clear basis for it. A surface inflow, deep water outflow circulation cell is present in the zonal overturning stream function and a surface inflow, deep water outflow circulation cell connects the Adriatic waters with the Ionian waters of the basin. An important point to note is the existence of a significant in- and out flow through the open boundary. Water flows freely in and out of the system based on density differences at the open boundary, only constrained by the horizontal depth-averaged velocity. The magnitude of this density induced flow is about 1.1 Sv.

When temperature forcing through the implementation of a temperature field is added to the model the circulation patterns somewhat shift, but the two basic circulation systems described within the model remain the same. The main difference between the two cases is that the Adriatic-Ionian circulation cell has become larger and stronger, while the cell at the open boundary has become smaller and weaker. The overall circulation is salinity-, as well as temperature-based and can be considered to represent a Mediterranean like thermohaline flow. The lack of significant change when adding temperature forcing shows that the implementation of net evaporation alone may be enough to simulate a Mediterranean like flow under the right conditions. When a horizontal depth-averaged two-way flow is imposed at the open boundary no significant change is observed in the overturning circulation. As previously mentioned a significant in and outflow (1.1 Sv) is already present at the open boundary through the process of free flow, so the addition of an imposed in and outflow (1.0 Sv) likely only makes a small difference to the resulting total in and outflow (1.2 Sv) observed. The relation between the imposed depth-averaged flow velocity, the density at the open boundary, and the resulting in and outflow at the open boundary may be examined in future research. Surprisingly, the imposed shape of the area of in and outflow along the open boundary also has little effect on the system. While a clear distinction between the streams of in and outflowing water can be observed one grid cell east of the open boundary, this distinction disappears almost completely within the following ten grid cells.

4.2 Seasonal atmospheric temperature variation

The addition of a seasonal variation of the temperature field causes a dip in terms of the yearly average temperature, going from a volume average of 18.7 to 18 °C. This is likely caused by the reduction in temperature banding of the sea surface in the latitudal direction. Where first a constant atmospheric temperature field was present the new field now shifts causing the sea surface temperature to be more spread out. This reduction of temperature banding reduces the effect of the sea surface temperature on deeper parts of the ocean, thus also reducing the volume average temperature. This causes a more depth-dependent ocean temperature field to form in the system. The seasonal temperature variation has little effect on the yearly average salinity of the system, only lowering it by a small margin (0.1

ppt). This decrease in salinity is small compared to the decrease in temperature, causing the average yearly density of the system to go down as well. The overturning circulation pattern in both the zonal direction and the meridional direction remains largely the same on a yearly average. The main difference is the intensity of the flow. This is likely caused by a reduced lateral temperature variation, but further research into the specific dynamics of the intensity of the deepwater flux is needed.

4.3 Geostrophic currents

Since a sea surface elevation map of the region is produced for each experiment a link with the sea surface particle trace map and the barotropic stream function can be made. A clockwise 90° rotation of the flow between high and low surfacemelevation is expected due to the Coriolis effect, and due to the fact that the Mediterranean is located in the northern hemisphere. When combining the data from the surface elevation map with the barotropic stream function this effect can be observed. An area of positive sea surface deviation exists in the south of the Ionian Sea creating an area of high pressure. This area corresponds to a clockwise flowing circulation cell created by the flow of water from this area of high pressure to an area of low pressure and rotated clockwise by the Coriolis effect. The surface flow in the model region cannot be fully explained through geostrophic currents since the flow is also effected by the model geography, the location of the open boundary and the underlying thermohaline currents.

4.4 Density difference versus deep water flux

The implementation of a seasonal temperature variation produced a relatively constant fluctuation in density difference between the Adriatic Sea and the Ionian box (fig. L1b). The deepwater flux shows a similar fluctuation, but it is much more irregular (fig. L1a). This irregularity, especially at the high frequencies, can be explained by existing background fluctuations in the deepwater flux. These fluctuations can be observed in the reference experiment (panel A1.1), which is a system with no forcing factors present. They are caused by small instabilities in the system present at the open boundary which in turn

has a small scale effect on the model region. These fluctuations are mostly lost in the averaging of the deepwater flux. When the ten-year period average of the deepwater flux is plotted against this graph a linear relation can be observed. This was confirmed by the trendline plotted through the deep water flux versus density graph. This result confirms that a relation exists between deepwater flow from a marginal to a deep water basin, and the corresponding density difference between these two basins. However, only a small variation of density difference between the Adriatic Sea and Ionian box is observed in the model. This means that the data points occupy a relatively small range of density variation. Because of this small range, no definite conclusion can be made about the most appropriate formulation for the relation between the density difference and the deepwater flux. When the simplest case of a linear relationship is considered the following formulation is found:

$$y = 3.46x + 1.93 \qquad (Eq. 2)$$

Where y is the deepwater flux in Sv and x is the difference in density in kg/m^3. The value of 3.46 can be considered a constant expressed in x 10^6 m^6/kg s and the value of 1.9307 can be considered a background value expressed in x 10^6 m^3/s. The corresponding coefficient of determination R^2 is 0.96, which shows a good data point fit. However, when a case is considered where the density difference is close to zero, the formulation will not hold. Considering this, a different formulation might provide better representation. When a power-law relation is considered a better fit ($R^2 = 0.97$) is found, admittedly only by a small margin. The associated formulation reads:

$$y = 5.17x^{0.48} \qquad (Eq. 3)$$

In this case, when a density difference of zero is considered, this will correspond to a deep water flux of zero as well, making it a better overall fit for the model. Despite this, a larger data range will still be needed to find a more definitive formulation for the relation between density and deep water flux. This could be achieved by a change in the forcing

conditions of the Adriatic Sea and the Ionian box. Examples include the implementation of a higher temperature variation in the north or a lower temperature variation in the south, and the implementation of a seasonal varying net evaporation rate.

4.5 Box model comparison

The 2019 paper "The mechanism of sapropel formation in the Mediterranean Sea: Insight from long-duration box-model experiments" by Dirksen and Meijer was chosen as a reference paper to assert if the comprehensive model supports the assumptions made in comparable box models. In this paper the magnitude of the vertical downward flux D_1 between the shallow margins (Box 1) and the deep Mediterranean (Box 3) is dependent on the oceanographic conditions at each time step. This relation was implemented by imposing a linear relationship between the density difference and the magnitude of the flux (D_1) via the following formulation:

$$D1 = max(0, c13 \cdot (\rho1 - \rho3))$$

Where $(\rho1 - \rho3)$ is the density difference between the two boxes and c13 is a efficiency constant which value was based on the occurrence of a realistic deep water flux at a present-day density difference (Dirksen & Meijer, 2019). A value of 1×10^6 m^6 kg^{-1} s^{-1} is used for the efficiency constant (c13). The data points of the comprehensive model showing the relations between deep water flux and density difference can be used to find a comparable value for c13. When a line is plotted from the origin through the data points, a c13 value of about 5.5×10^6 m^6 kg^{-1} s^{-1} is found. This shows a possible underestimation of the deepwater flow within the compared box model. However, since only density data points within the 0.3 to 0.8 kg/m^3 range were used in the comprehensive model the accuracy of this assumption could be debated.

5. Conclusion

A POM implementation was used to further the understanding of the relation between a number of forcing factors imposed on the system and the deep water flux. It was asserted that no deep water flux forms within a system with zero forcing and an open boundary. Once net evaporation is added to the system a significant overturning circulation develops, which provide a basis for a Mediterranean like circulation. The addition of a temperature field causes a shift in the circulation pattern and the observed circulation can be considered a Mediterranean like thermohaline flow. Any additional forcing factors show only small changes in this circulation pattern. The addition of a seasonal temperature variation has a dampening effect on the circulation, while the addition of a two-way flow at the open boundary has little to no effect. The variation in density difference between the marginal and depth basin was compared to the deep water flux and quantification was attempted. A linear relation was considered but seemed inaccurate for lower density values close to zero. Instead, a power-law relation was found to be the best fit since it also proved accurate at a zero-density difference. No definite conclusion was made about the most appropriate formulation since the data points used only spanned a small range in density variations. The results were compared to a comparable box model which showed a possible underestimation of the deepwater flow between the boxes used in the model. Further research using a wider data range was proposed to acquire a more definitive formulation for the relation between the density difference variation and the deep water flow.

References

1. Alhammoud, B., Meijer, P. T., & Dijkstra, H. A. (2010). Sensitivity of Mediterranean thermohaline circulation to gateway depth: A model investigation. Paleoceanography, 25(2).

2. Blumberg, A. F., & Mellor, G. L. (1987). A description of a three-dimensional coastal ocean circulation model. Three-dimensional coastal ocean models, 4, 1-16.

3. Courant, R., Friedrichs, K., & Lewy, H. (1928). Über die partiellen Differenzengleichungen der mathematischen Physik. Mathematische annalen, 100(1), 32-74.

4. Dirksen, J. P., & Meijer, P. T. (2019). The mechanism of sapropel formation in the Mediterranean Sea: Insight from long duration box-model experiments.

5. Drakopoulos, P. G., & Lascaratos, A. (1999). Modelling the Mediterranean Sea: climatological forcing. Journal of Marine Systems, 20(1-4), 157-173.

6. Ezer, T., Arango, H., & Shchepetkin, A. F. (2002). Developments in terrain-following ocean models: intercomparisons of numerical aspects. Ocean Modelling, 4(3-4), 249-267.

7. Fundació de la Comunitat Valenciana Centro d'Estudis Ambientals del Mediterrani, 2019. *Available on the world wide web on 24/02/2020: http://ceam.es/ceamet/SST/index.html*

8. *Haines, K., & Wu, P. L. (1995). A modelling study of the thermohaline circulation of the Mediterranean Sea: water formation and dispersal. Oceanologica Acta, 18(4), 401-417.*

9. Karami, M. P., De Leeuw, A., Krijgsman, W., Meijer, P. T., & Wortel, M. J. R. (2011). The role of gateways in the evolution of temperature and salinity of semi-enclosed basins: An oceanic box model for the Miocene Mediterranean Sea and Paratethys. Global and Planetary Change, 79(1-2), 73-88.

10. Manzella, G. M., Gasparini, G. P., & Astraldi, M. (1988). Water exchange between the eastern and western Mediterranean through the Strait of Sicily. Deep Sea Research Part A. Oceanographic Research Papers, 35(6), 1021-1035.

11. *Marshall, J., & Schott, F. (1999). Open-ocean convection: Observations, theory, and models. Reviews of Geophysics, 37(1), 1-64.*

12. *Mellor, G. L. (1991). An equation of state for numerical models of oceans and estuaries. Journal of Atmospheric and Oceanic Technology, 8(4), 609-611.*

13. Mellor, G. L. (2002). User Guide for a Three-Dimensional, Primitive Equation, Numerical Ocean Model (Okt/2002 Version), 42 pp. Atmos. & Oceanic Sci. Prog., Princeton Univ. NJ, USA.

14. Myers, P. G., Haines, K., & Josey, S. (1998). On the importance of the choice of wind stress forcing to the modeling of the Mediterranean Sea circulation. Journal of Geophysical Research: Oceans, 103(C8), 15729-15749.

15. National Centers for Environmental Information, 2019. *Available on the world wide web on 24/02/2020: https://www.ncei.noaa.gov/*

16. Paklar, G. B., Isakov, V., Koračin, D., Kourafalou, V., & Orlić, M. (2001). A case study of bora-driven flow and density changes on the Adriatic shelf (January 1987). Continental Shelf Research, 21(16-17), 1751-1783.

17. Phillips, N. A. (1957). A coordinate system having some special advantages for numerical forecasting. Journal of Meteorology, 14(2), 184-185.

18. *Roether, W., Manca, B. B., Klein, B., Bregant, D., Georgopoulos, D., Beitzel, V., ... & Luchetta, A. (1996). Recent changes in eastern Mediterranean deep waters. Science, 271(5247), 333-335.*

19. Winton, M., & Sarachik, E. S. (1993). Thermohaline oscillations induced by strong steady salinity forcing of ocean general circulation models. Journal of Physical Oceanography, 23(7), 1389-1410.
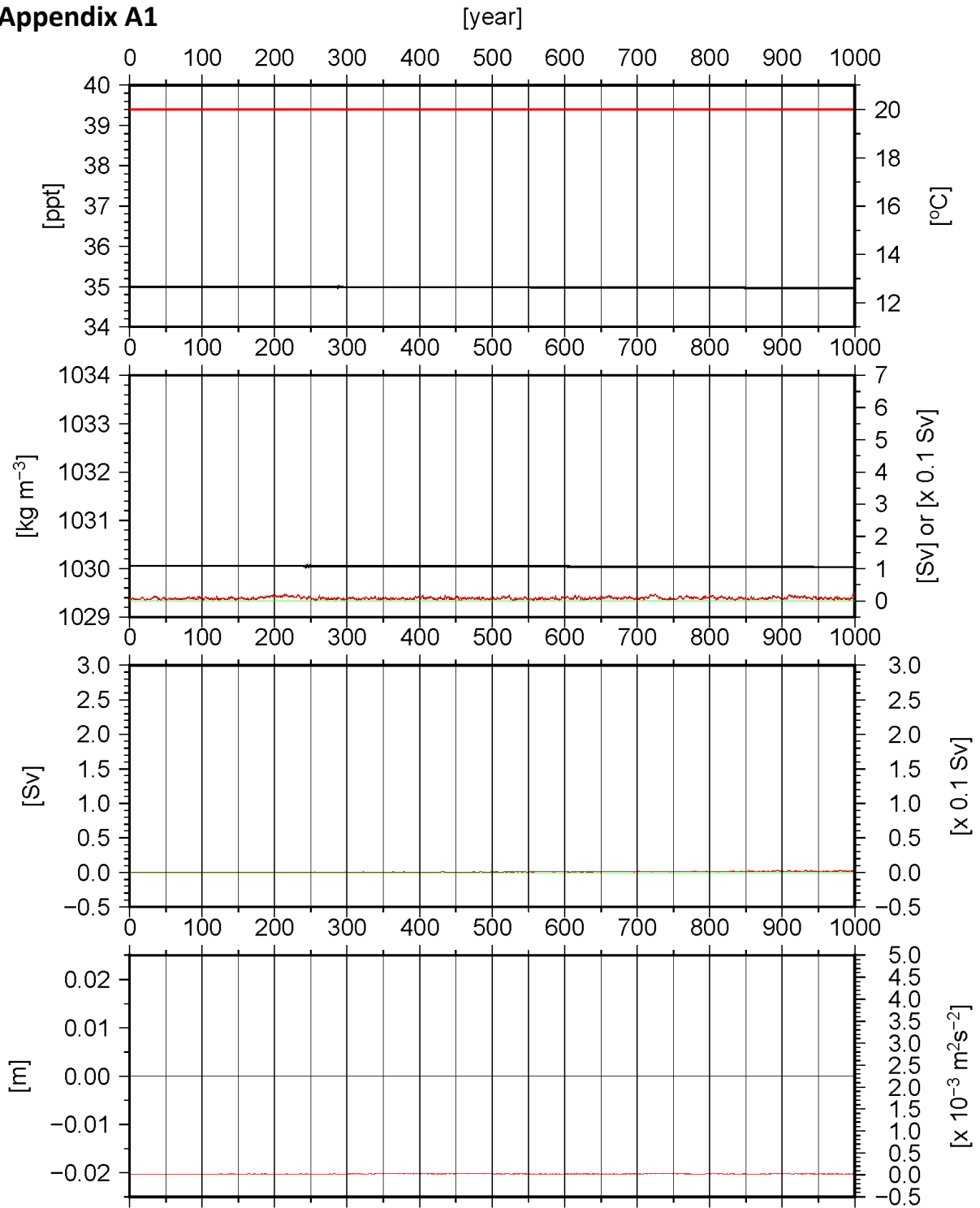
Panel A1.1: Volume average salinity [ppt] (black) (1st image), temperature [°C] (red) (1st image), density [kg m-3] (black) (2nd image) and the mean kinetic energy [10-3 m2 s-2] (red) (4th image). Northward and southward (red) [Sv] and net (green) [0.1 Sv] flow of the strait of Otranto (2nd image). Eastward and westward (red) [Sv] and net (green) [0.1 Sv] flow of the strait of Sicily (3rd image). Average surface elevation [m] (black) (4th image). All data is recorded over the 1000 year run time of experiment 2060.
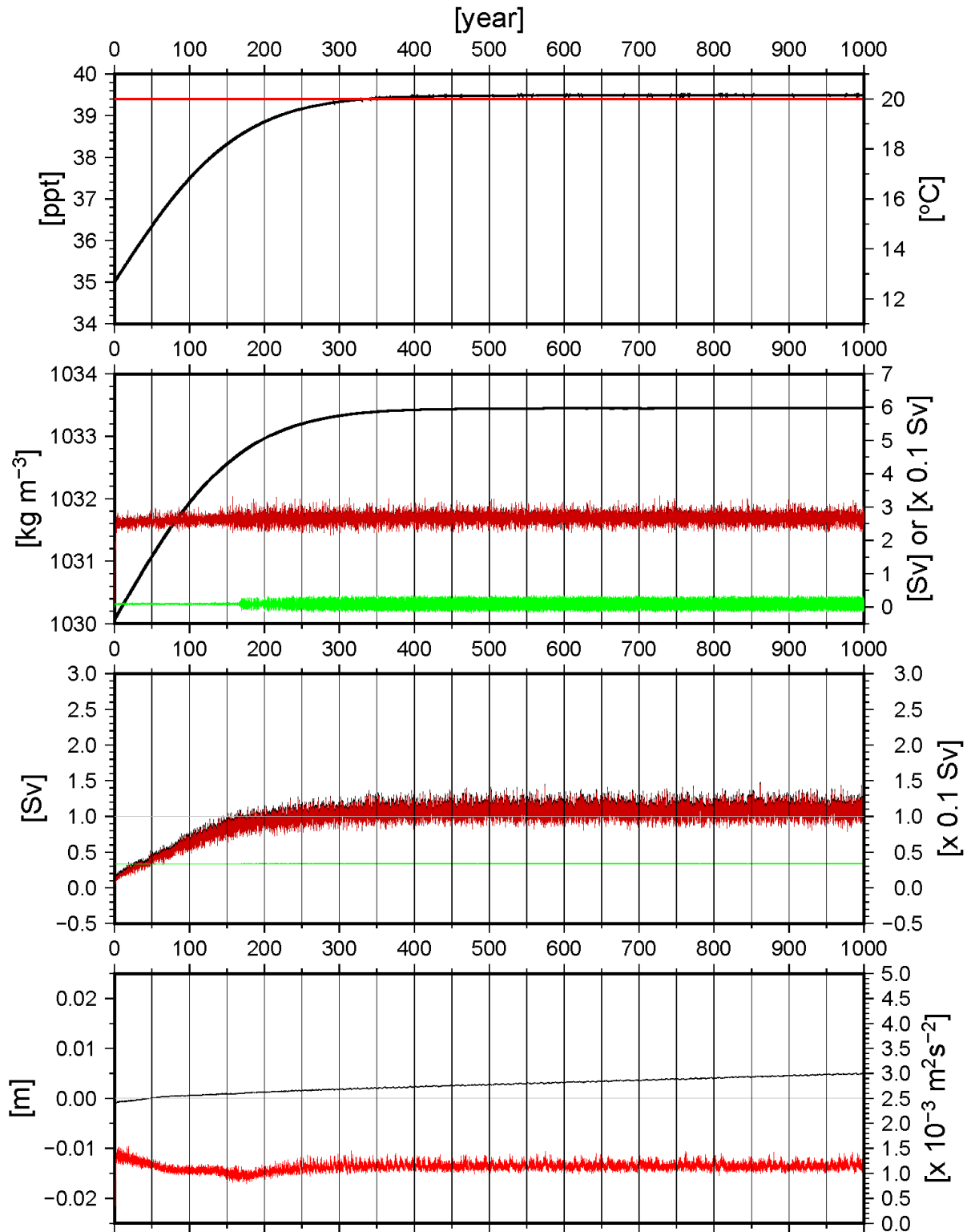
Panel A1.2: Volume average salinity [ppt] (black) (1st image), temperature [°C] (red) (1st image), density [kg m-3] (black) (2nd image) and the mean kinetic energy [10-3 m2 s-2] (red) (4th image). Northward (black) [Sv], southward (red) [Sv] and net (green) [0.1 Sv] flow of the strait of Otranto (2nd image). Eastward (black) [Sv], westward (red) [Sv] and net (green) [0.1 Sv] flow of the strait of Sicily (3rd image). Average surface elevation [m] (black) (4th image). All data is recorded over the 1000 year run time of experiment 2020.
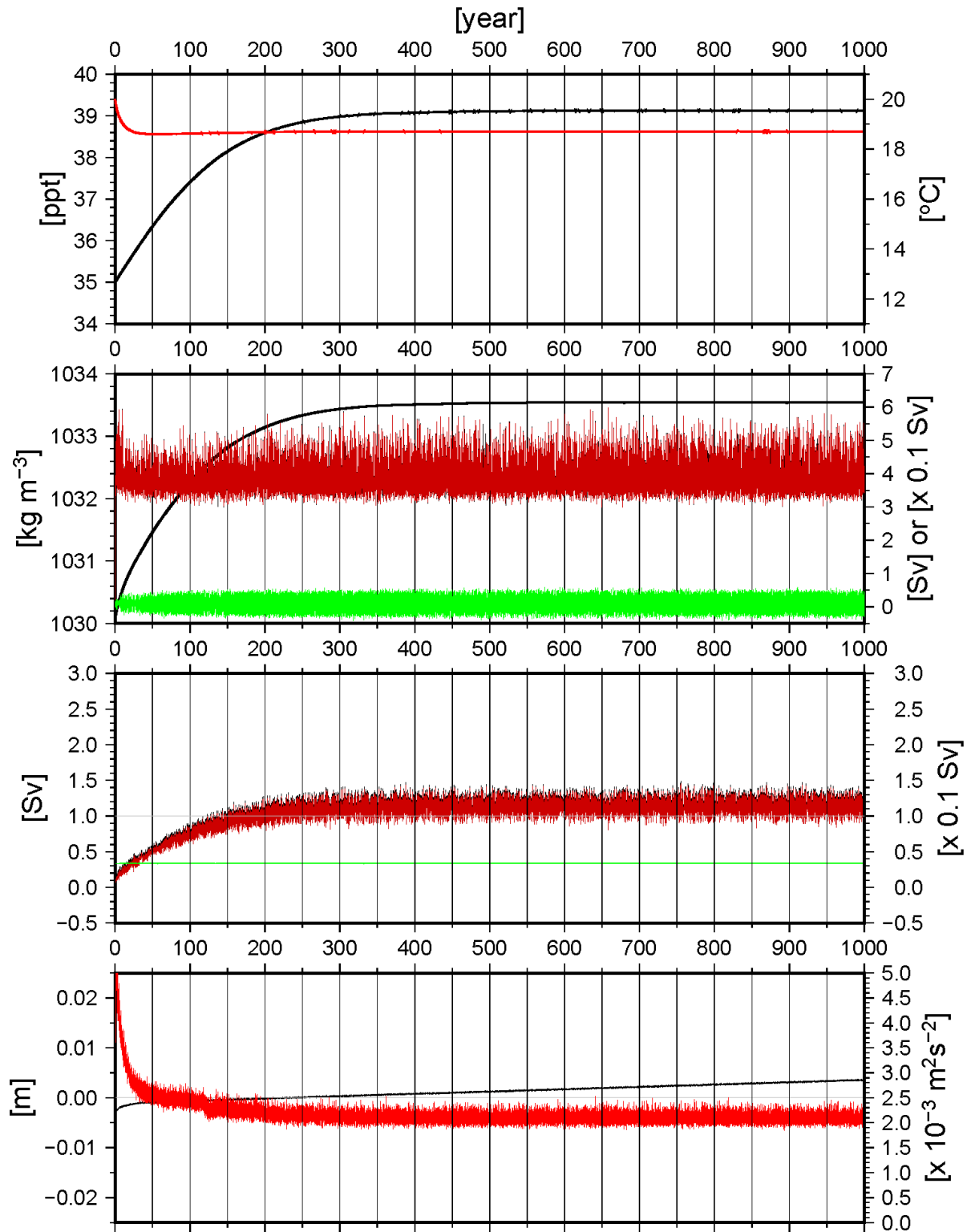
Panel A1.3: Volume average salinity [ppt] (black) (1st image), temperature [°C] (red) (1st image), density [kg m-3] (black) (2nd image) and the mean kinetic energy [10-3 m2 s-2] (red) (4th image). Northward (black) [Sv], southward (red) [Sv] and net (green) [0.1 Sv] flow of the strait of Otranto (2nd image). Eastward (black) [Sv], westward (red) [Sv] and net (green) [0.1 Sv] flow of the strait of Sicily (3rd image). Average surface elevation [m] (black) (4th image). All data is recorded over the 1000 year run time of experiment 2041.
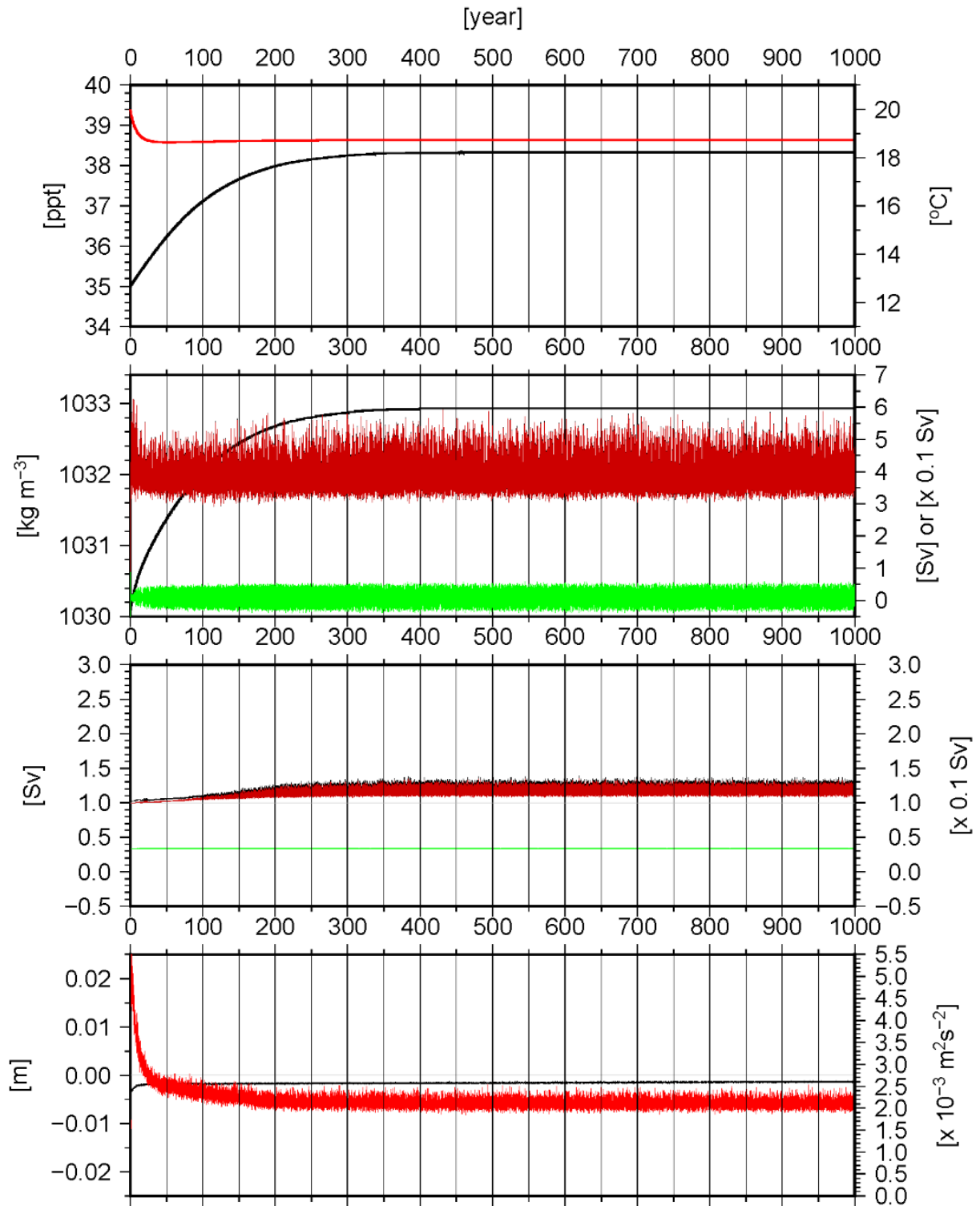
Panel A1.4: Volume average salinity [ppt] (black) (1st image), temperature [°C] (red) (1st image), density [kg m-3] (black) (2nd image) and the mean kinetic energy [10-3 m2 s-2] (red) (4th image). Northward (black) [Sv], southward (red) [Sv] and net (green) [0.1 Sv] flow of the strait of Otranto (2nd image). Eastward (black) [Sv], westward (red) [Sv] and net (green) [0.1 Sv] flow of the strait of Sicily (3rd image). Average surface elevation [m] (black) (4th image). All data is recorded over the 1000 year run time of experiment 2042
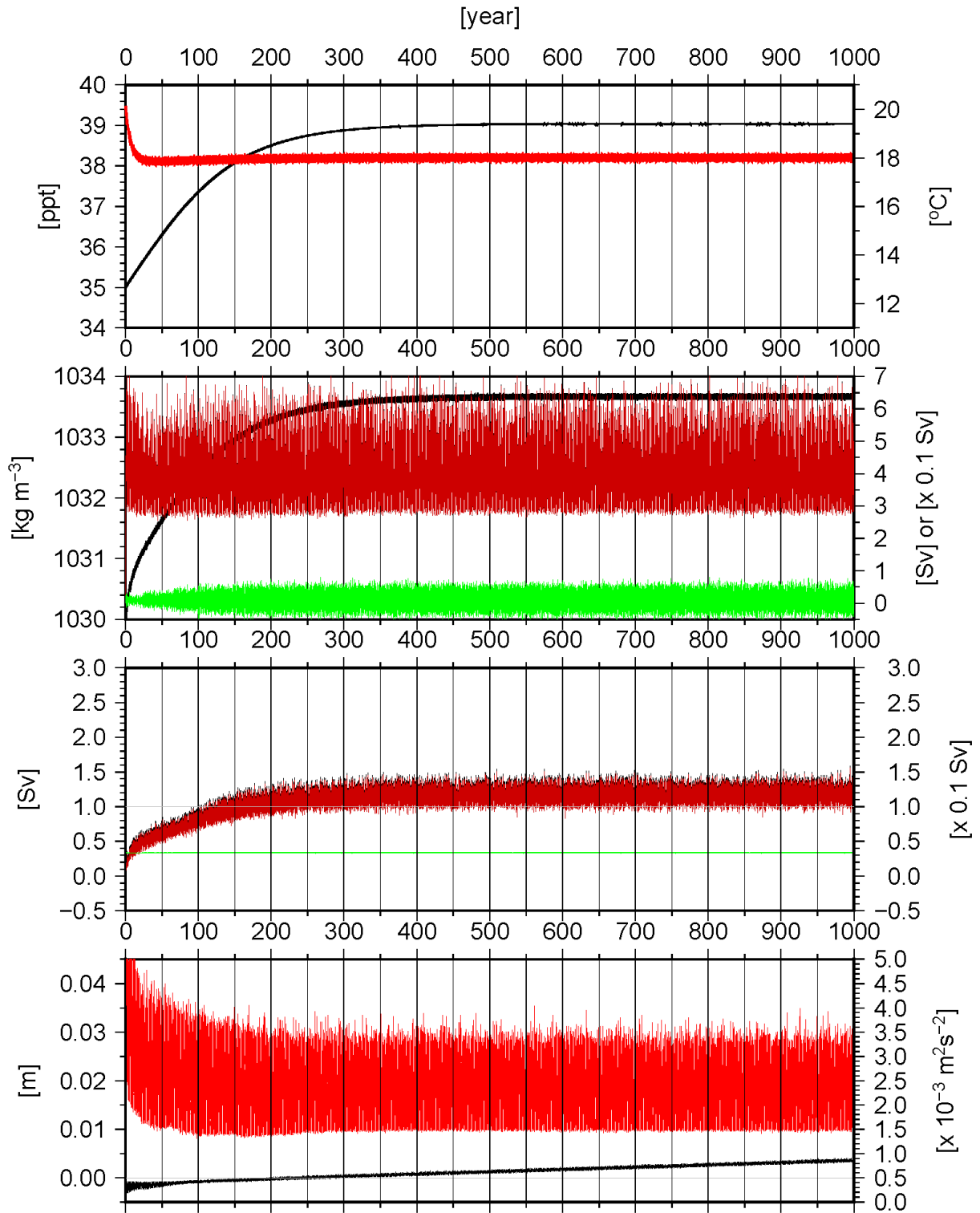
Panel A1.5: Volume average salinity [ppt] (black) (1st image), temperature [°C] (red) (1st image), density [kg m⁻³] (black) (2nd image) and the mean kinetic energy [10⁻³ m² s⁻²] (red) (4th image). Northward (black) [Sv], southward (red) [Sv] and net (green) [0.1 Sv] flow of the strait of Otranto (2nd image). Eastward (black) [Sv], westward (red) [Sv] and net (green) [0.1 Sv] flow of the strait of Sicily (3rd image). Average surface elevation [m] (black) (4th image). All data is recorded over the 1000 year run time of experiment 2031.
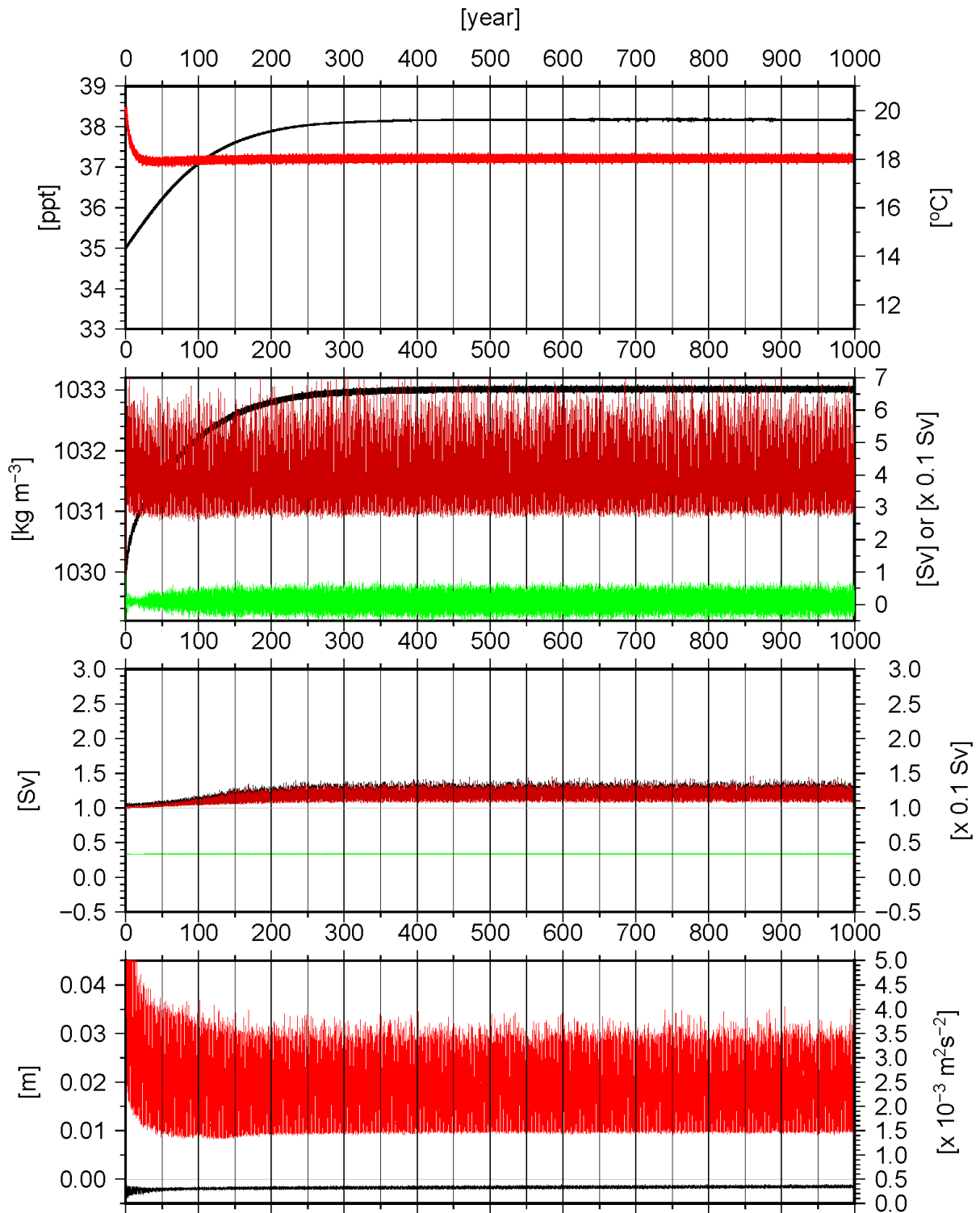
Panel A1.6: Volume average salinity [ppt] (black) (1st image), temperature [°C] (red) (1st image), density [kg m-3] (black) (2nd image) and the mean kinetic energy [10-3 m2 s-2] (red) (4th image). Northward (black) [Sv], southward (red) [Sv] and net (green) [0.1 Sv] flow of the strait of Otranto (2nd image). Eastward (black) [Sv], westward (red) [Sv] and net (green) [0.1 Sv] flow of the strait of Sicily (3rd image). Average surface elevation [m] (black) (4th image). All data is recorded over the 1000 year run time of experiment 2044.
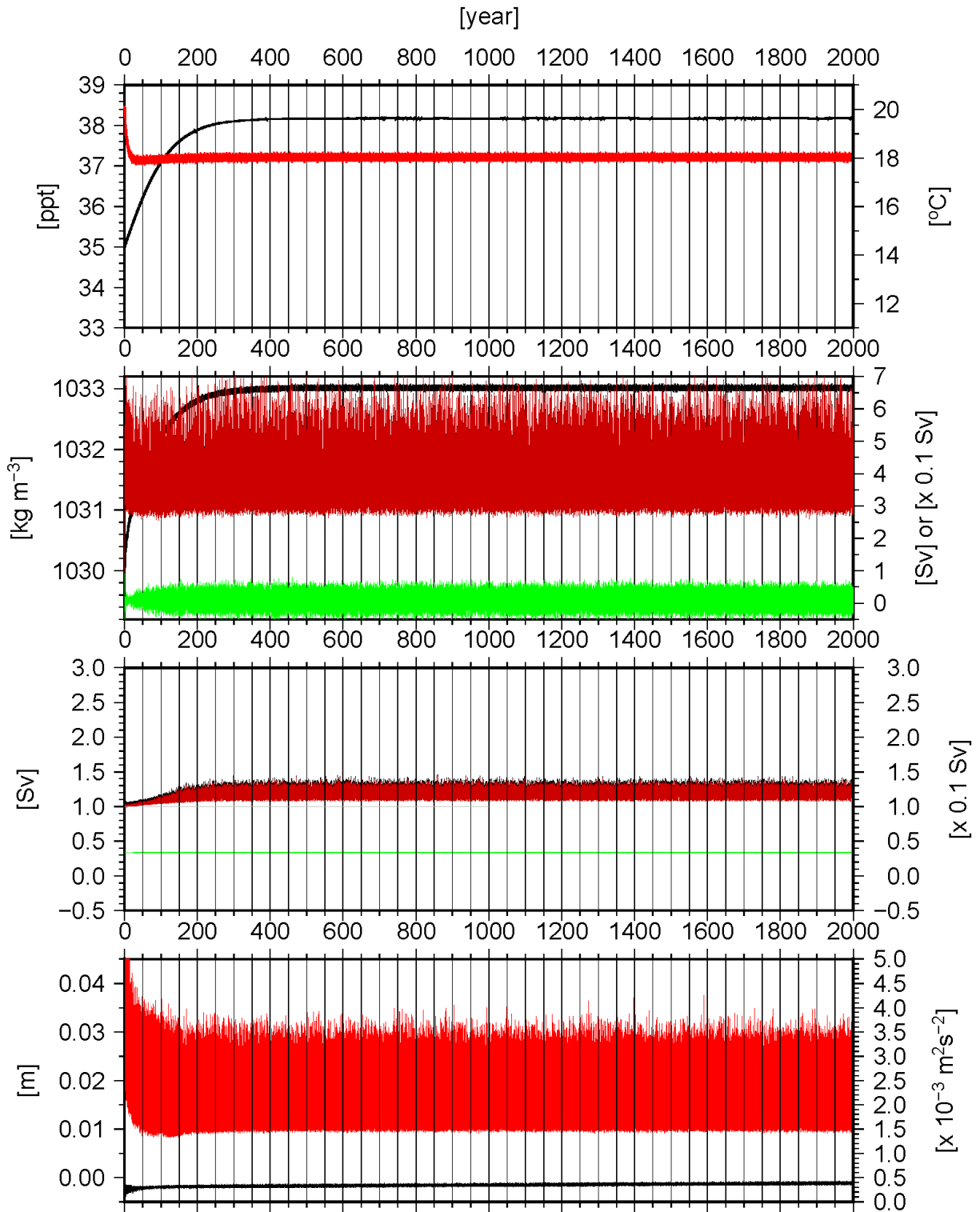
Panel A1.7: Volume average salinity [ppt] (black) (1st image), temperature [°C] (red) (1st image), density [kg m-3] (black) (2nd image) and the mean kinetic energy [10-3 m2 s-2] (red) (4th image). Northward (black) [Sv], southward (red) [Sv] and net (green) [0.1 Sv] flow of the strait of Otranto (2nd image). Eastward (black) [Sv], westward (red) [Sv] and net (green) [0.1 Sv] flow of the strait of Sicily (3rd image). Average surface elevation [m] (black) (4th image). All data is recorded over the 2000 year run time of experiment 2050.
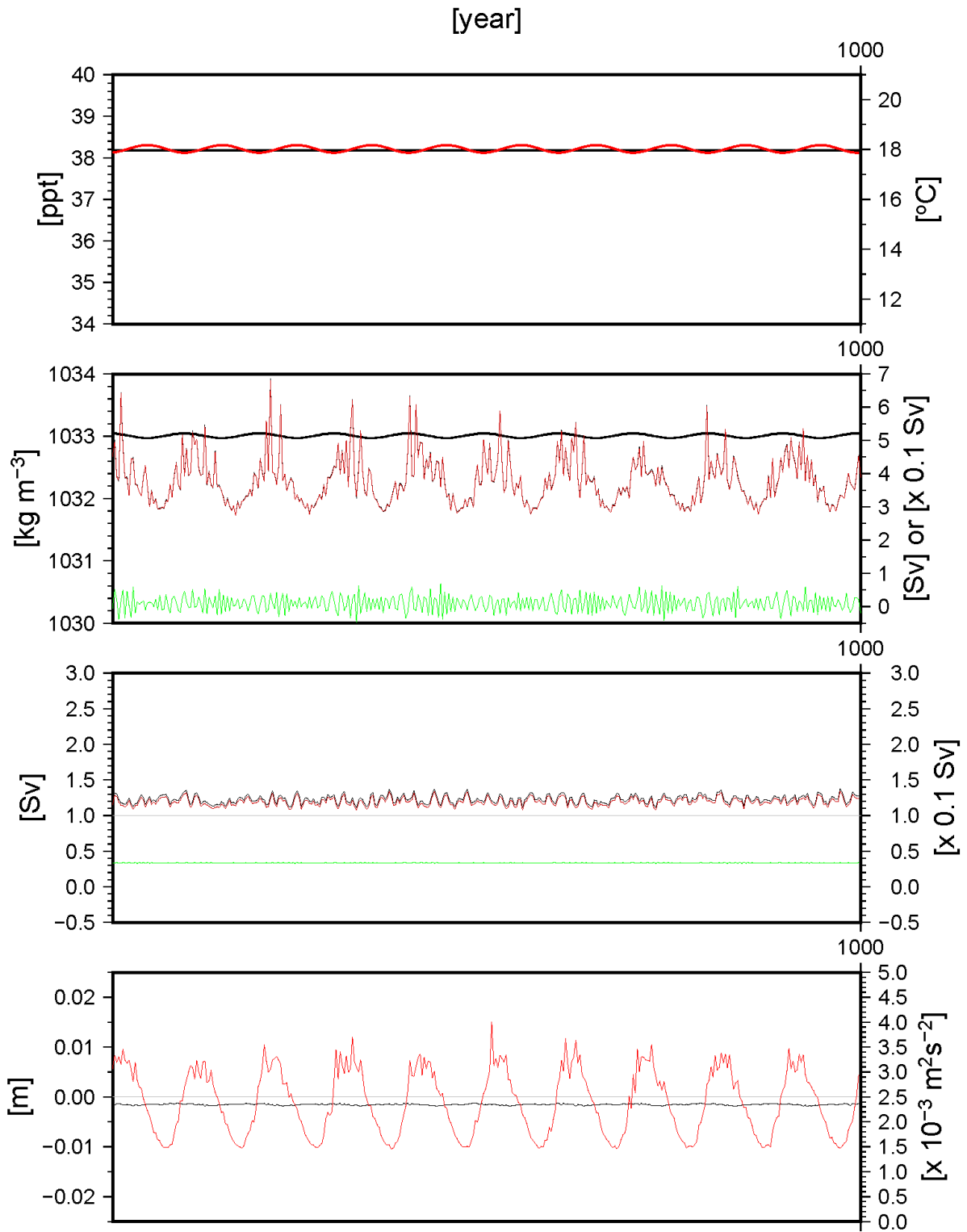
Panel A2.1: Volume average salinity [ppt] (black) (1st image), temperature [°C] (red) (1st image), density [kg m-3] (black) (2nd image) and the mean kinetic energy [10-3 m2 s-2] (red) (4th image). Northward and southward (red) [Sv] and net (green) [0.1 Sv] flow of the strait of Otranto (2nd image). Eastward and westward (red) [Sv] and net (green) [0.1 Sv] flow of the strait of Sicily (3rd image). Average surface elevation [m] (black) (4th image). All data was recorded over the last 10 years of experiment 2044.
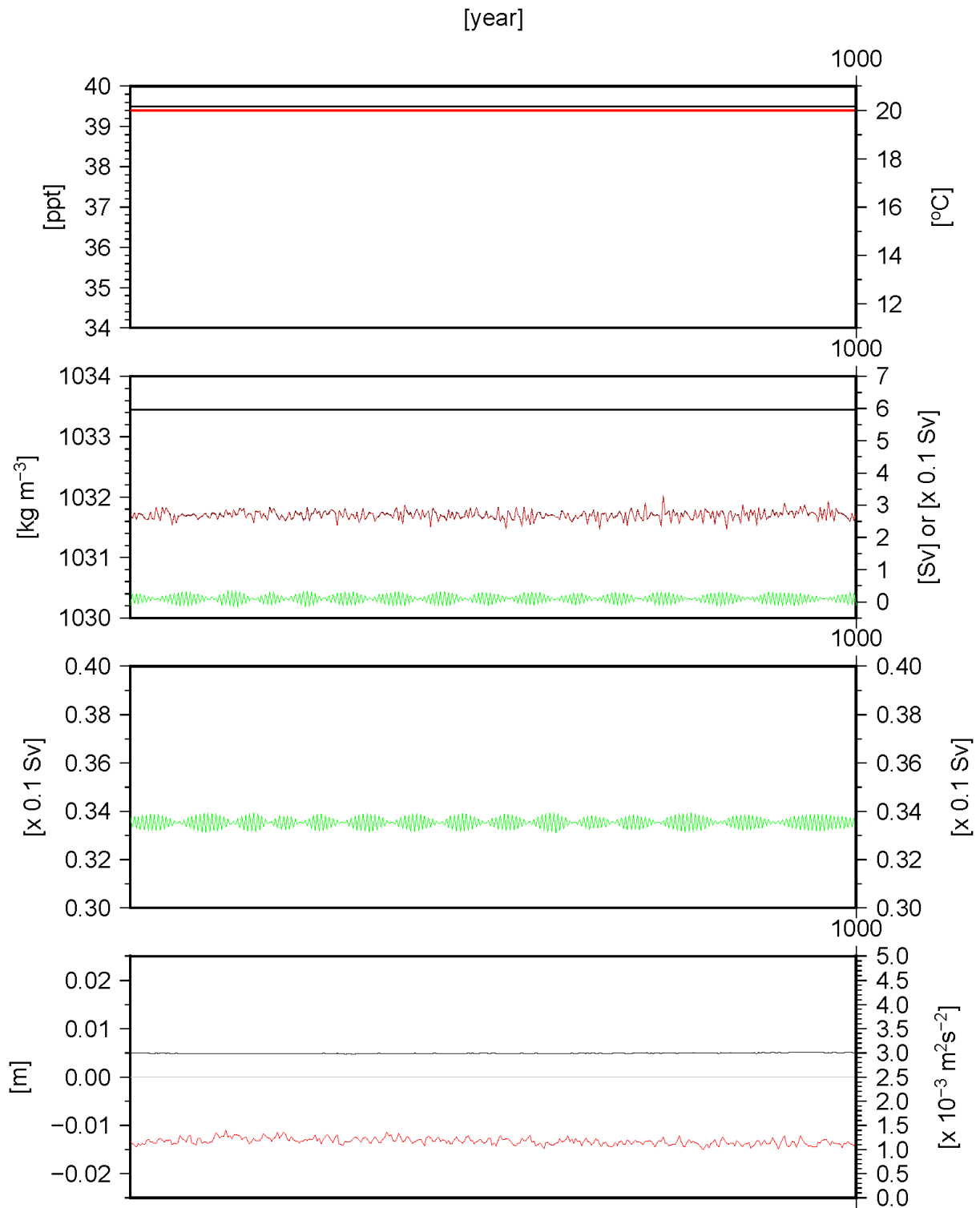
Panel A2.2: Volume average salinity [ppt] (black) (1st image), temperature [°C] (red) (1st image), density [kg m-3] (black) (2nd image) and the mean kinetic energy [10-3 m2 s-2] (red) (4th image). Northward and southward (red) [Sv] and net (green) [0.1 Sv] flow of the strait of Otranto (2nd image). Eastward and westward (red) [Sv] and net (green) [0.1 Sv] flow of the strait of Sicily (3rd image). Average surface elevation [m] (black) (4th image). All data was recorded over the last 10 years of experiment 2020.
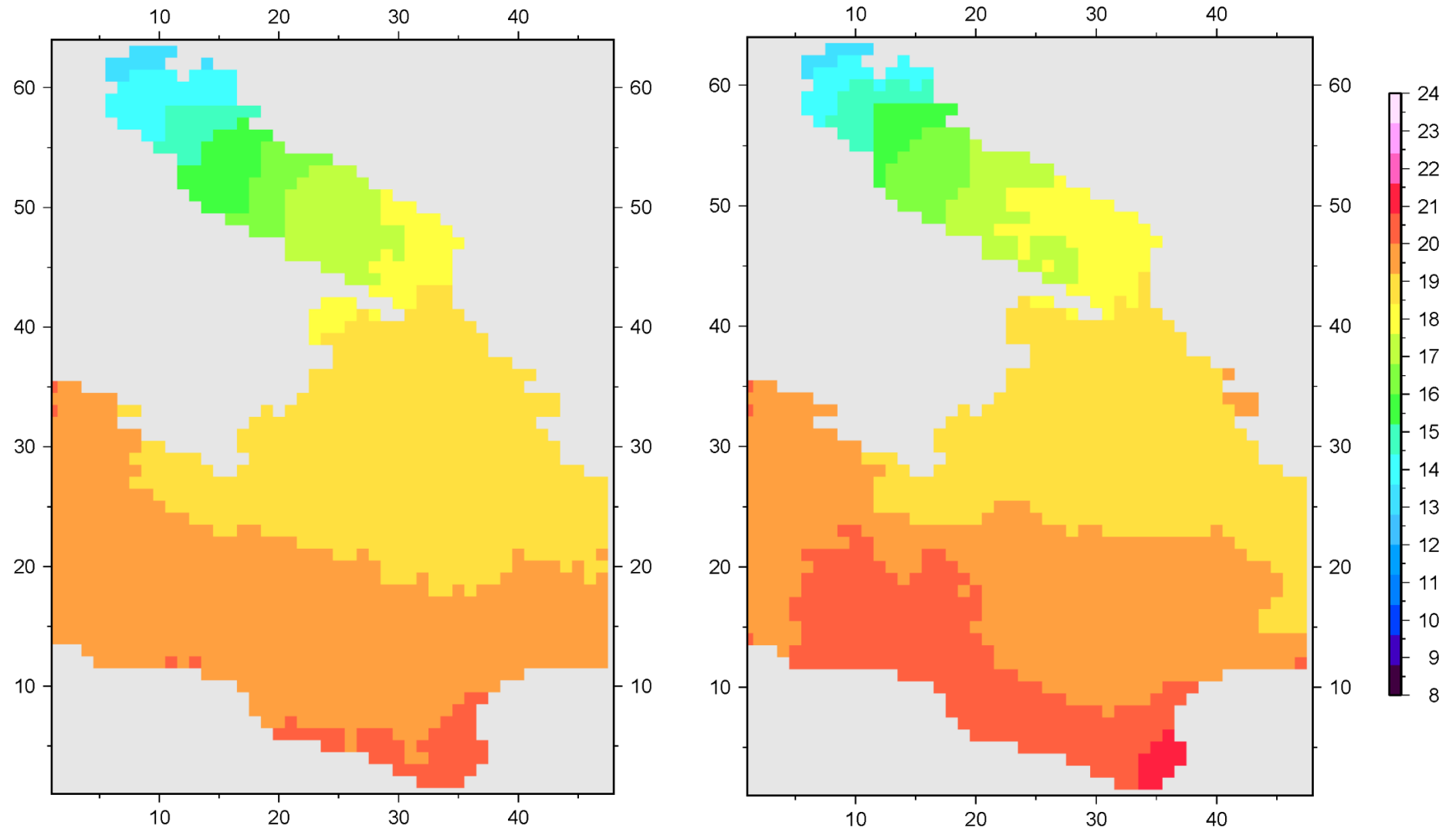
Panel B1: Surface temperature in °C of exp. 2041 (left) and exp. 2031 (right)
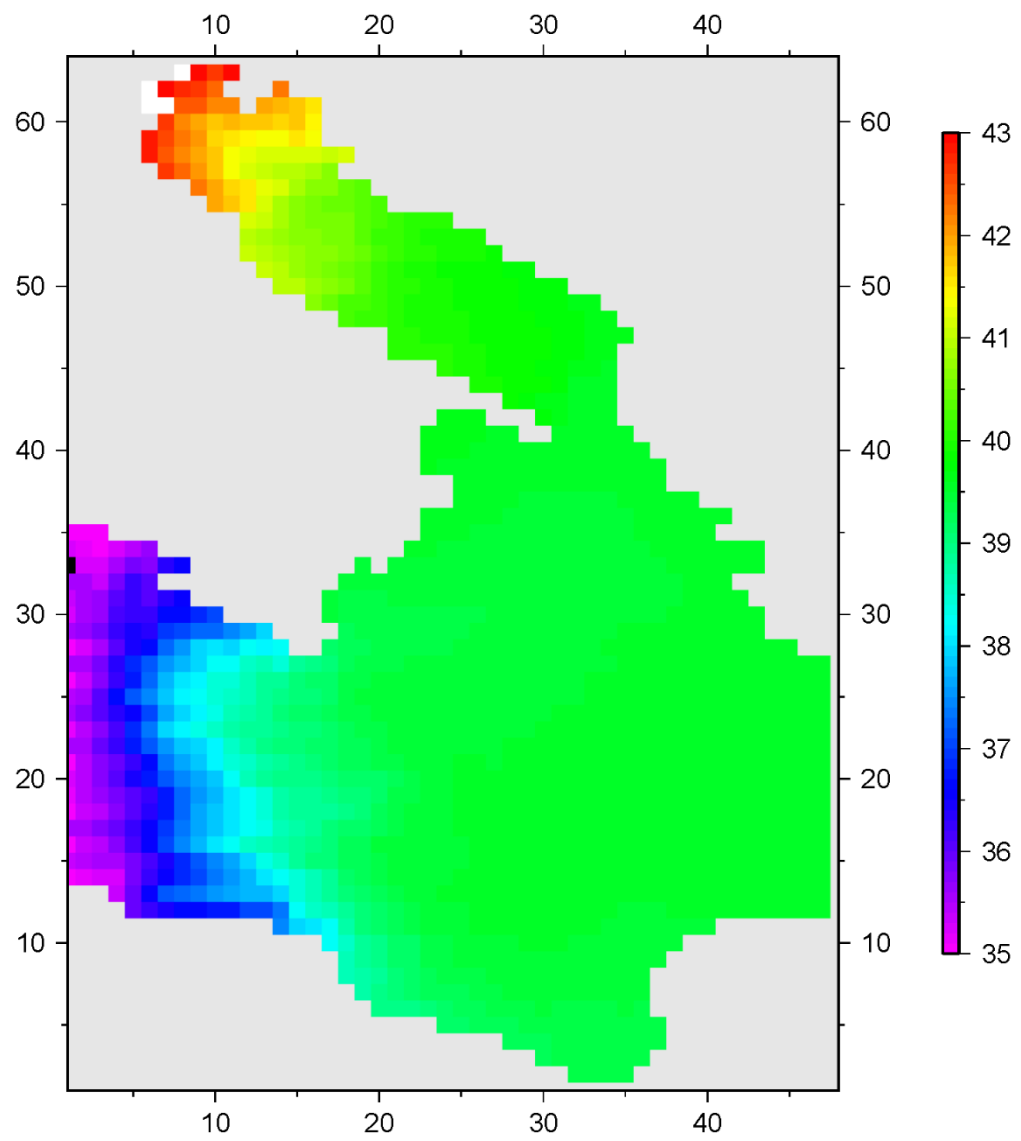
Figure B2: Surface salinity in psu of exp. 2020
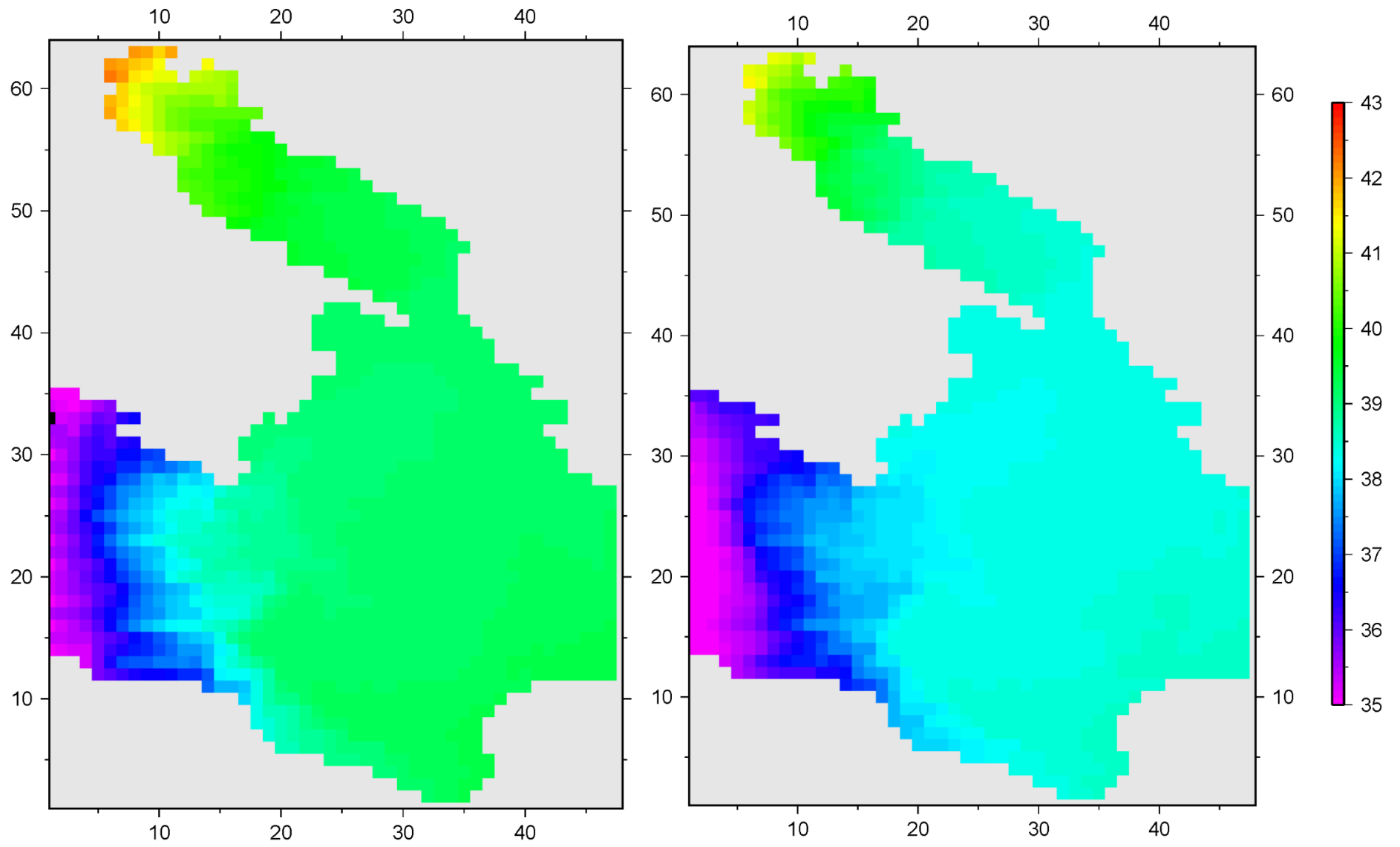
Panel B3: Surface salinity in psu of exp. 2041 (left) and exp. 2042 (right)
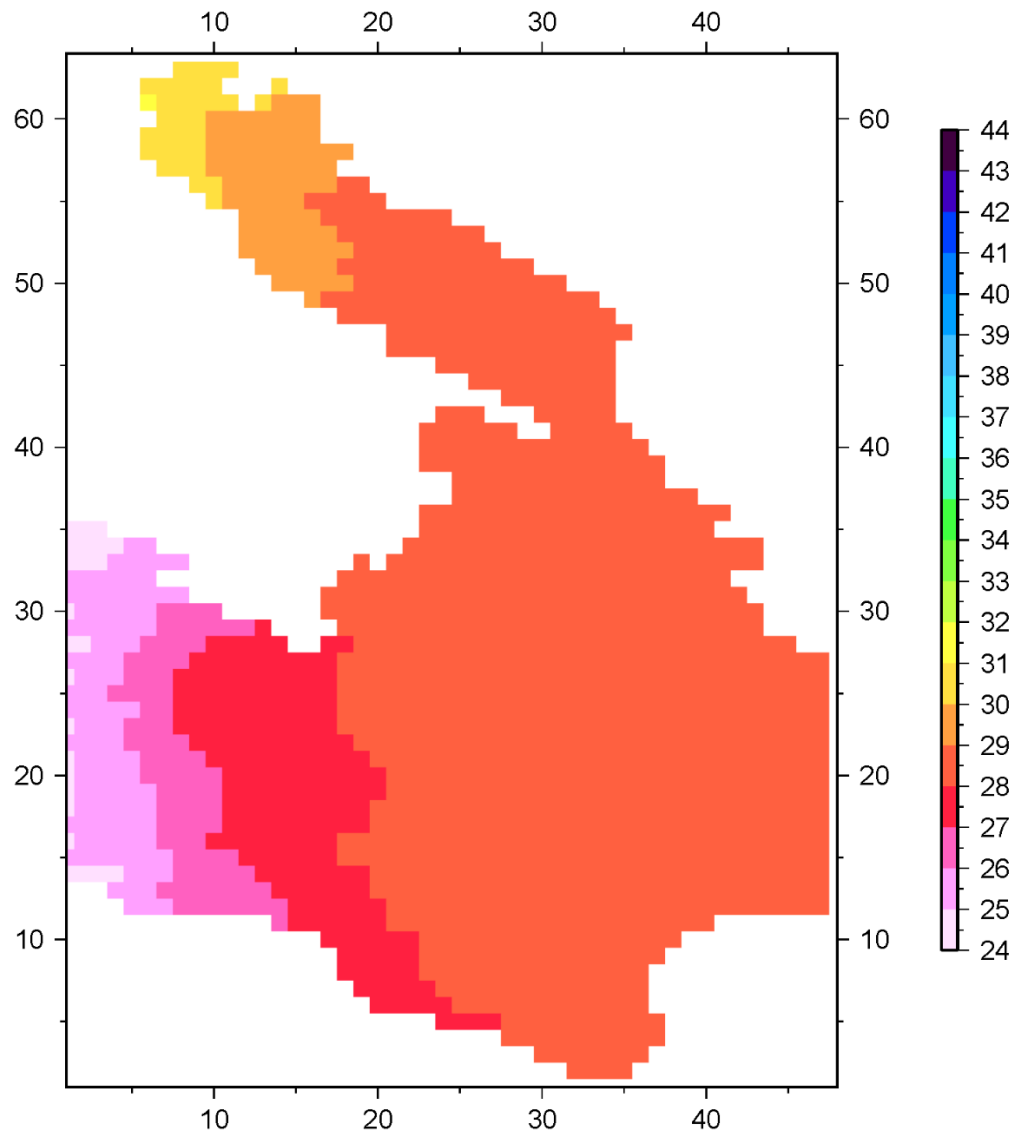
Figure B4: Surface density (ρ-1000) in kg/m³ of exp. 2020
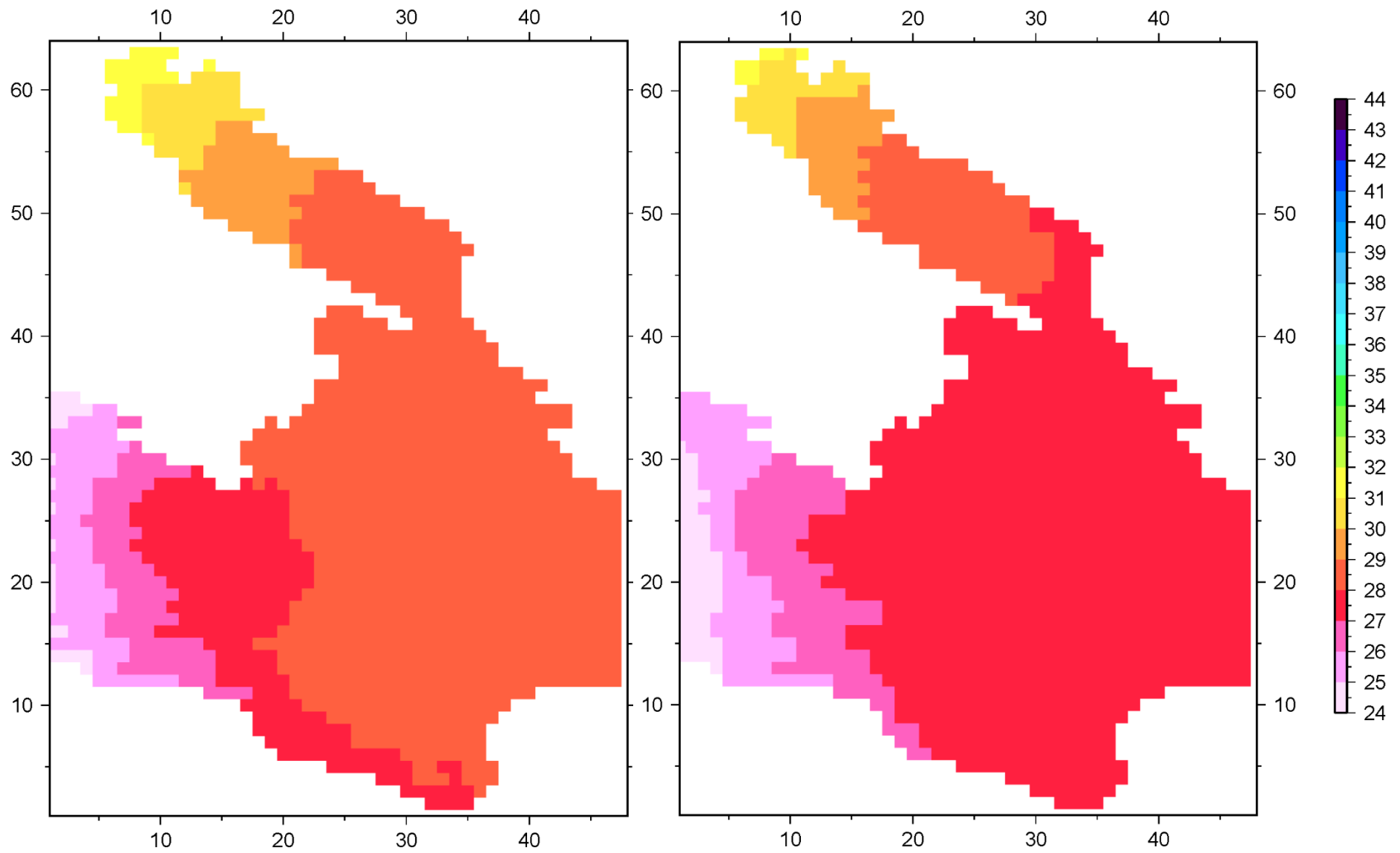
Panel B5: Surface density (ρ-1000) in kg/m³ of exp. 2041 (left) and exp. 2042 (right)
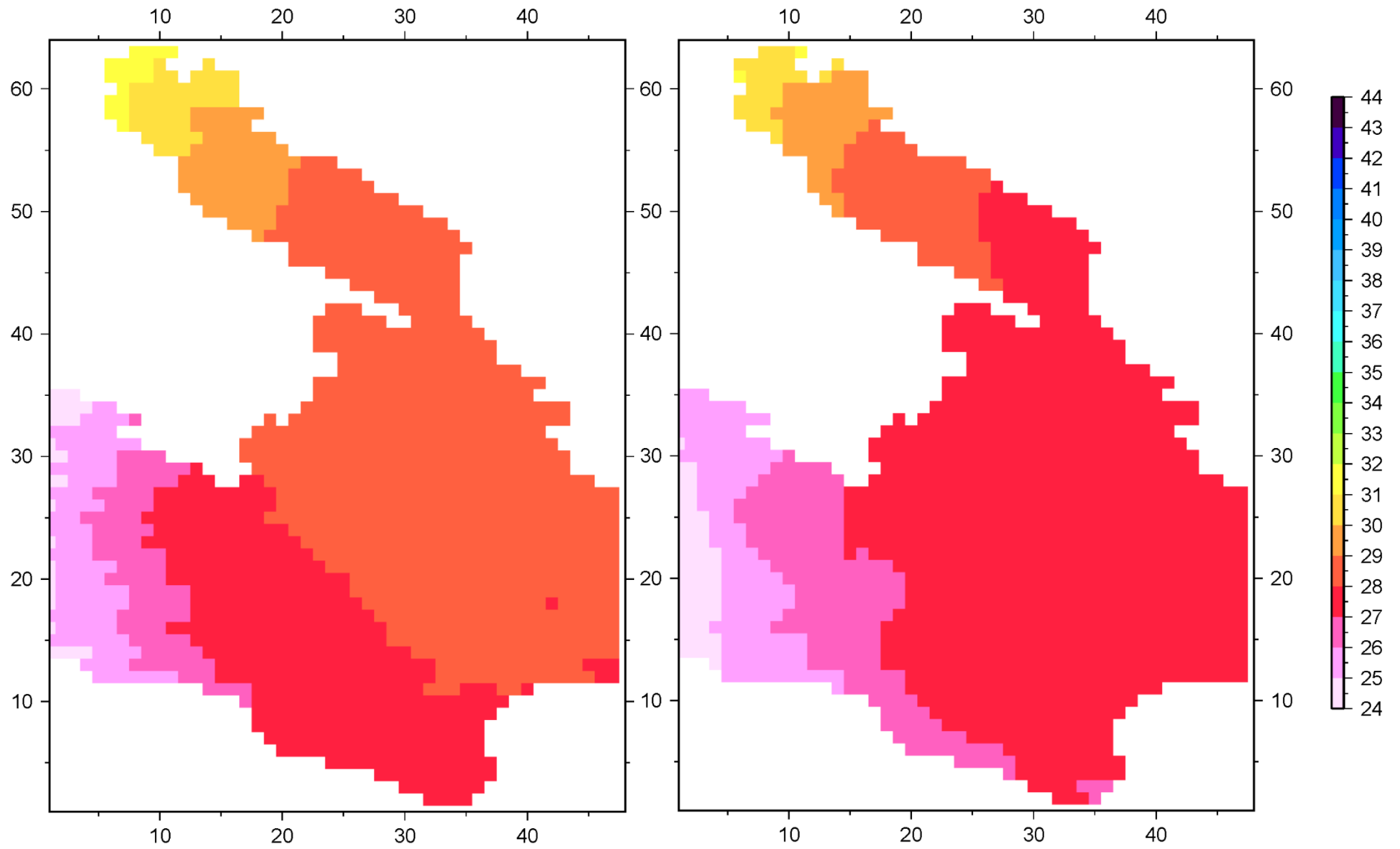
Panel B6: Surface density (ρ-1000) in kg/m³ of exp. 2031 (left) and exp. 2044 (right)

Appendix C
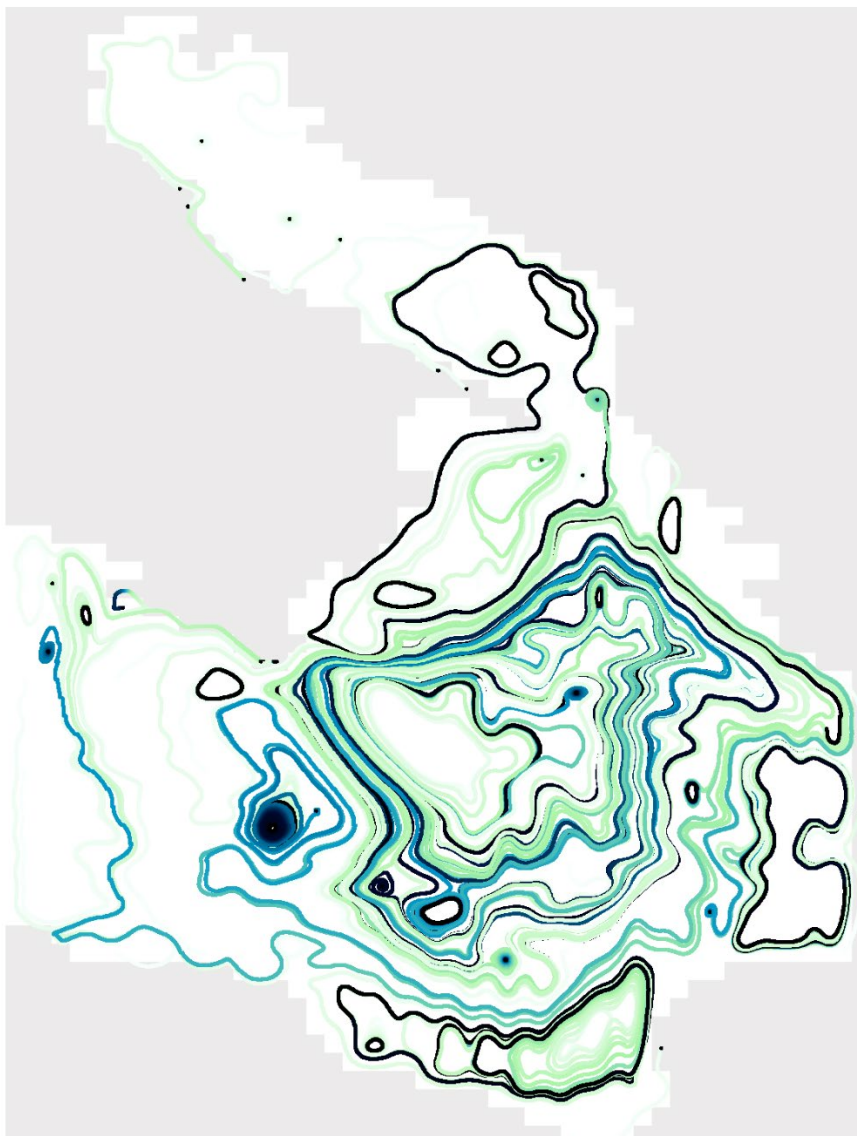
Figure C1: The traces of a selection of equally spaced surface particle through time of exp. 2020. The tail of each particle becomes lighter as the trace of the particle becomes longer.
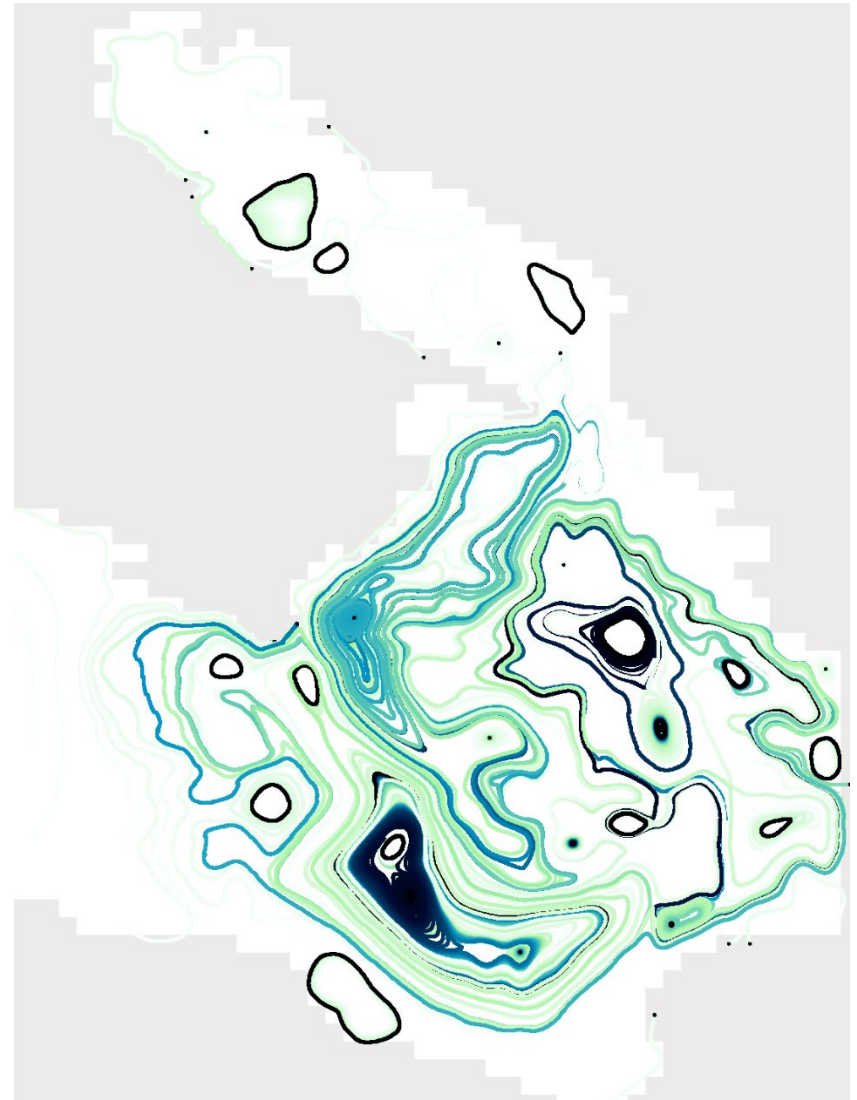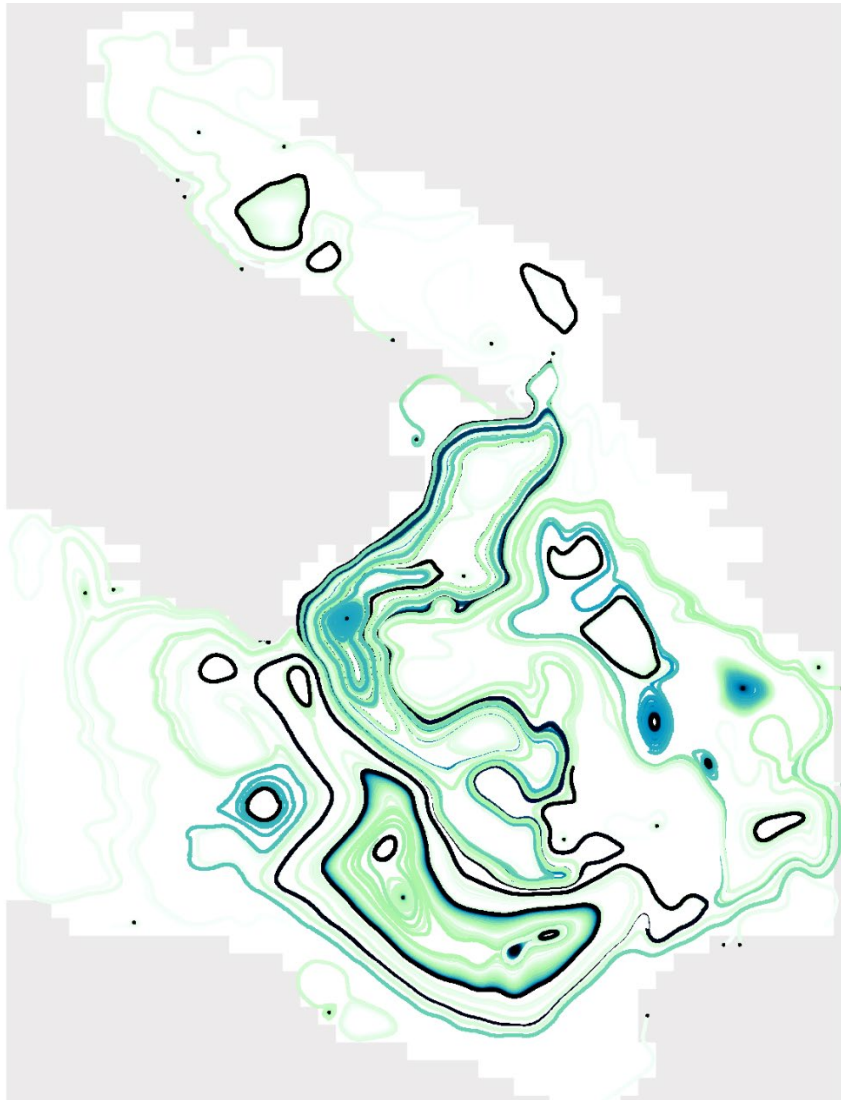
Panel C2: The traces of a selection of equally spaced surface particle through time of exp. 2041 (left) and exp. 2042 (right). The tail of each particle becomes lighter as the trace of the particle becomes longer.
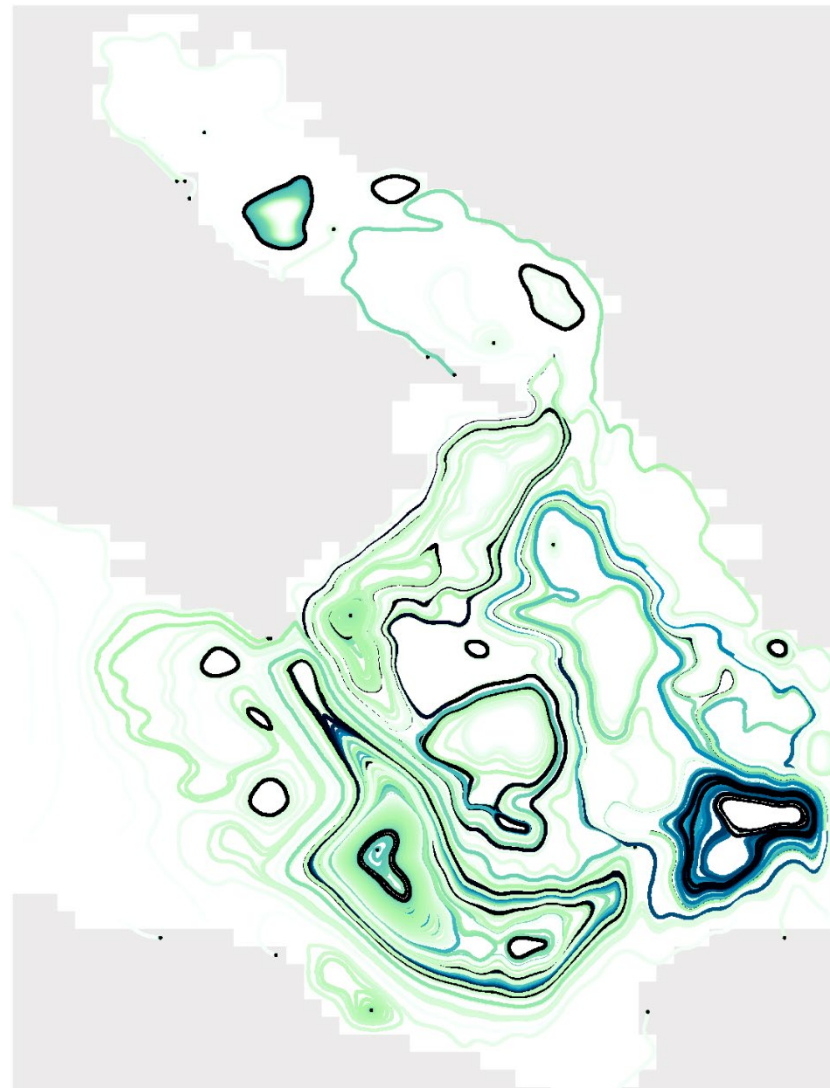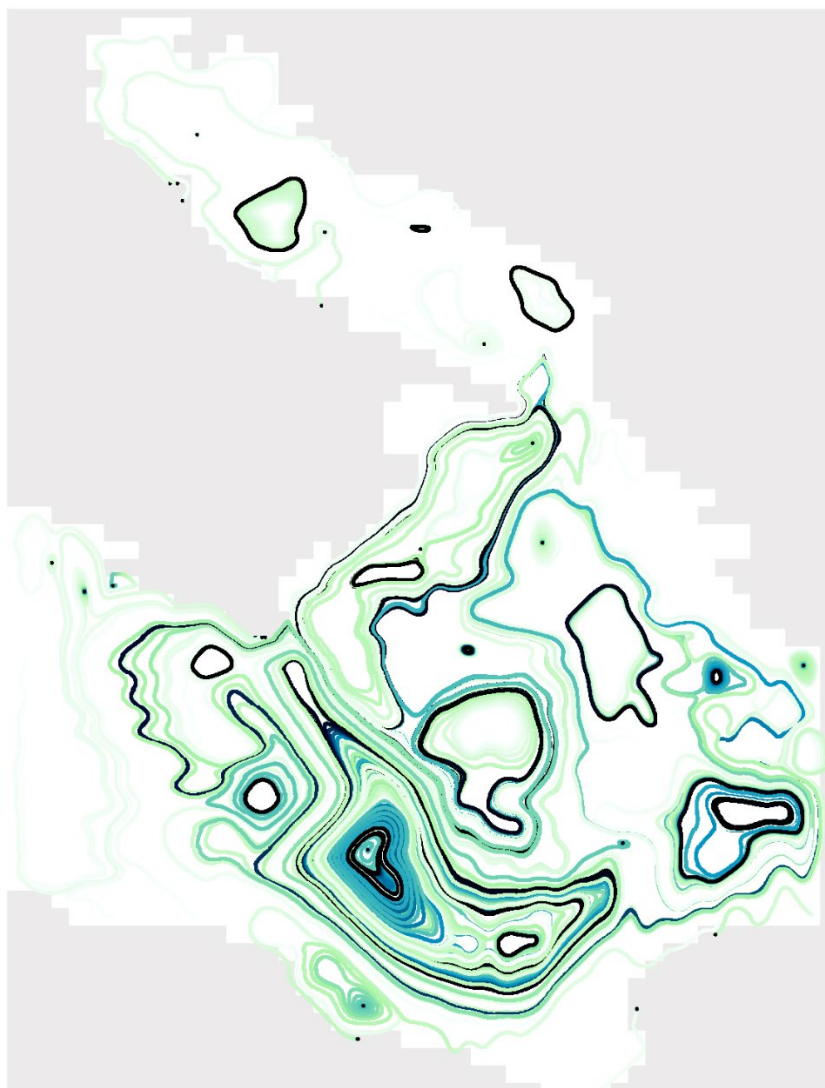
Panel C3: The traces of a selection of equally spaced surface particle through time of exp. 2031 (left) and exp. 2044 (right). The tail of each particle becomes lighter as the trace of the particle becomes longer.
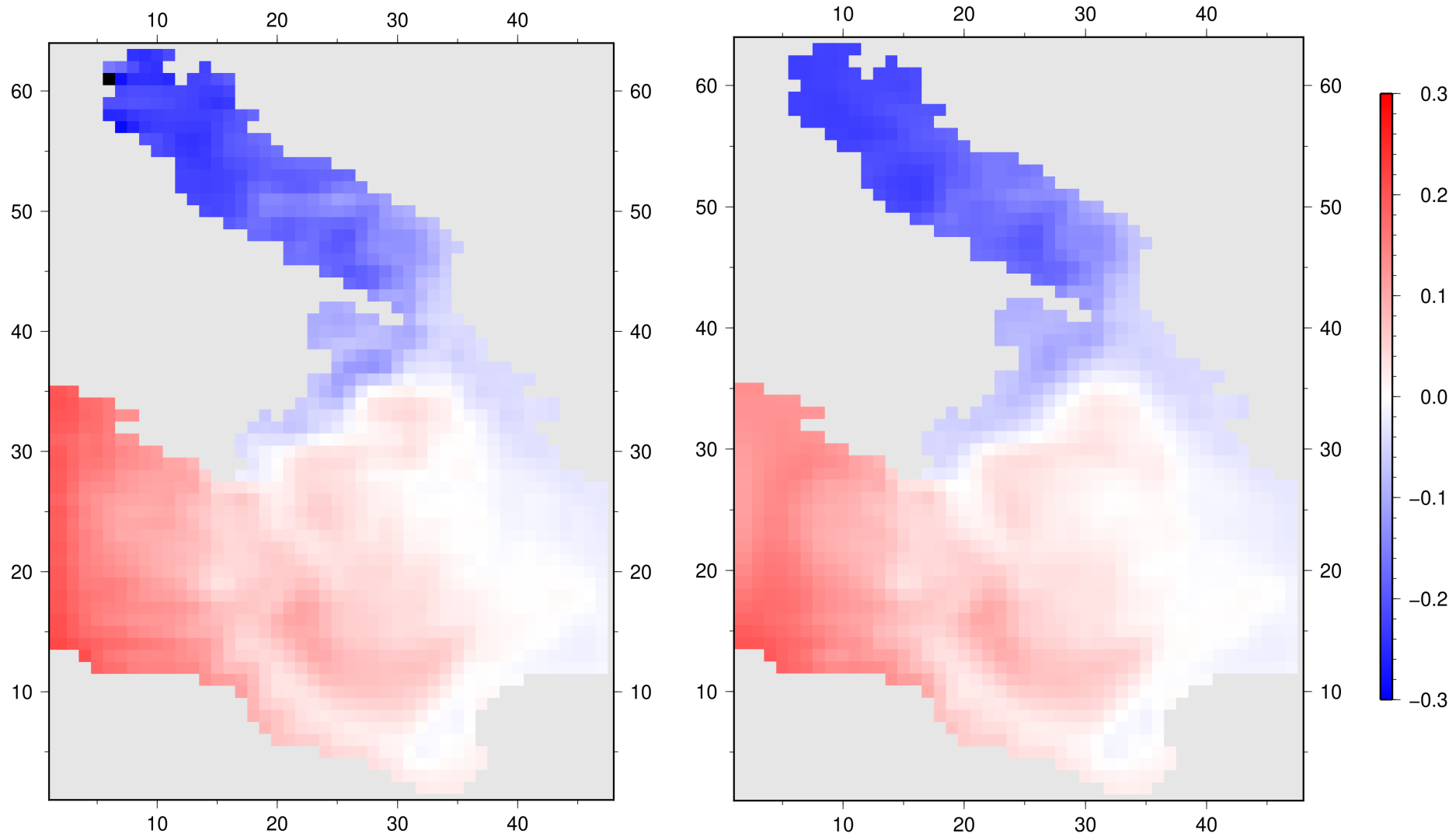
Panel C4: Surface elevation map of exp. 2041 (left) and exp. 2042 (right). (red=positive surface deviation, blue=negative surface deviation)
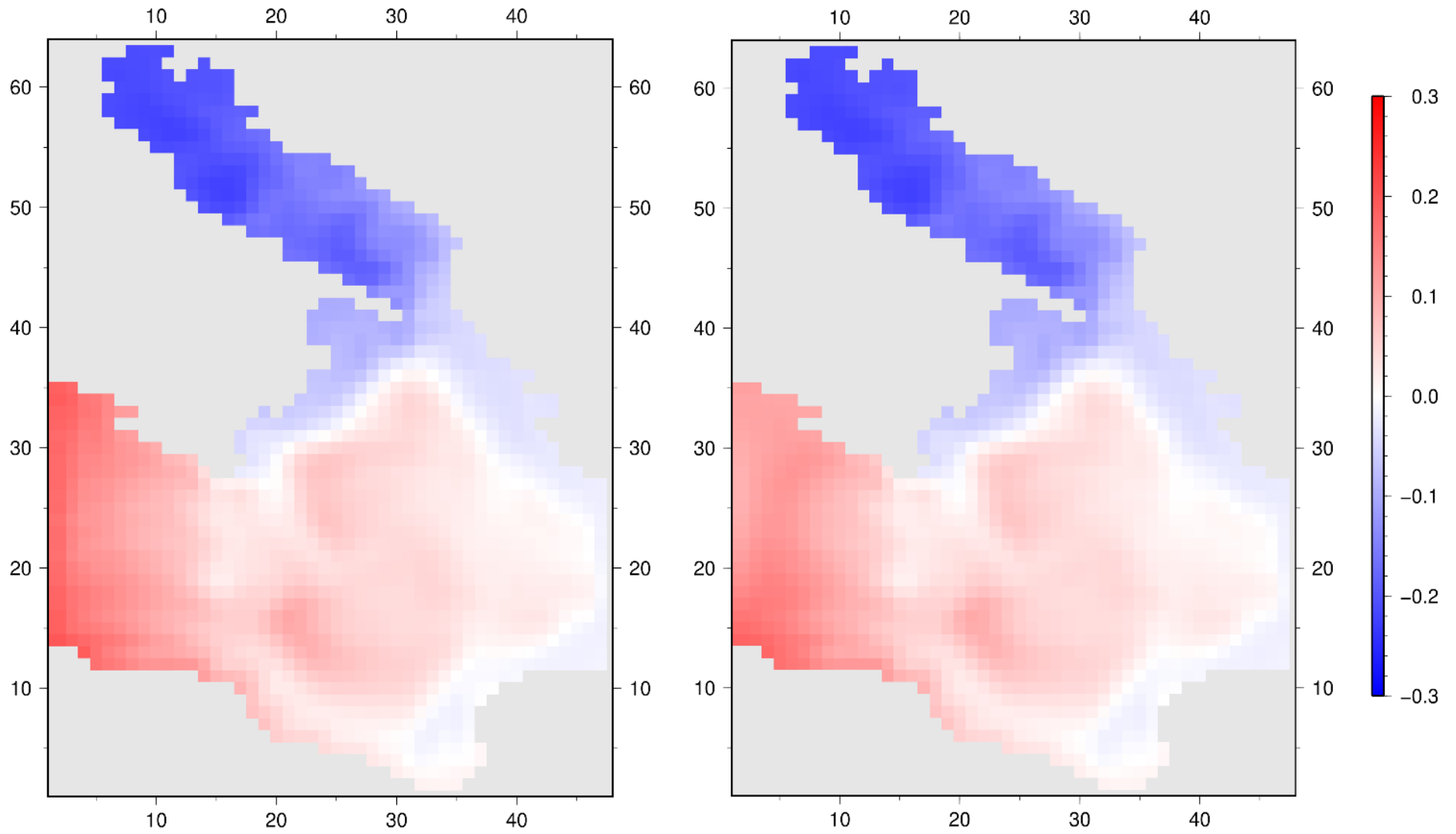
Panel C5: Surface elevation map of exp. 2041 (left) and exp. 2042 (right). (red=positive surface deviation, blue-blue=negative surface deviation)
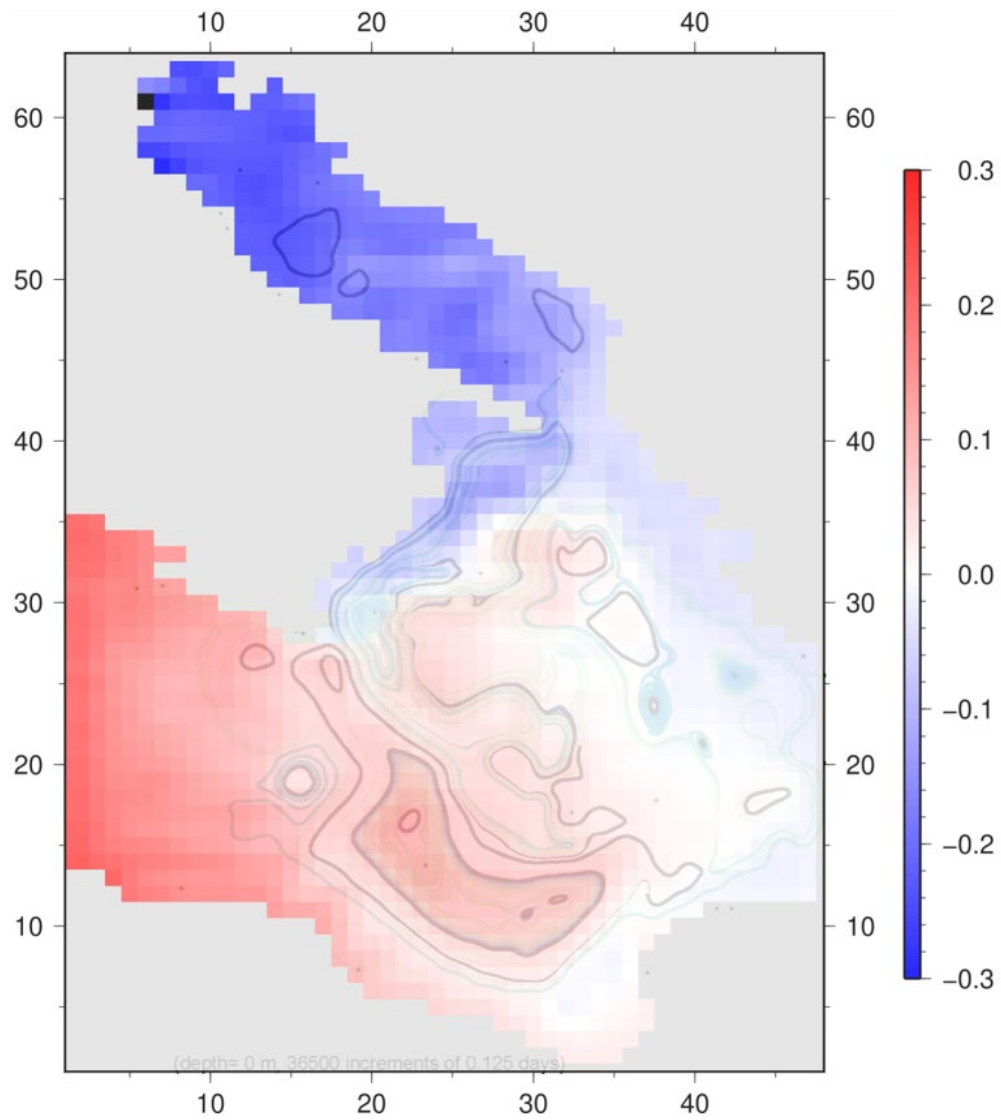
Figure C6: The particle trace map of exp. 2041 overlain by the surface elevation map of exp. 2041.

Appendix D
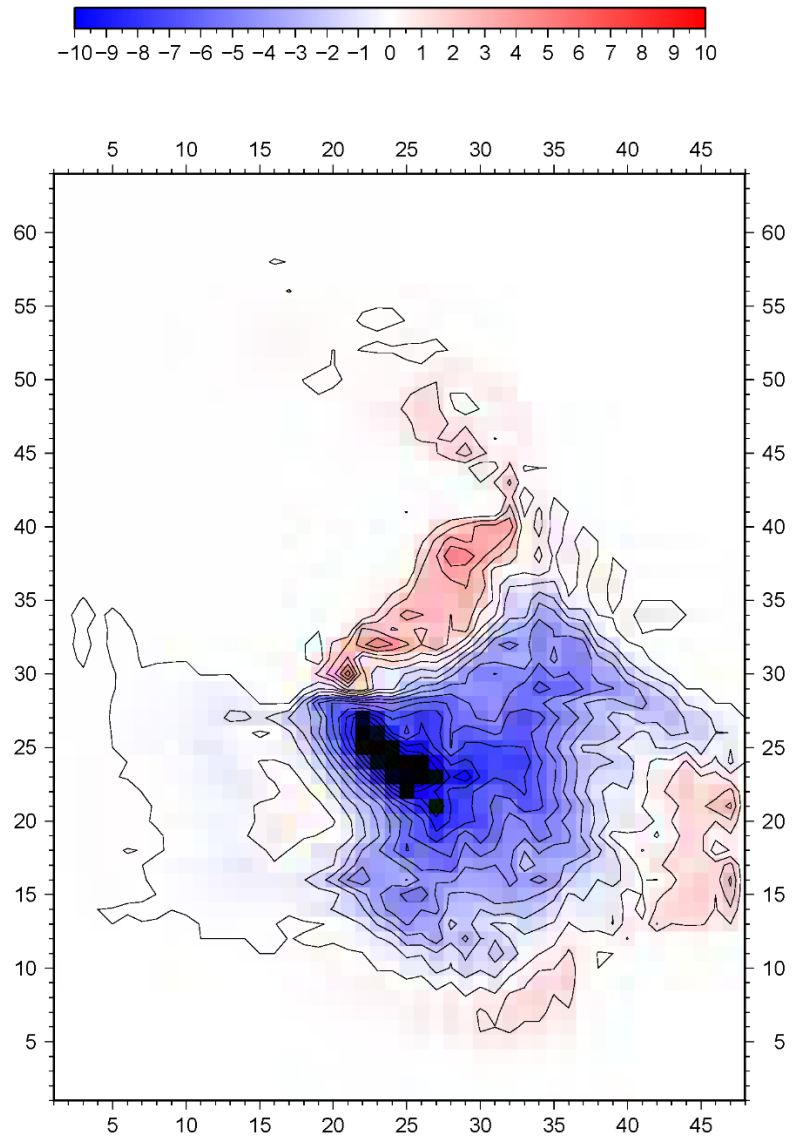
Figure D1: The depth integrated potential of flow in Sv of exp. 2020 (red=counter-clockwise, blue=clockwise)
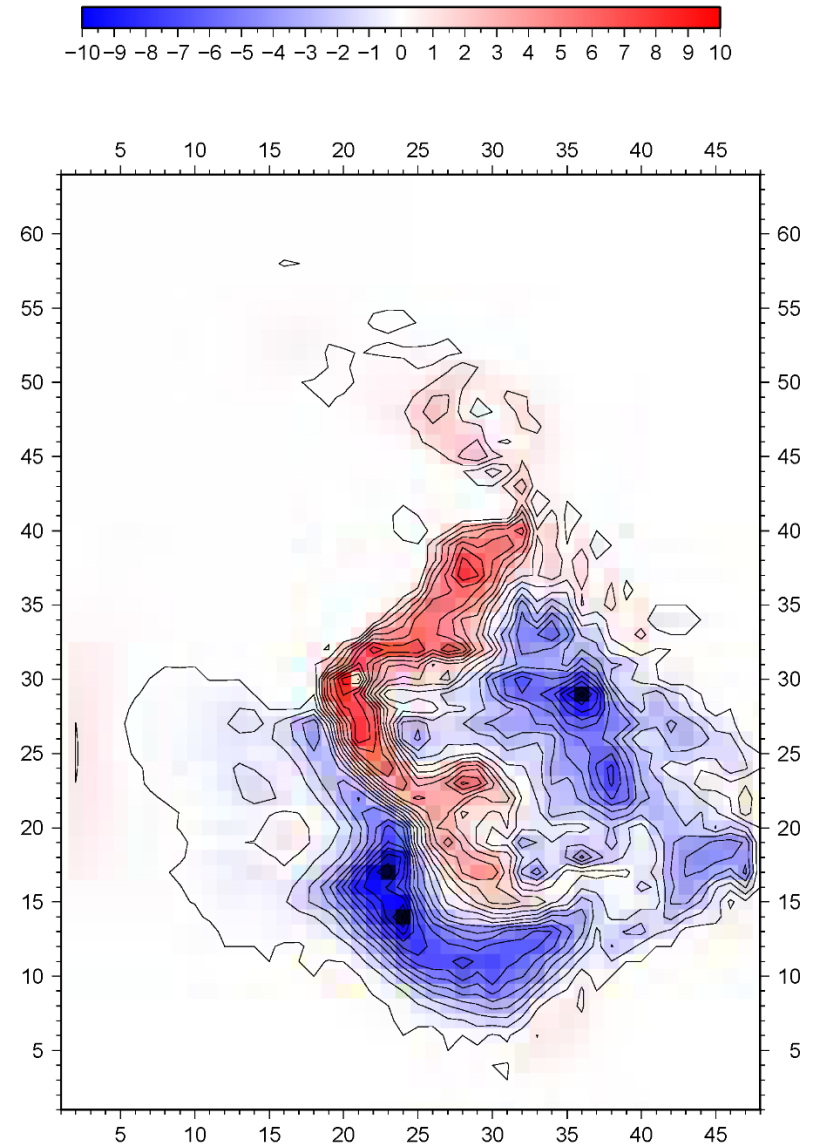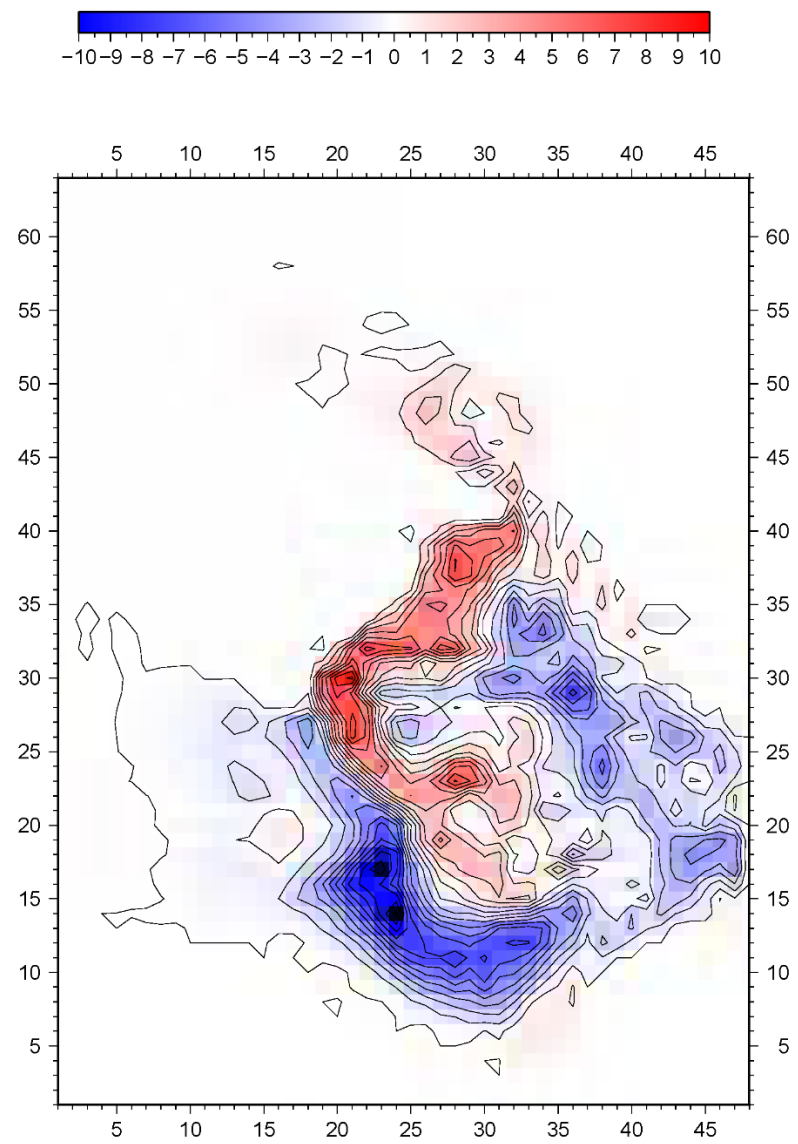
Panel D2: The depth integrated potential of flow in Sv of exp. 2041 (left) and exp. 2042 (right) (red=counter-clockwise, blue=clockwise)
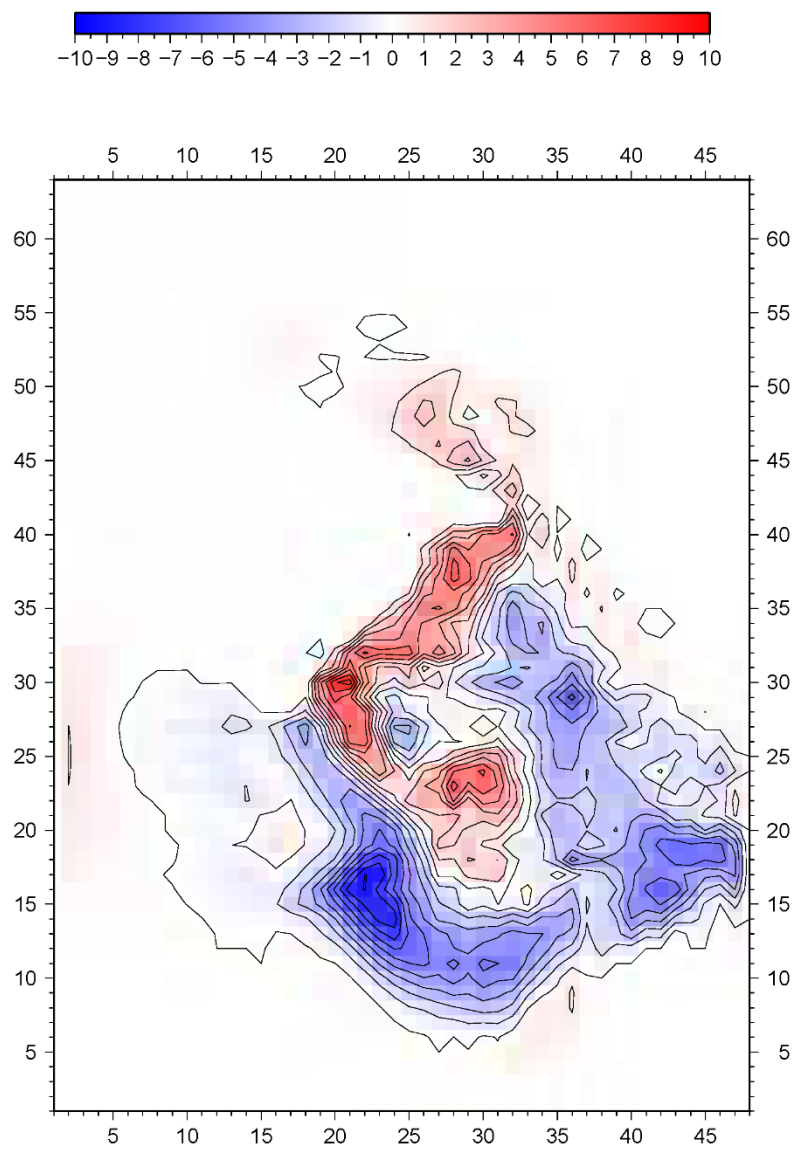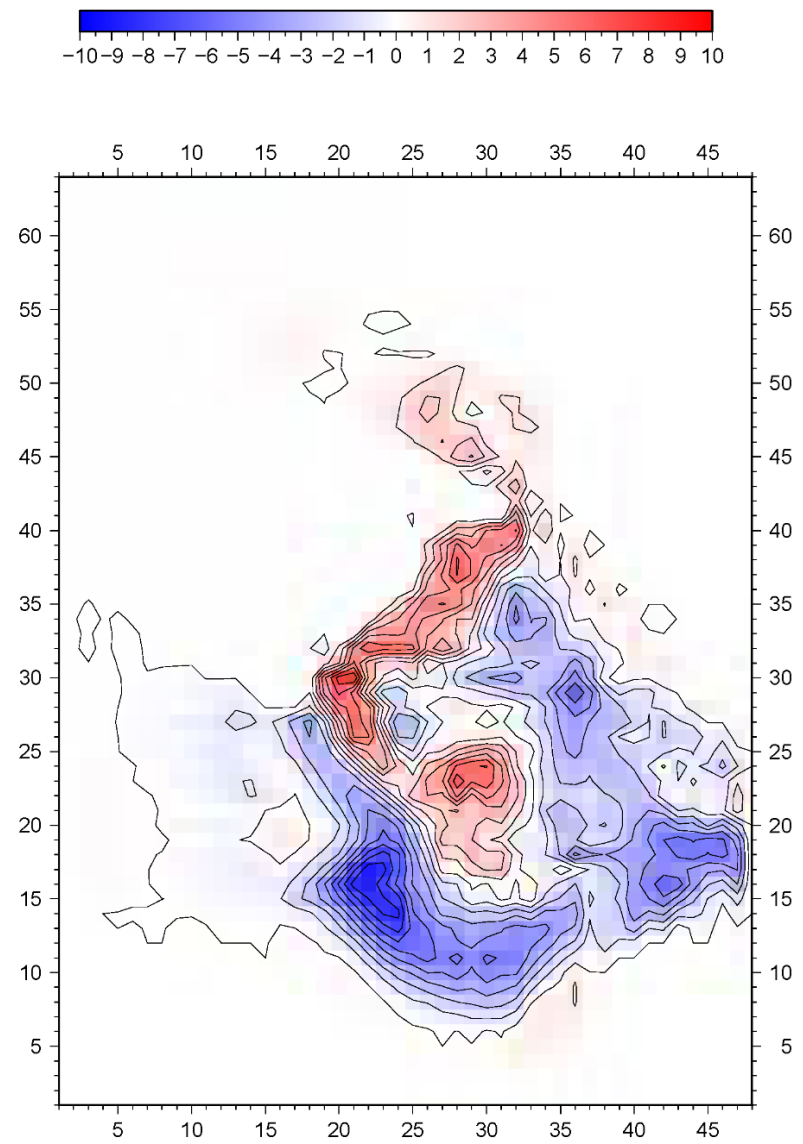
Panel D3: The depth integrated potential of flow in Sv of exp. 2031 (left) and exp. 2044 (right) (red=counter-clockwise, blue=clockwise)

Appendix E
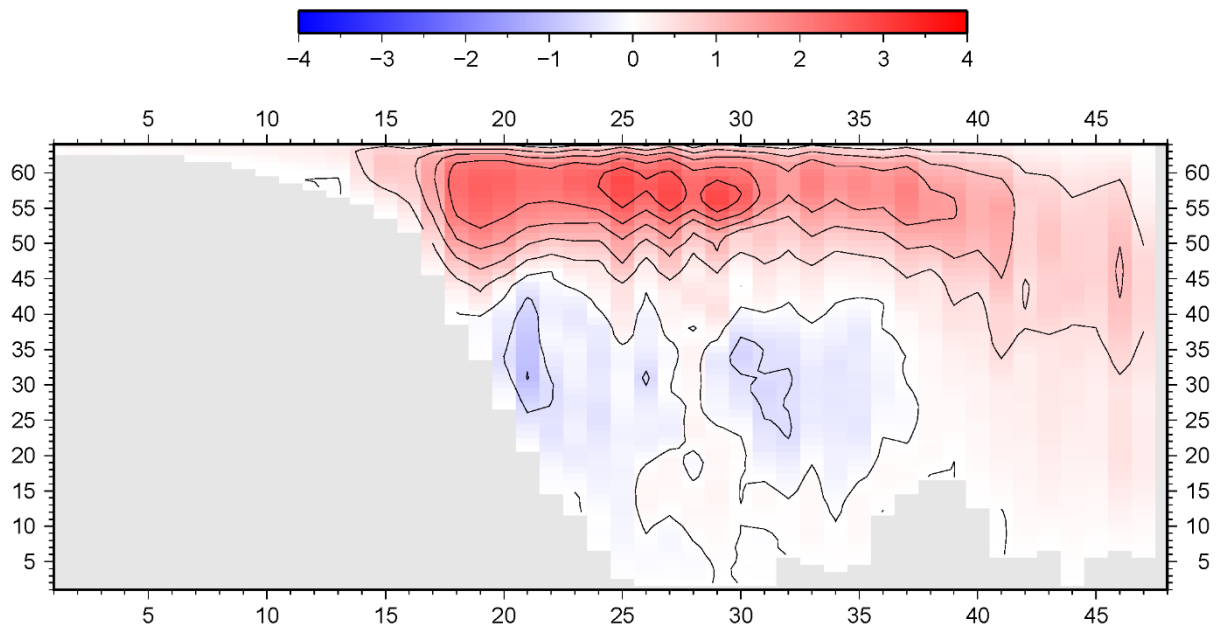
Figure E1: The zonal overturning stream function in Sv representing streamlines tangent to the flow velocity vector of exp. 2020 (red=clockwise, blue=counter clockwise). Depth [m] is represented on the y axis through the following formulation: depth = 65*(64-y).
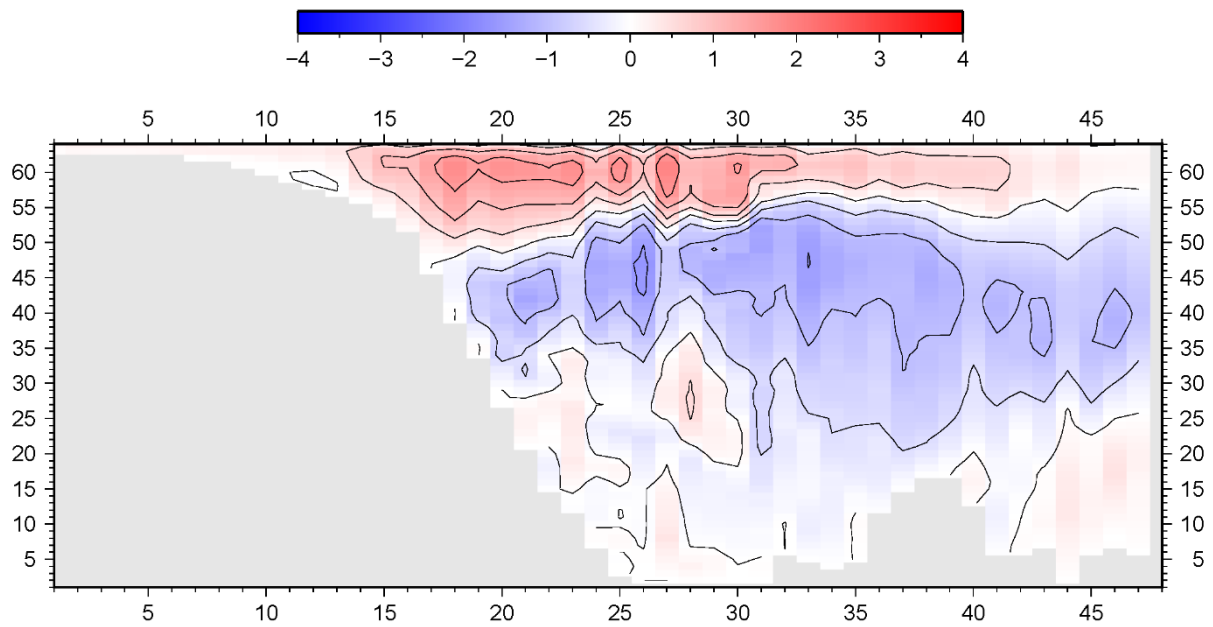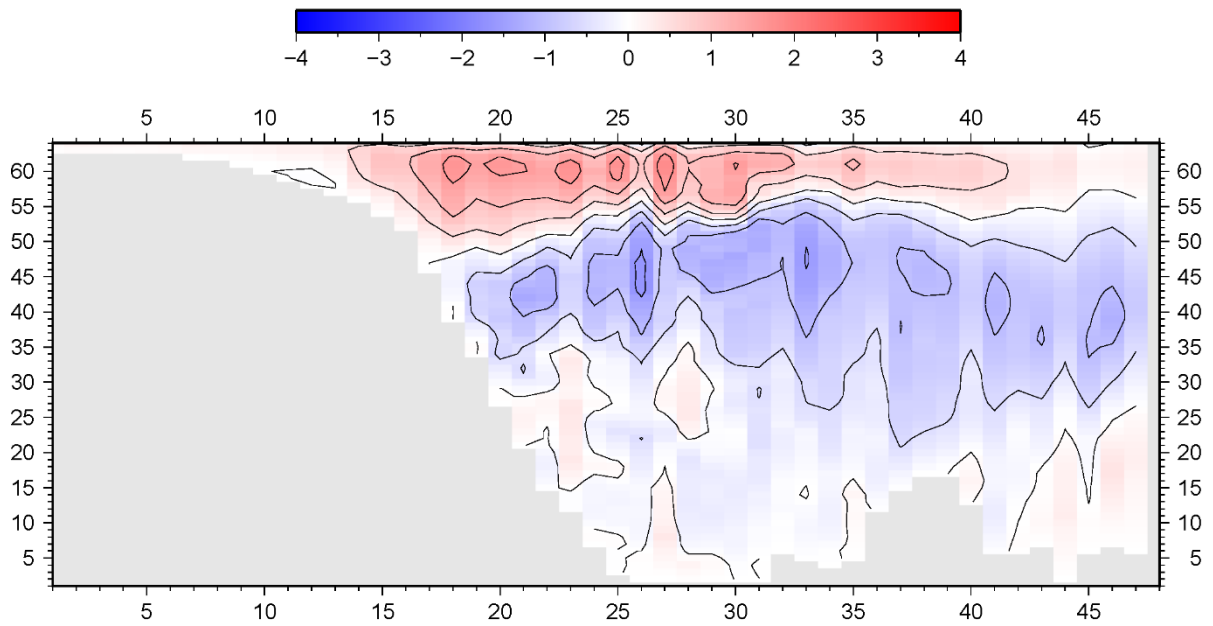
Panel E2: The zonal overturning stream function in Sv representing streamlines tangent to the flow velocity vector of exp. 2041 (top) and exp. 2042 (bottom) (red=clockwise, blue=counter clockwise). Depth [m] is represented on the y axis through the following formulation: depth = 65(64-y).*
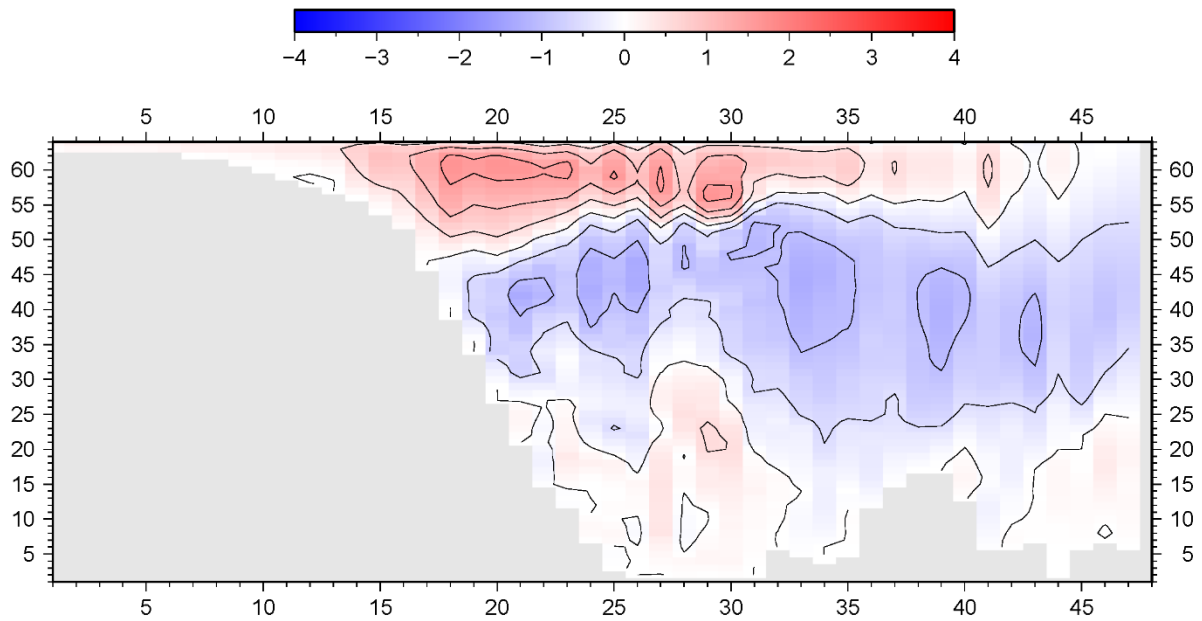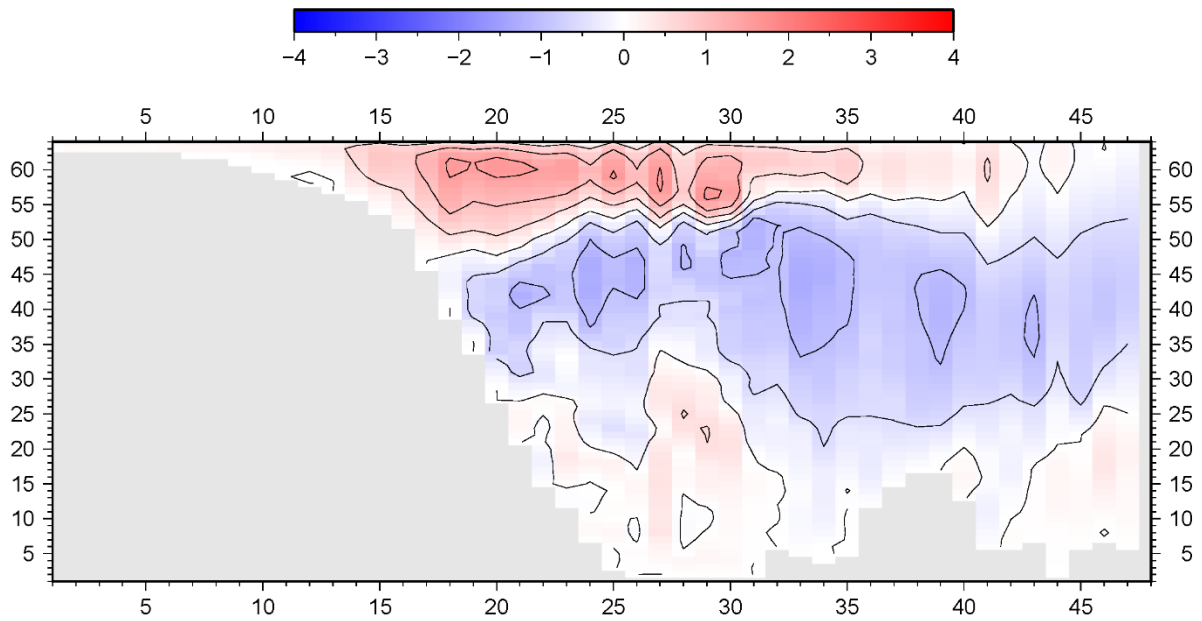
Panel E3: The zonal overturning stream function in Sv representing streamlines tangent to the flow velocity vector of exp. 2031 (top) and exp. 2044 (bottom) (red=clockwise, blue=counter clockwise). Depth [m] is represented on the y axis through the following formulation: depth = 65*(64-y).

Appendix F
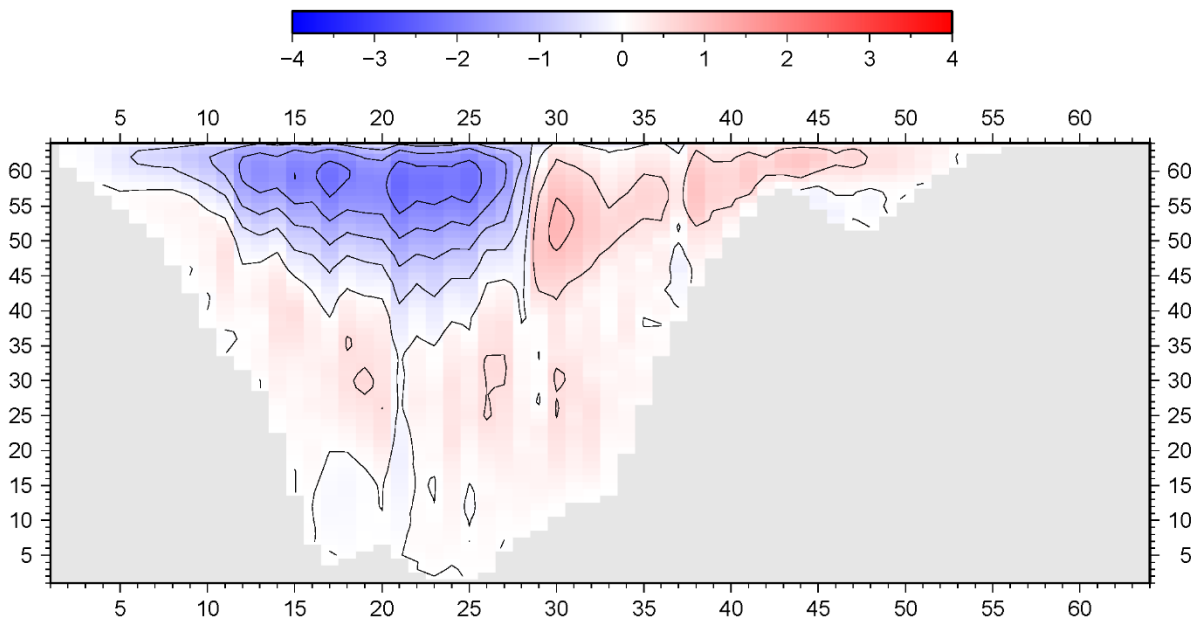
Figure F1: The meridional overturning stream function in Sv representing streamlines tangent to the flow velocity vector of exp. 2020 (red=clockwise, blue=counter clockwise). Depth [m] is represented on the y axis through the following formulation: depth = 65*(64-y).
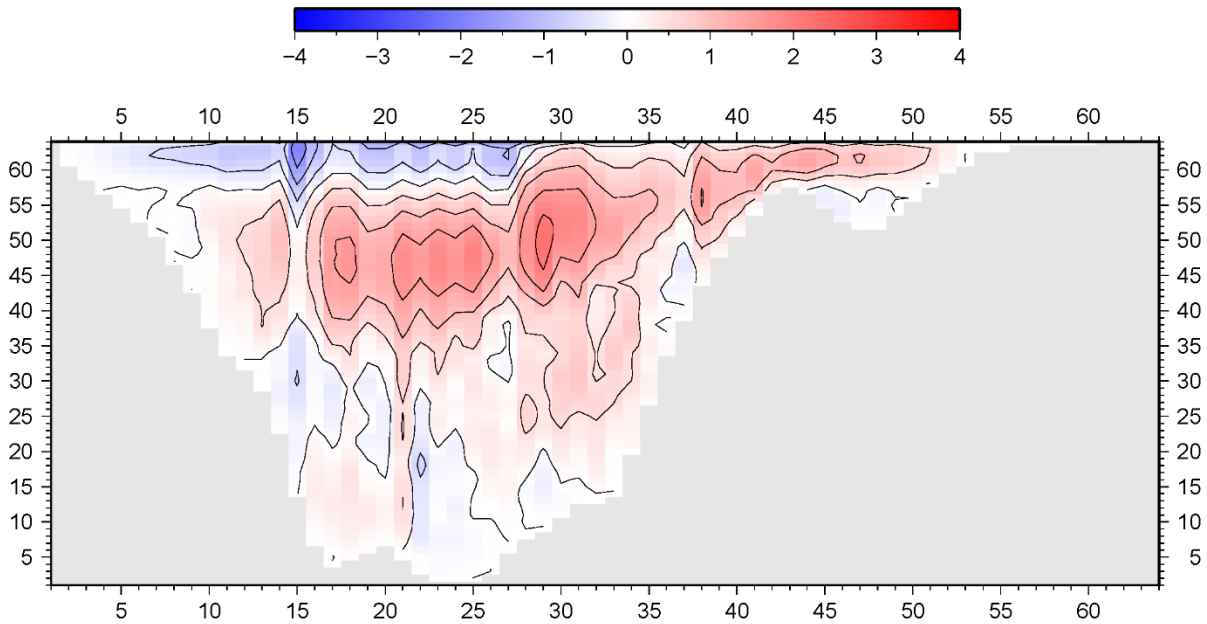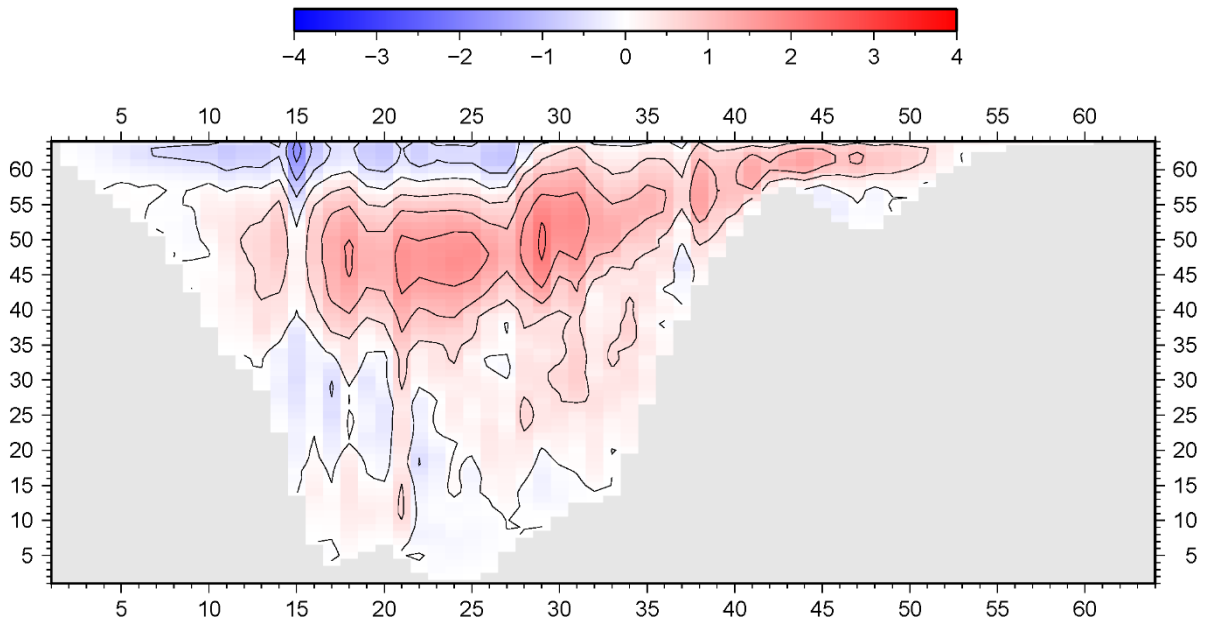
Panel F2: The meridional overturning stream function in Sv representing streamlines tangent to the flow velocity vector of exp. 2041 (top) and exp. 2042 (bottom) (red=clockwise, blue=counter clockwise). Depth [m] is represented on the y axis through the following formulation: depth = 65*(64-y).
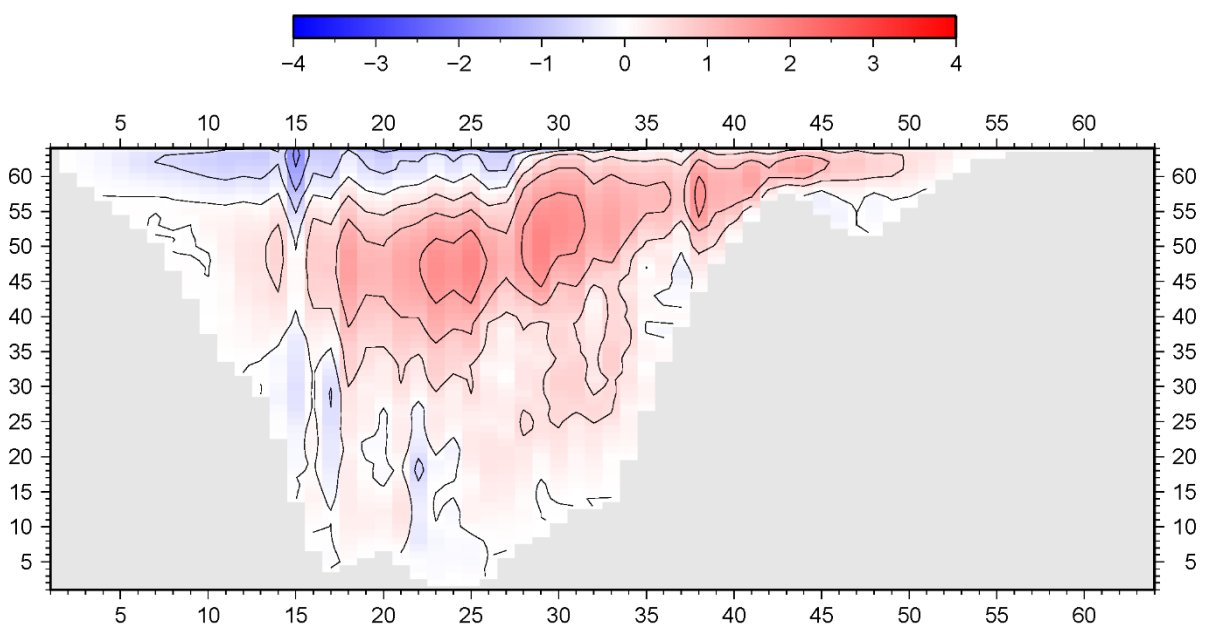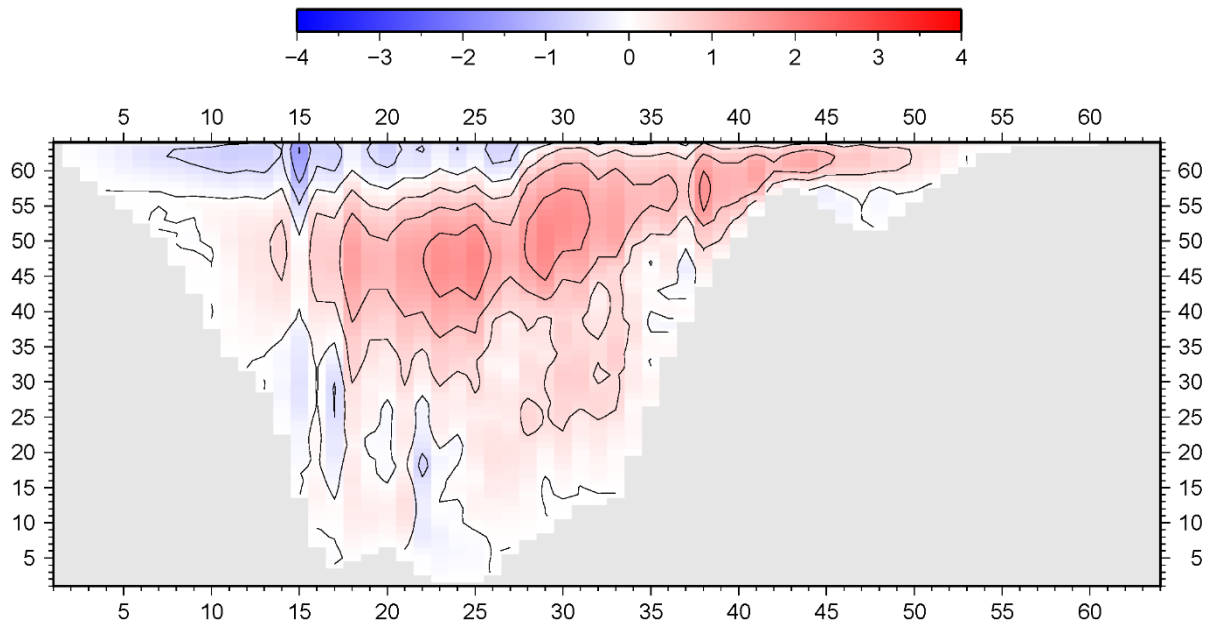
Panel F3: The meridional overturning stream function in Sv representing streamlines tangent to the flow velocity vector of exp. 2031 (top) and exp. 2044 (bottom) (red=clockwise, blue=counter clockwise). Depth [m] is represented on the y axis through the following formulation: depth = 65(64-y).*

Appendix G
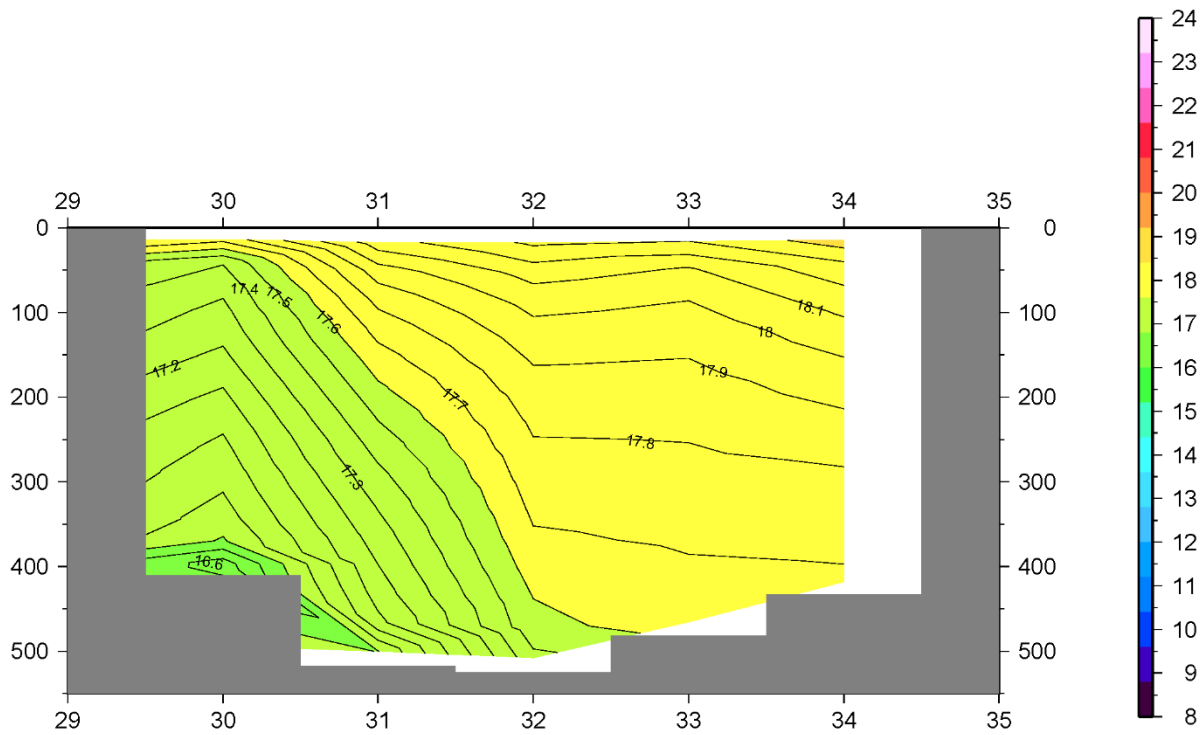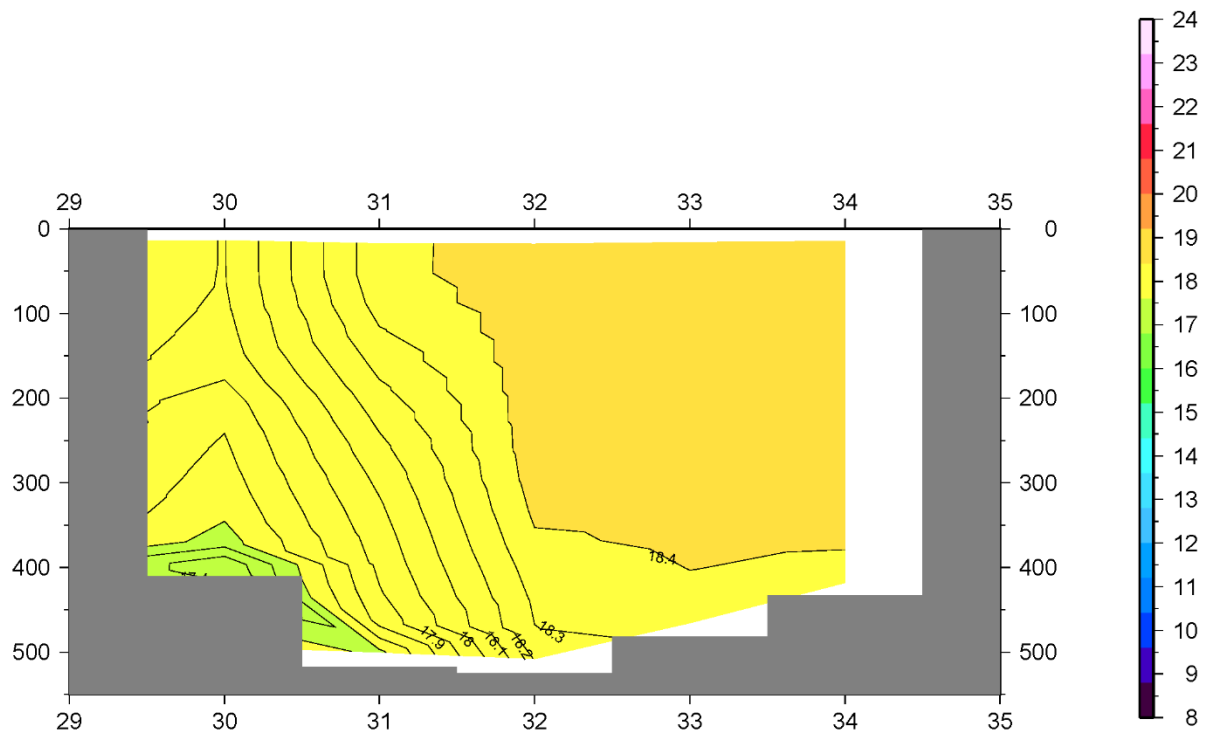
Panel G1: Section H_1 temperature in °C of exp. 2041 (top) and exp. 2031 (bottom). The y axis represents the depth of the section while the x axis represents the ith grid cell.
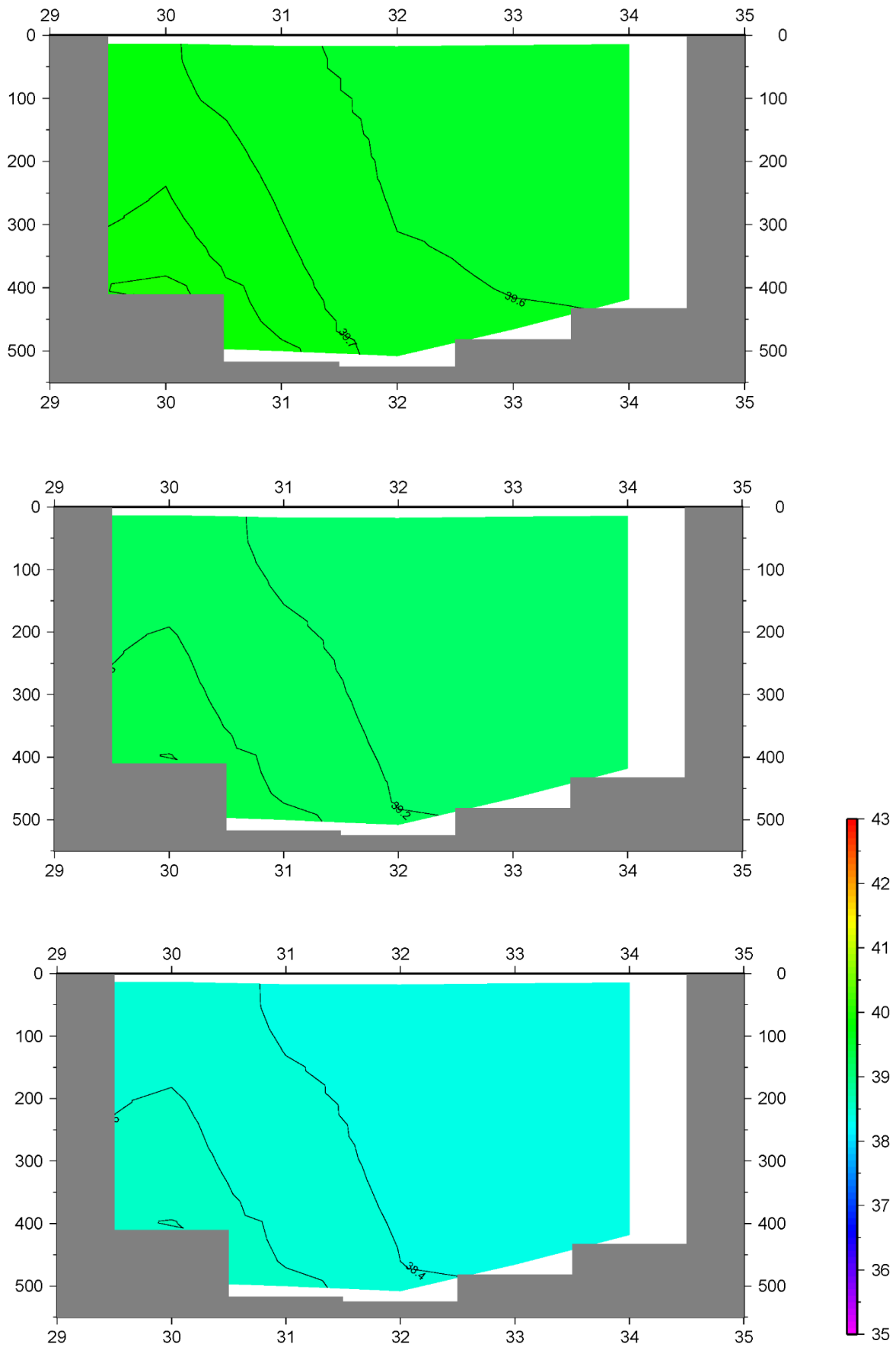
Panel G2: Section H_1 salinity in ppt of exp. 2020 (top), exp. 2041 (middle) and exp. 2042 (bottom). The y axis represents the depth of the section while the x axis represents the ith grid cell.
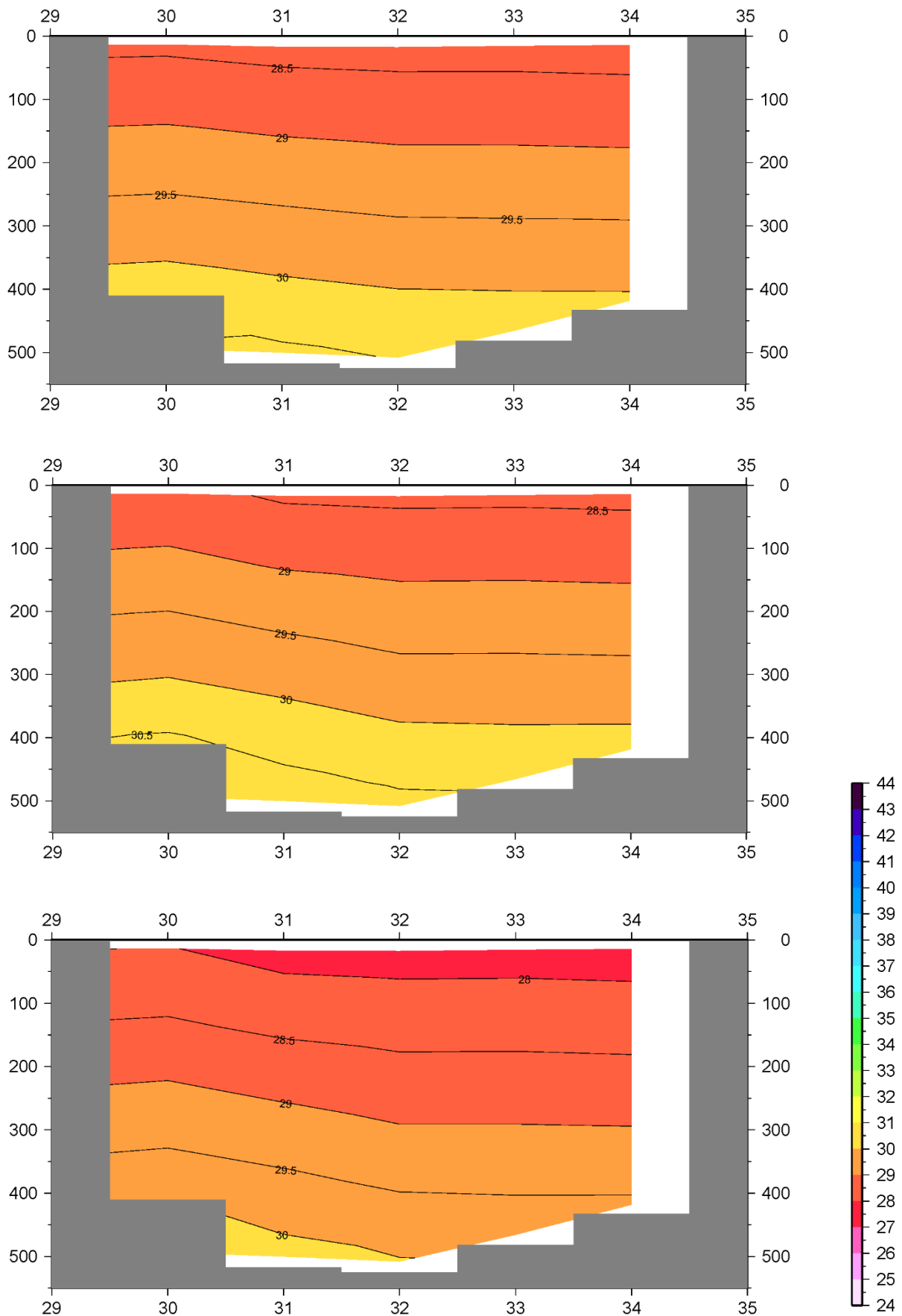
Panel G3: Section H_1 density (ρ-1000) in kg/m³ of exp. 2020 (top), exp. 2041 (middle) and exp. 2042 (bottom). The y axis represents the depth of the section while the x axis represents the ith grid cell.
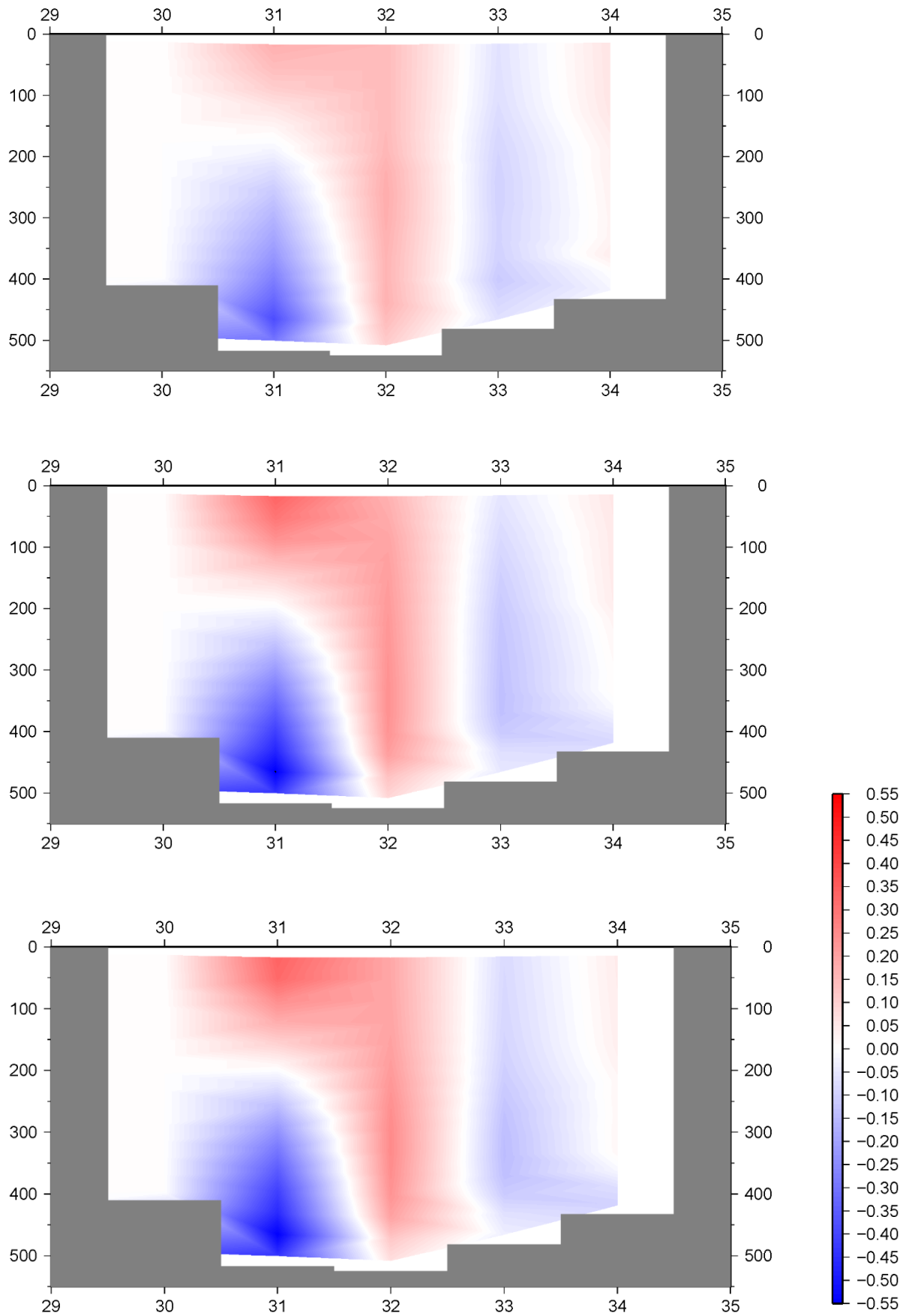
Panel G4: Section H_1 velocity of in- and outflow in m/s of exp. 2020 (top), exp. 2041 (middle) and exp. 2031 (bottom). (red=northward flow, blue=southward flow). The y axis represents the depth of the section while the x axis represents the ith grid cell.

Appendix H
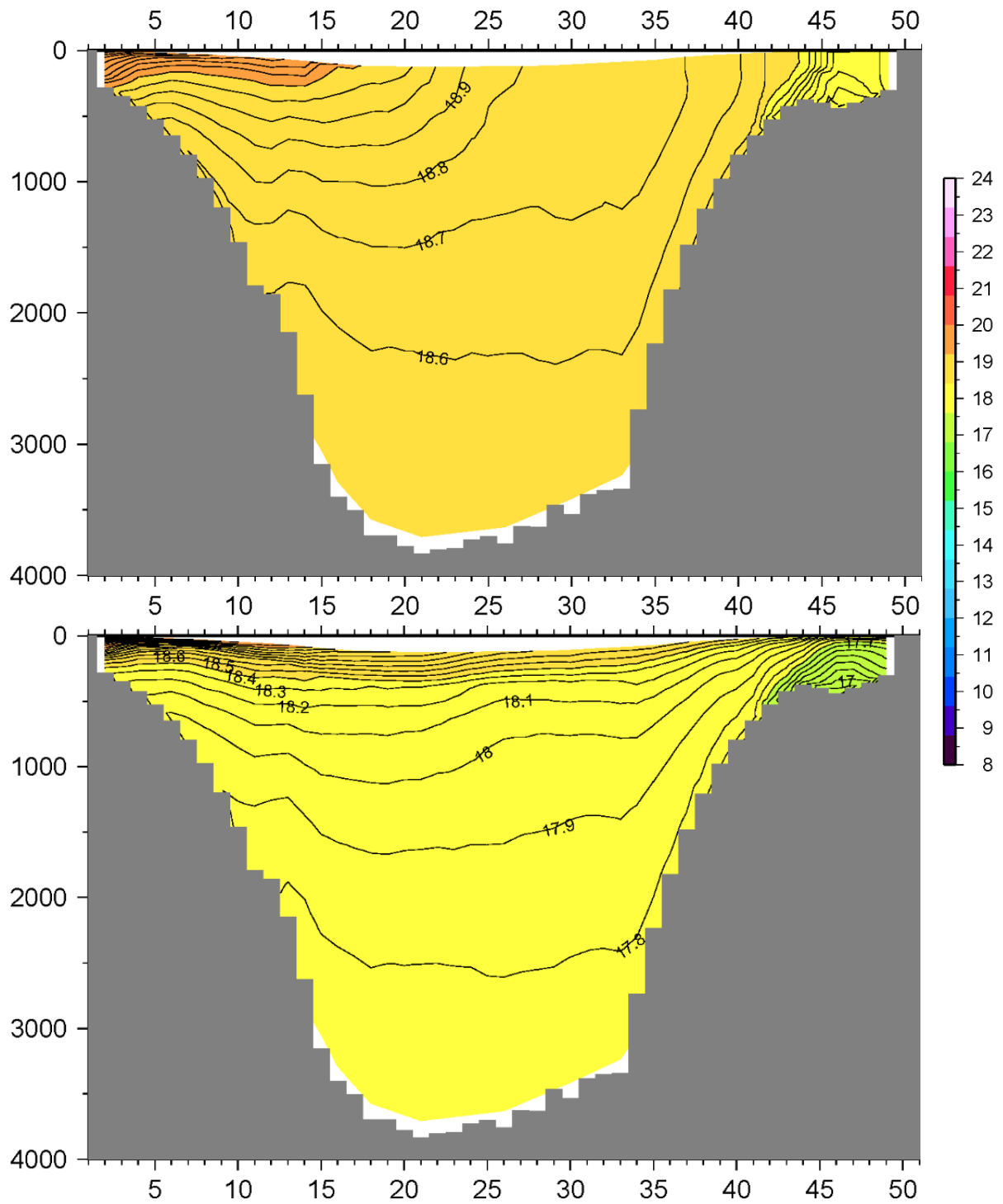
Panel H1: Section V temperature in °C of exp. 2041 (top) and exp. 2031 (bottom). The y axis represents the depth of the section while the x axis represents the jth grid cell.
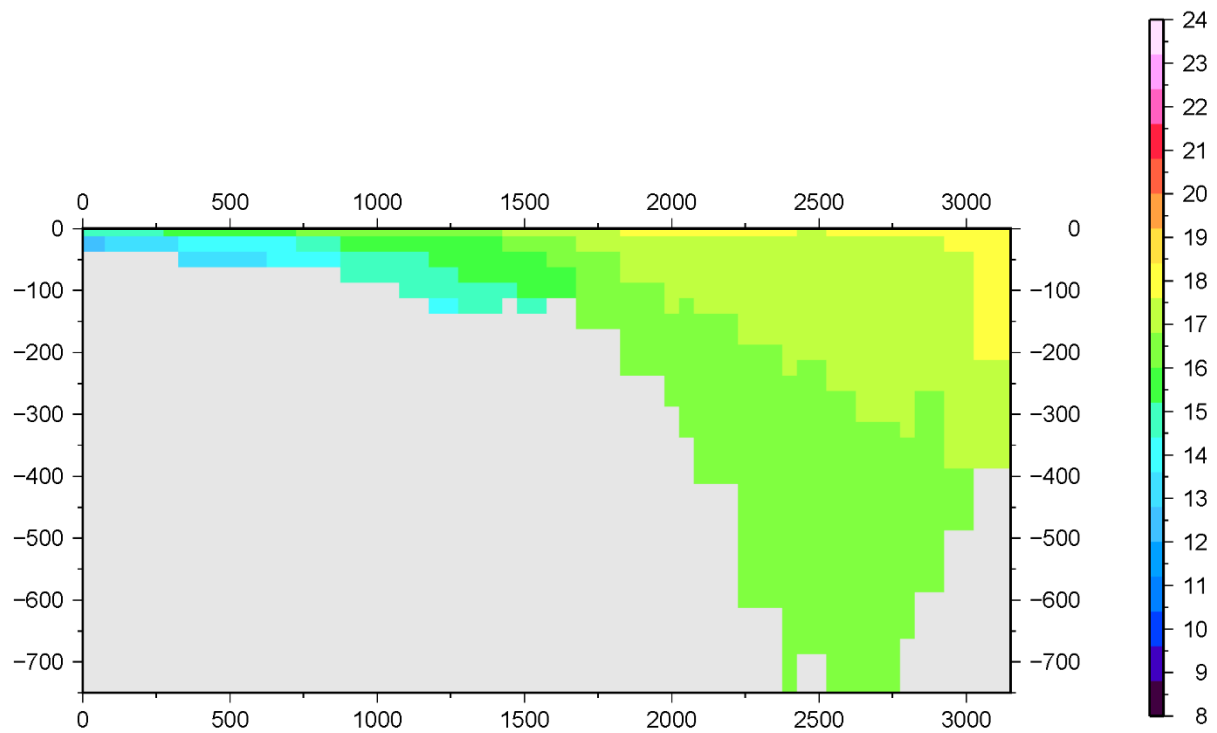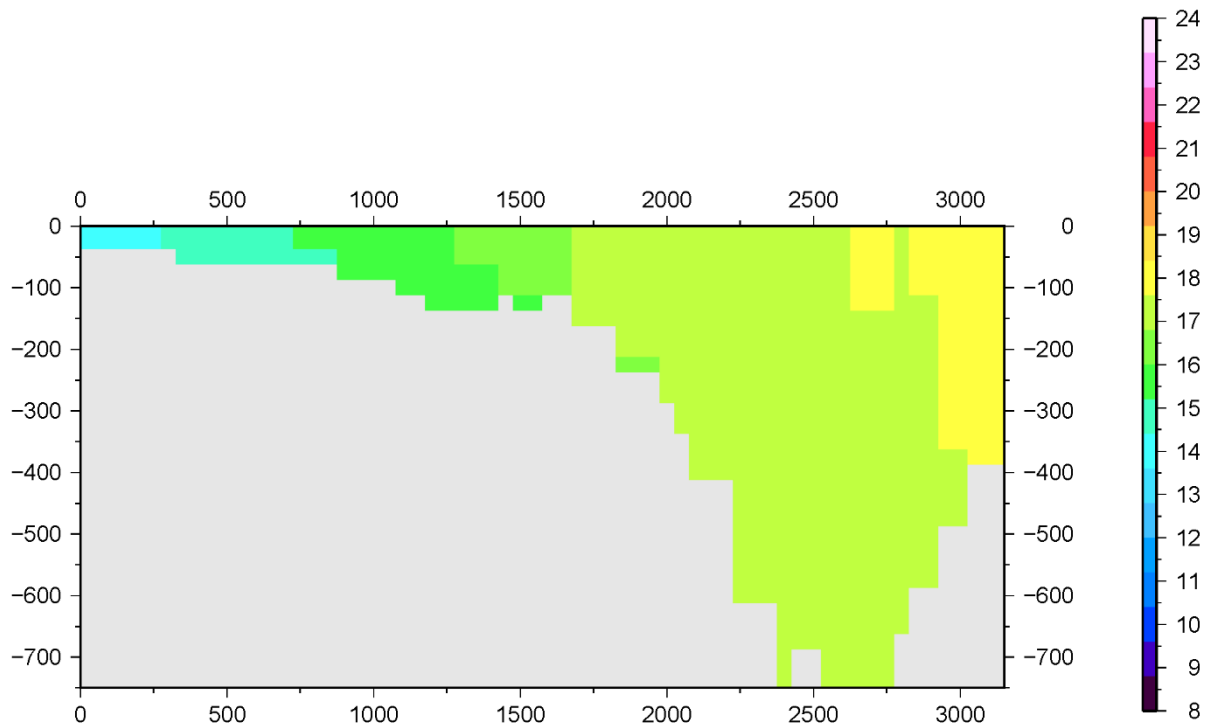
Panel H2: Section D_1 temperature in °C of exp. 2041 (top) and exp. 2031 (bottom). The y axis represents the depth of the section while the x axis represents the distance in km along the cross section starting in the north-west and ending in the south-east.
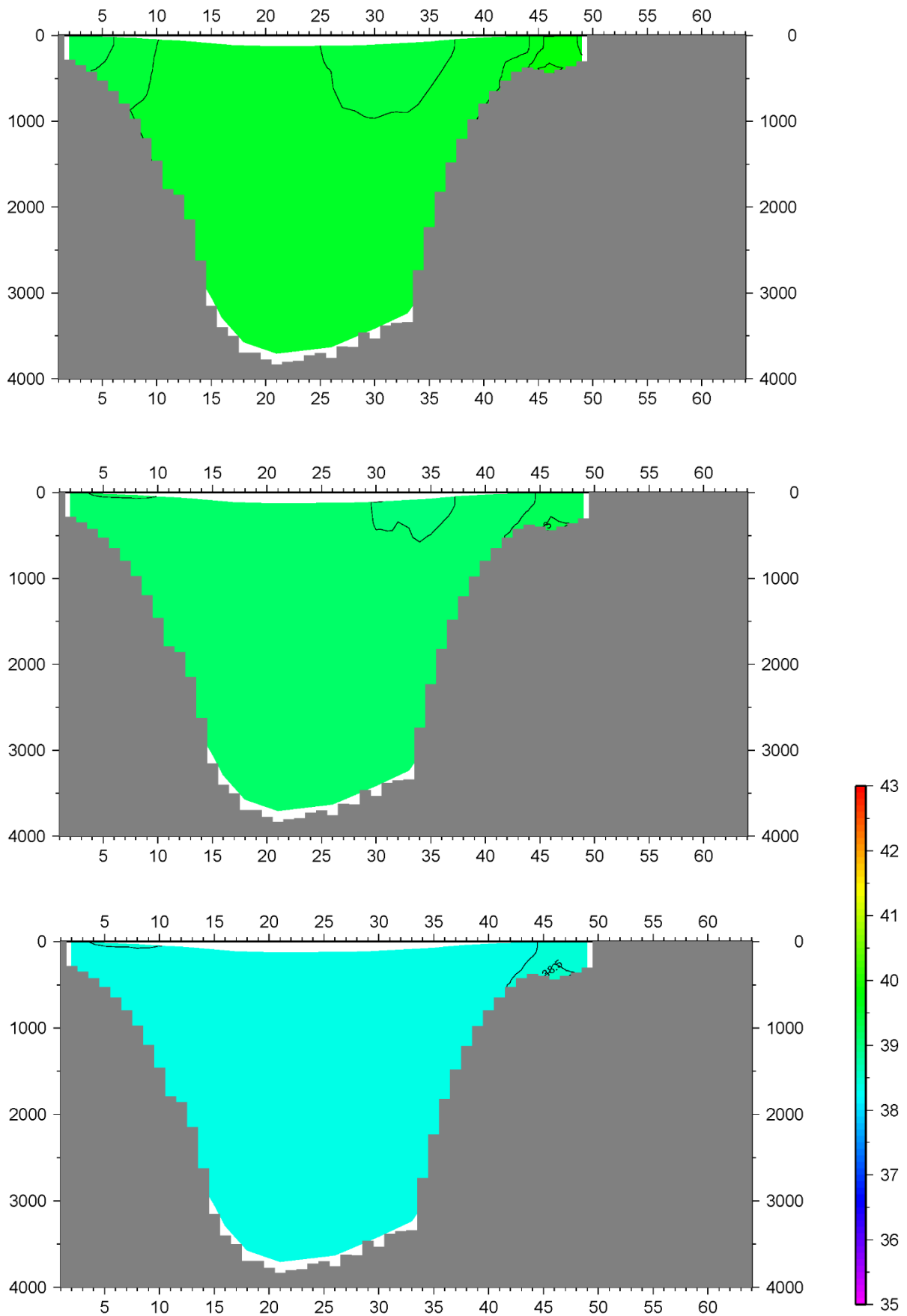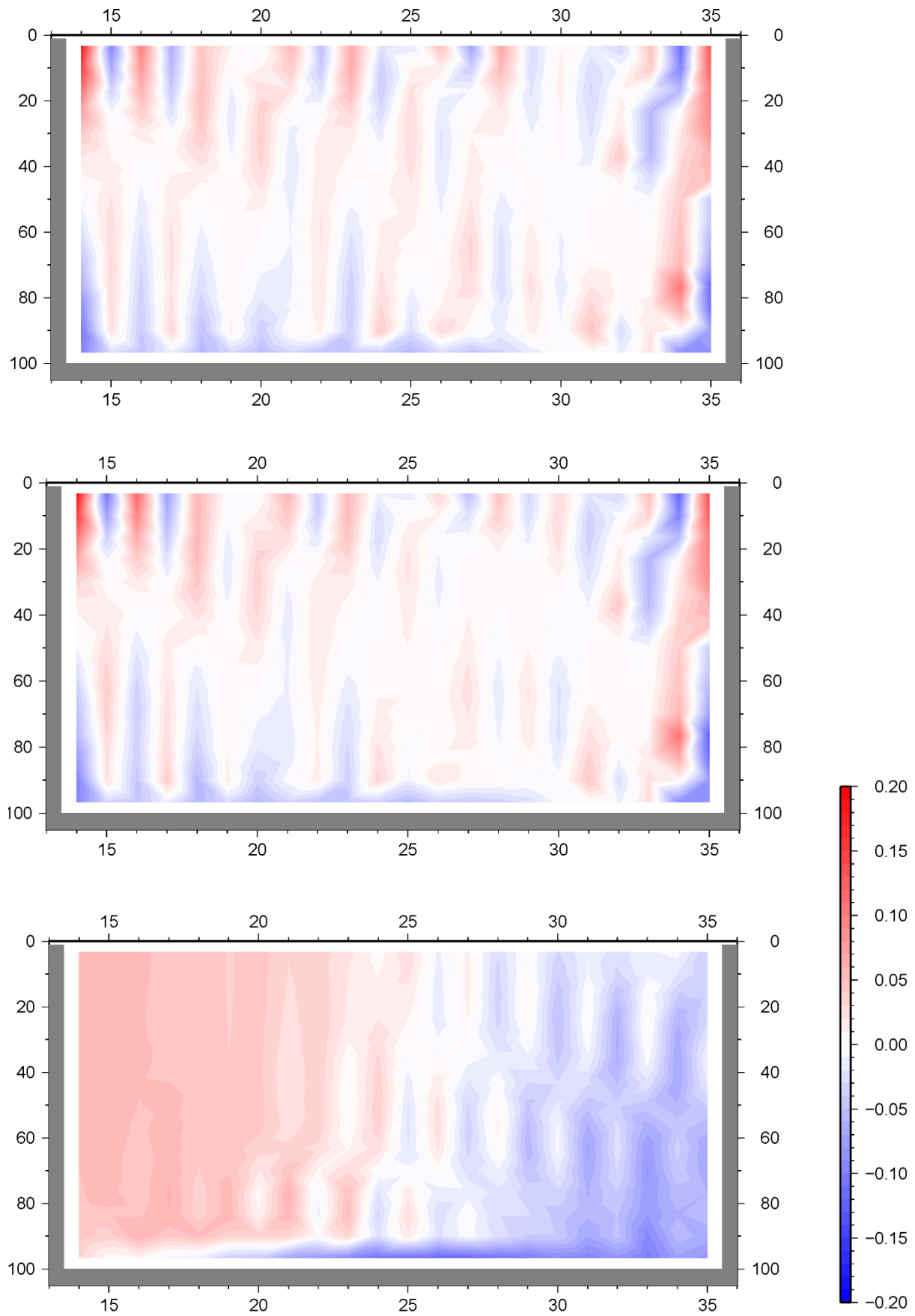
Panel H3: Section V salinity in ppt of exp. 2020 (top), exp. 2041 (middle) and exp. 2042 (bottom). The y axis represents the depth of the section while the x axis represents the jth grid cell.
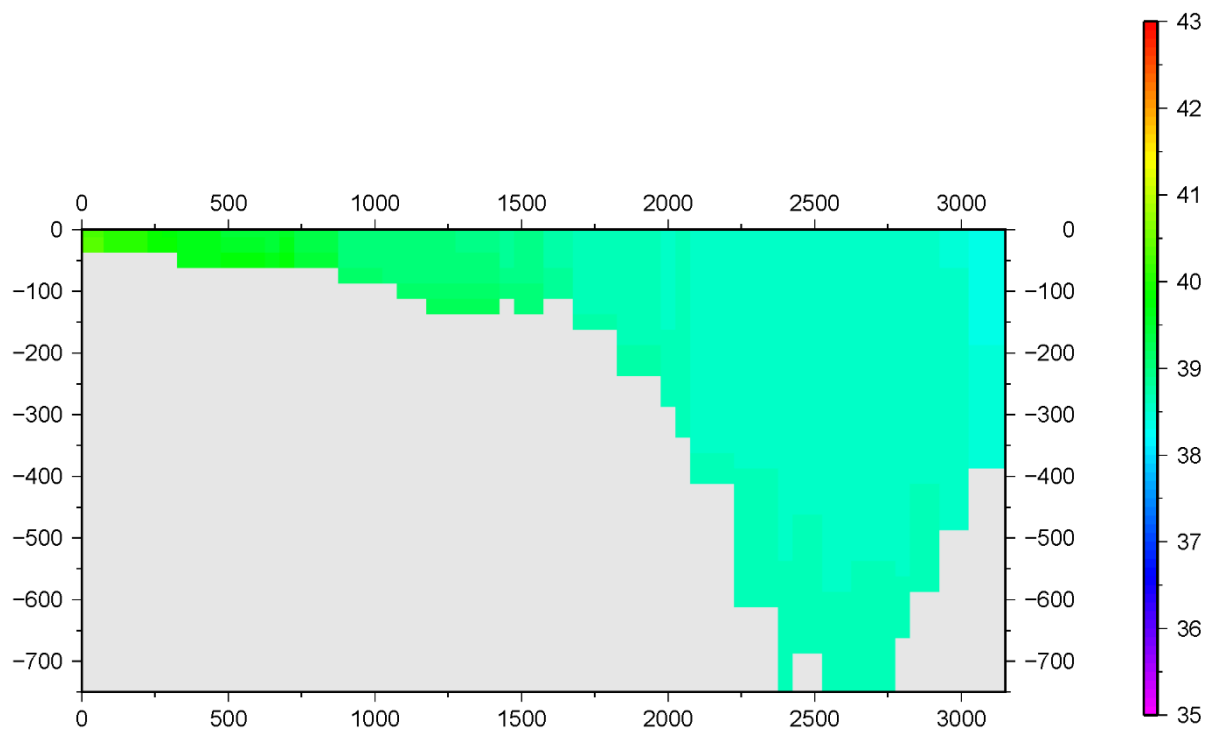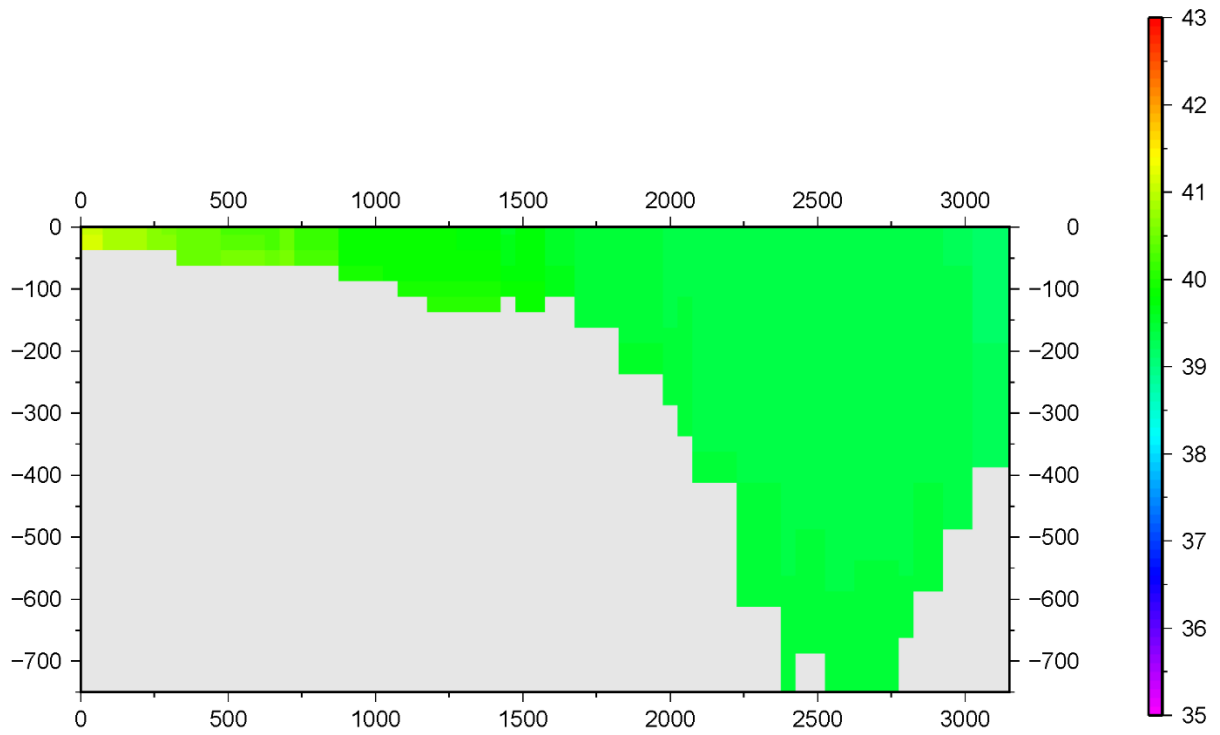
Panel H4: Section D_1 salinity in ppt of exp. 2041 (top) and exp. 2042 (bottom). The y axis represents the depth of the section while the x axis represents the distance in km along the cross section starting in the north-west and ending in the south-east.
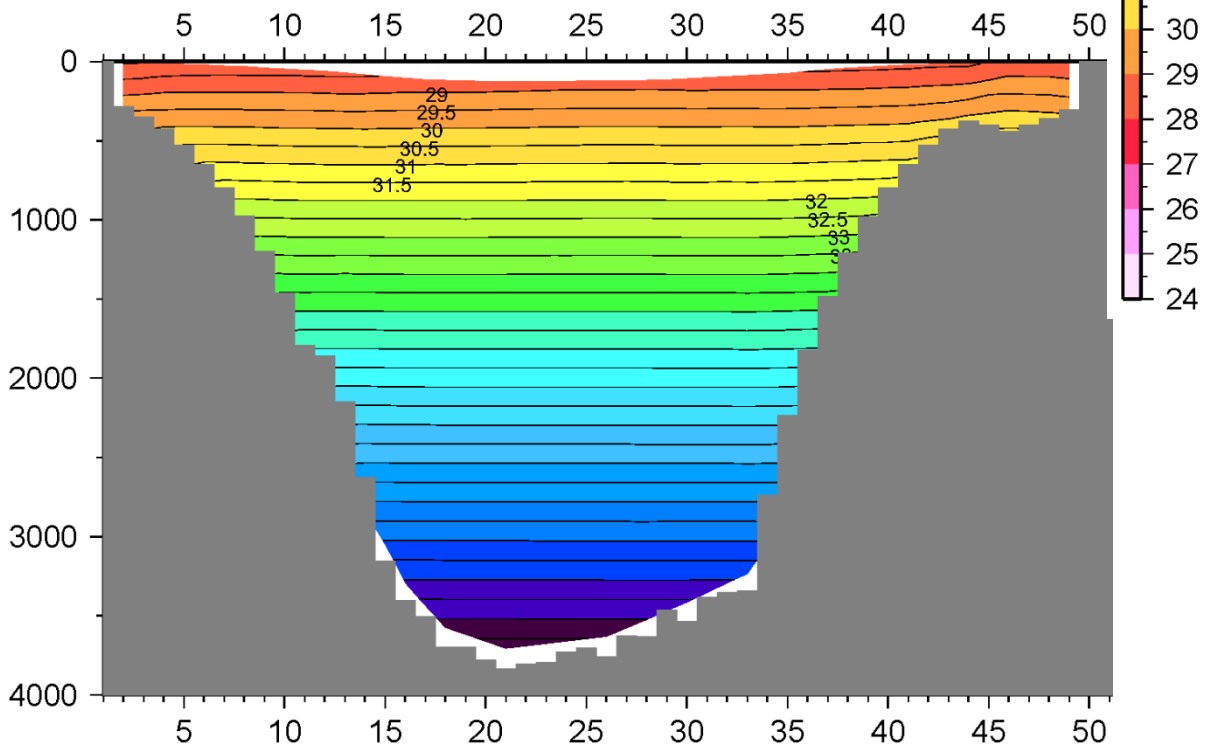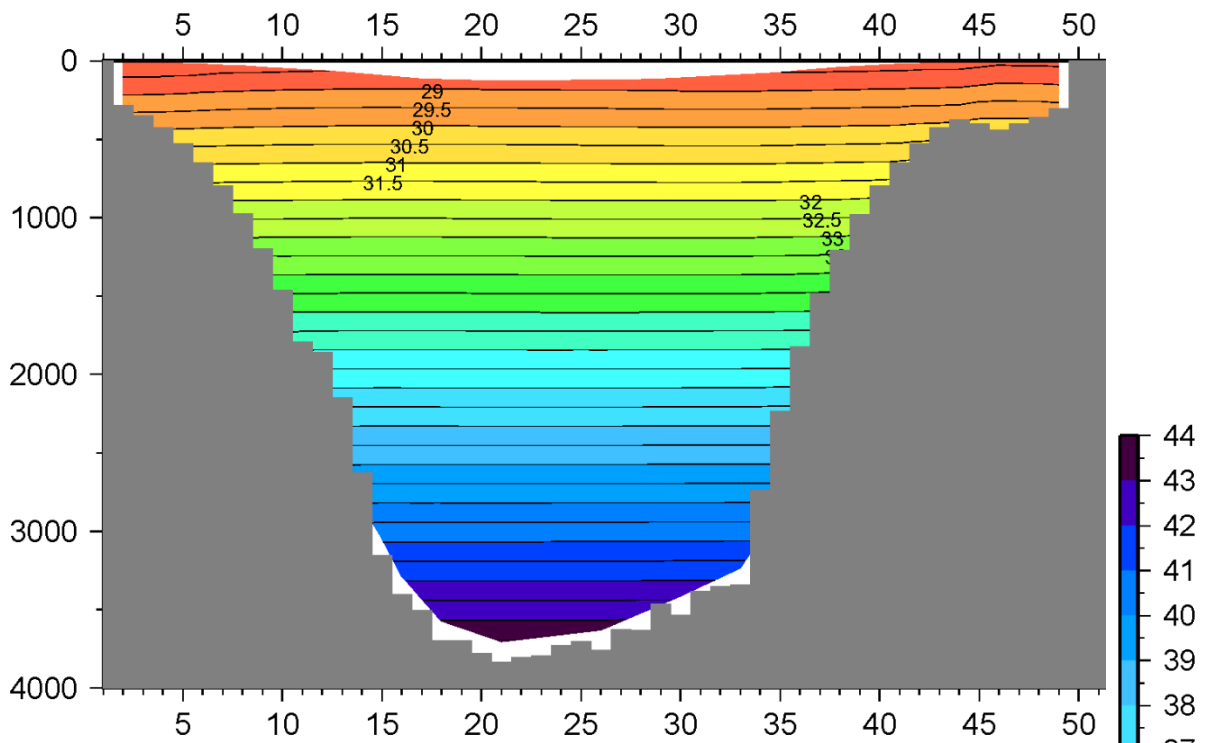
Panel H5: Section V density (ρ-1000) in kg/m³ of exp. 2020 (top) and exp. 2041 (bottom). The y axis represents the depth of the section while the x axis represents the jth grid cell.
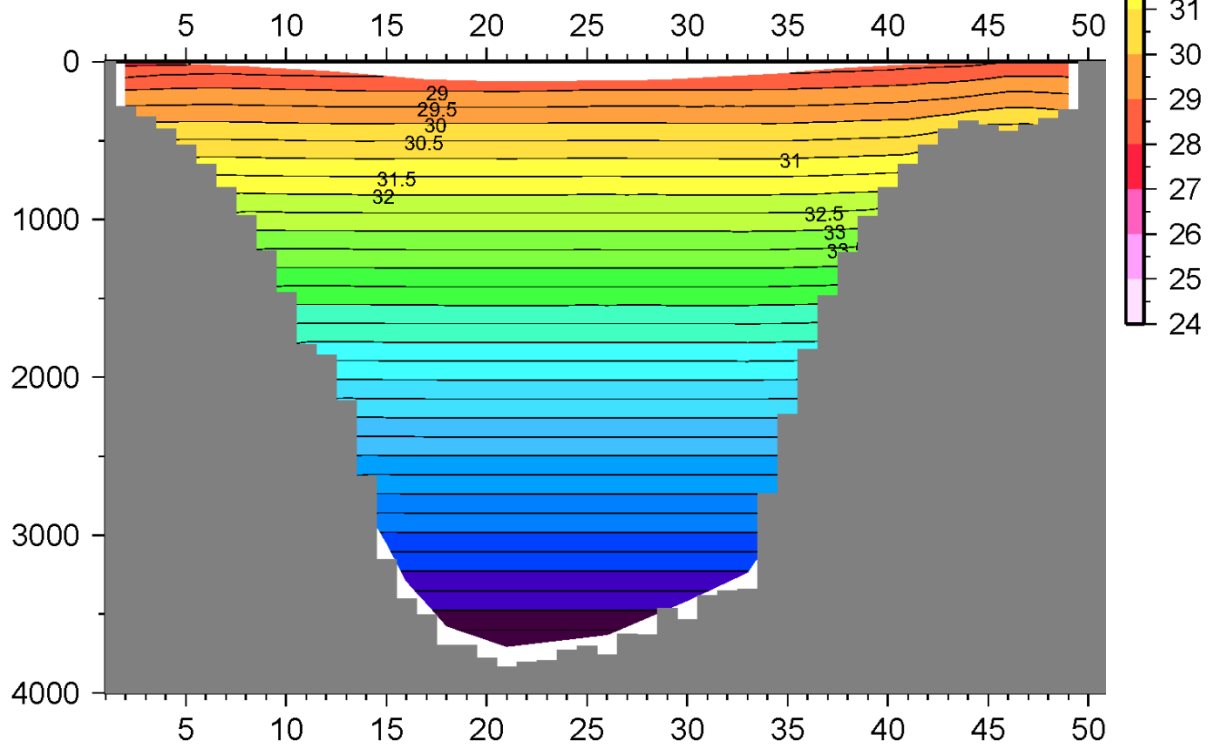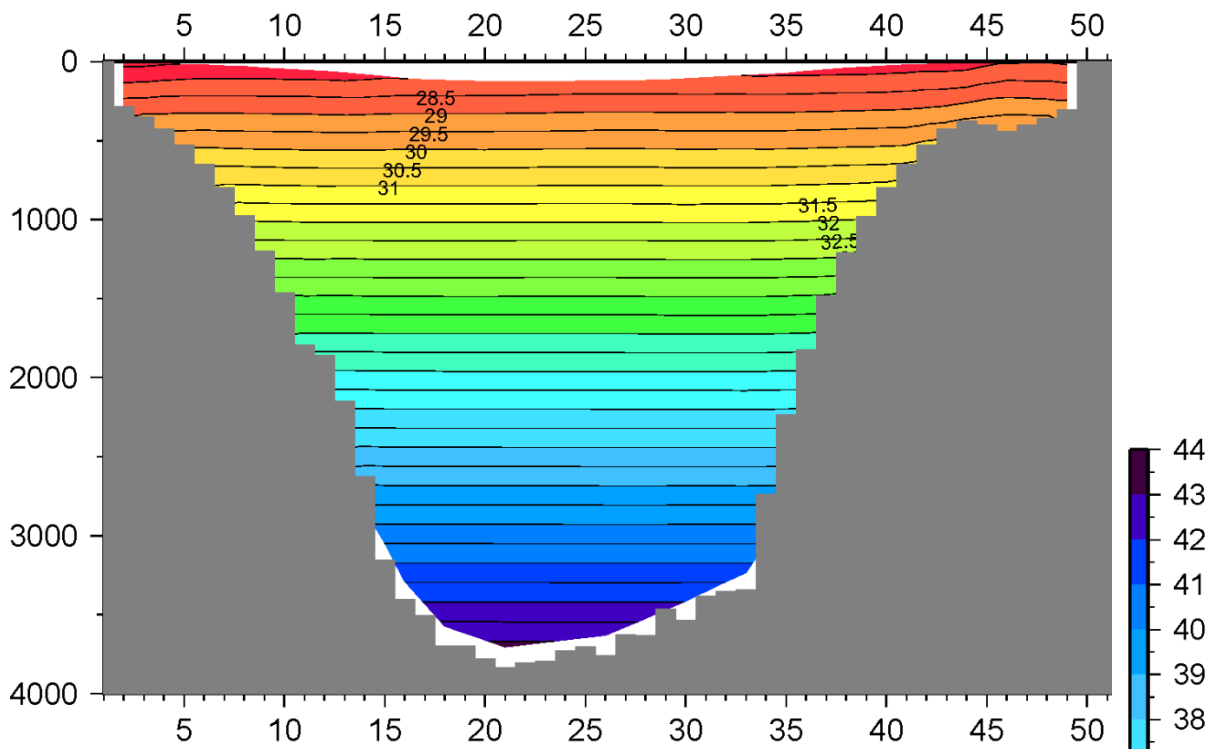
Panel H6: Section V density (ρ-1000) in kg/m³ of exp. 2042 (top) and exp. 2031 (bottom). The y axis represents the depth of the section while the x axis represents the jth grid cell.

Appendix I
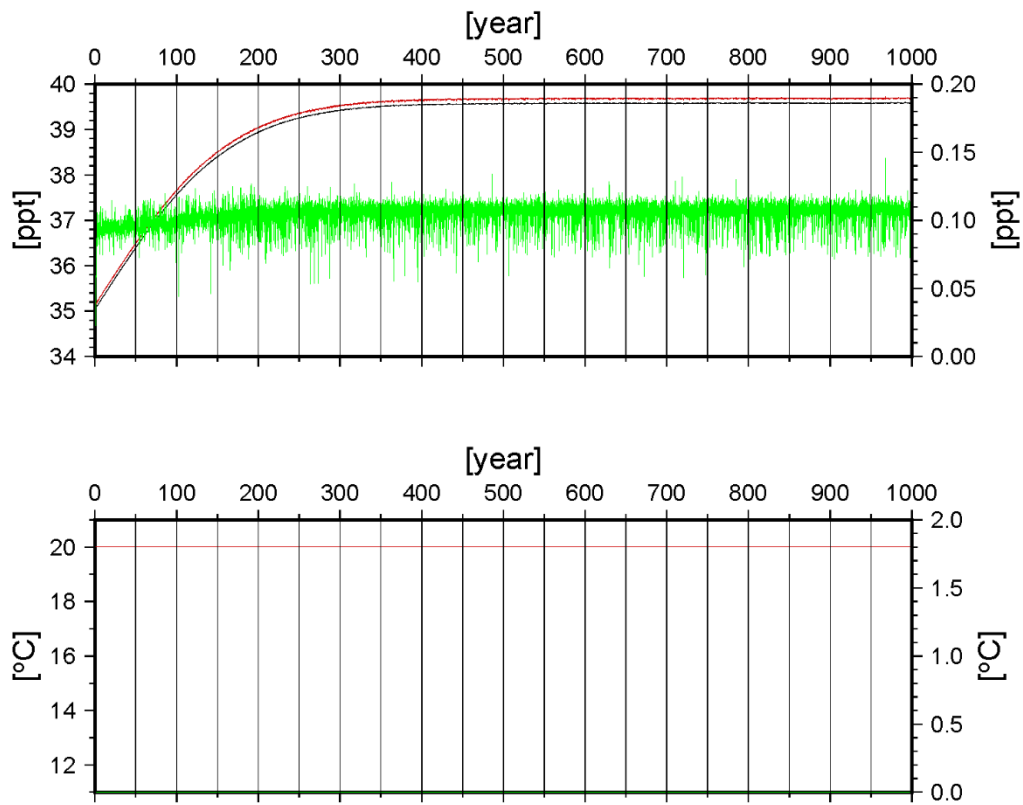

Figure I1: Average salinity [ppt] and temperature [°C] of the northward (black) and southward (red) flow through the strait of Otranto. The y axis on the right corresponds to the difference between the northward and southward flow (green) in ppt and °C. All data is recorded over the 1000 year run time of experiment 2020.
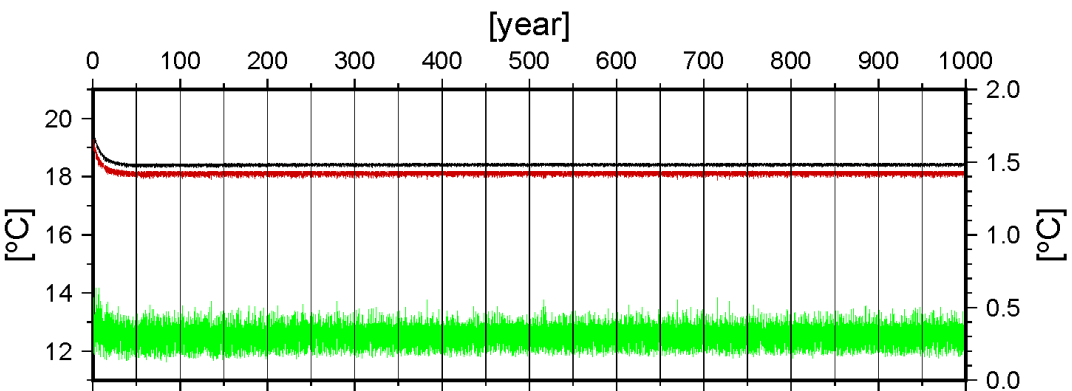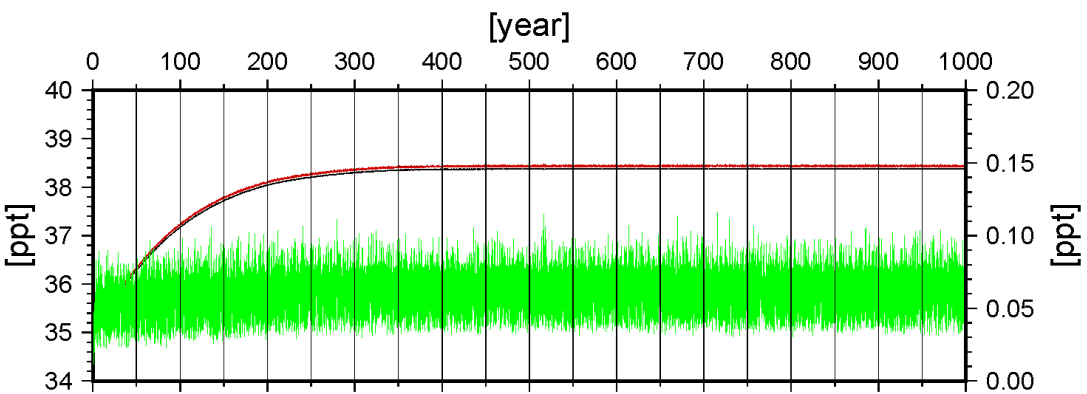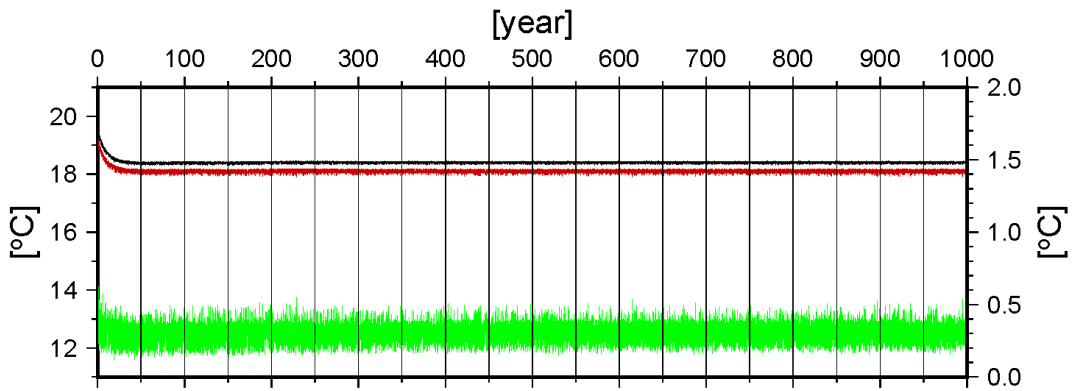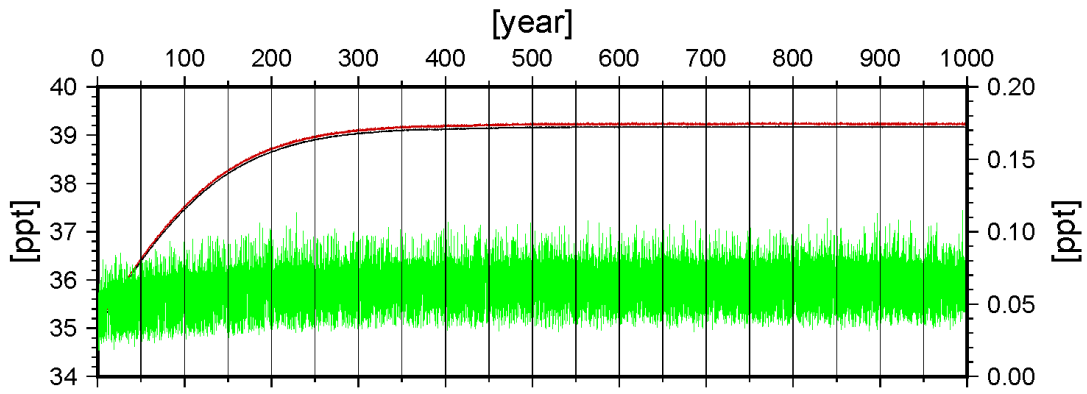
Panel I2: Average salinity [ppt] and temperature [°C] of the northward (black) and southward (red) flow through the strait of Otranto. The y axis on the right corresponds to the difference between the northward and southward flow (green) in ppt and °C. All data is recorded over the 1000 year run time of exp. 2041 (top) and exp. 2042 (bottom).
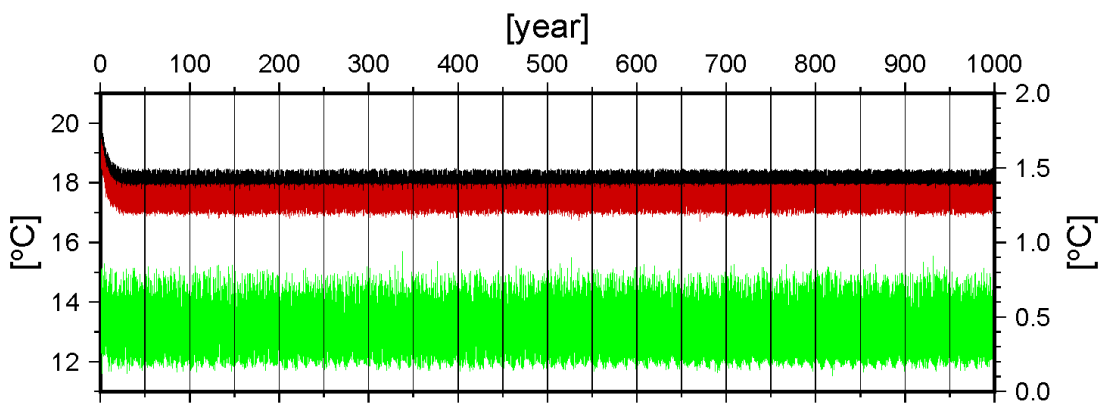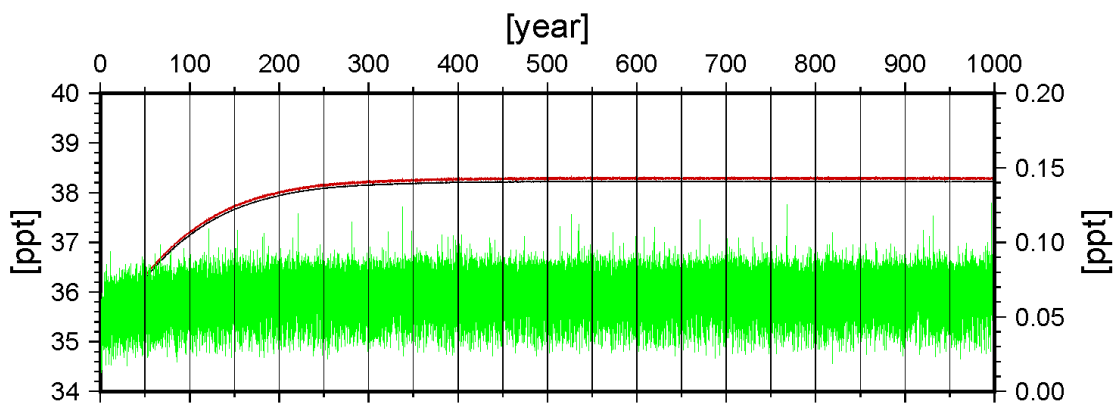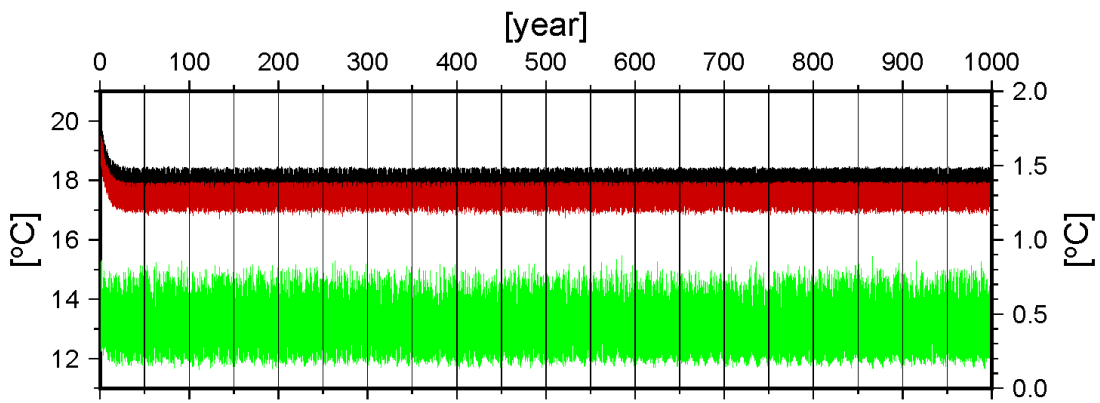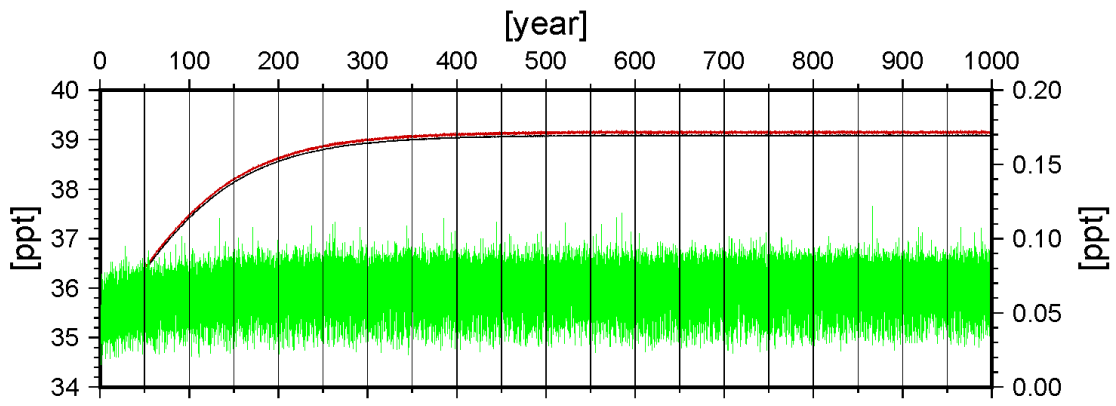
Panel I3: Average salinity [ppt] and temperature [°C] of the northward (black) and southward (red) flow through the strait of Otranto. The y axis on the right corresponds to the difference between the northward and southward flow (green) in ppt and °C. All data is recorded over the 1000 year run time of exp. 2031 (top) and exp. 2044 (bottom)
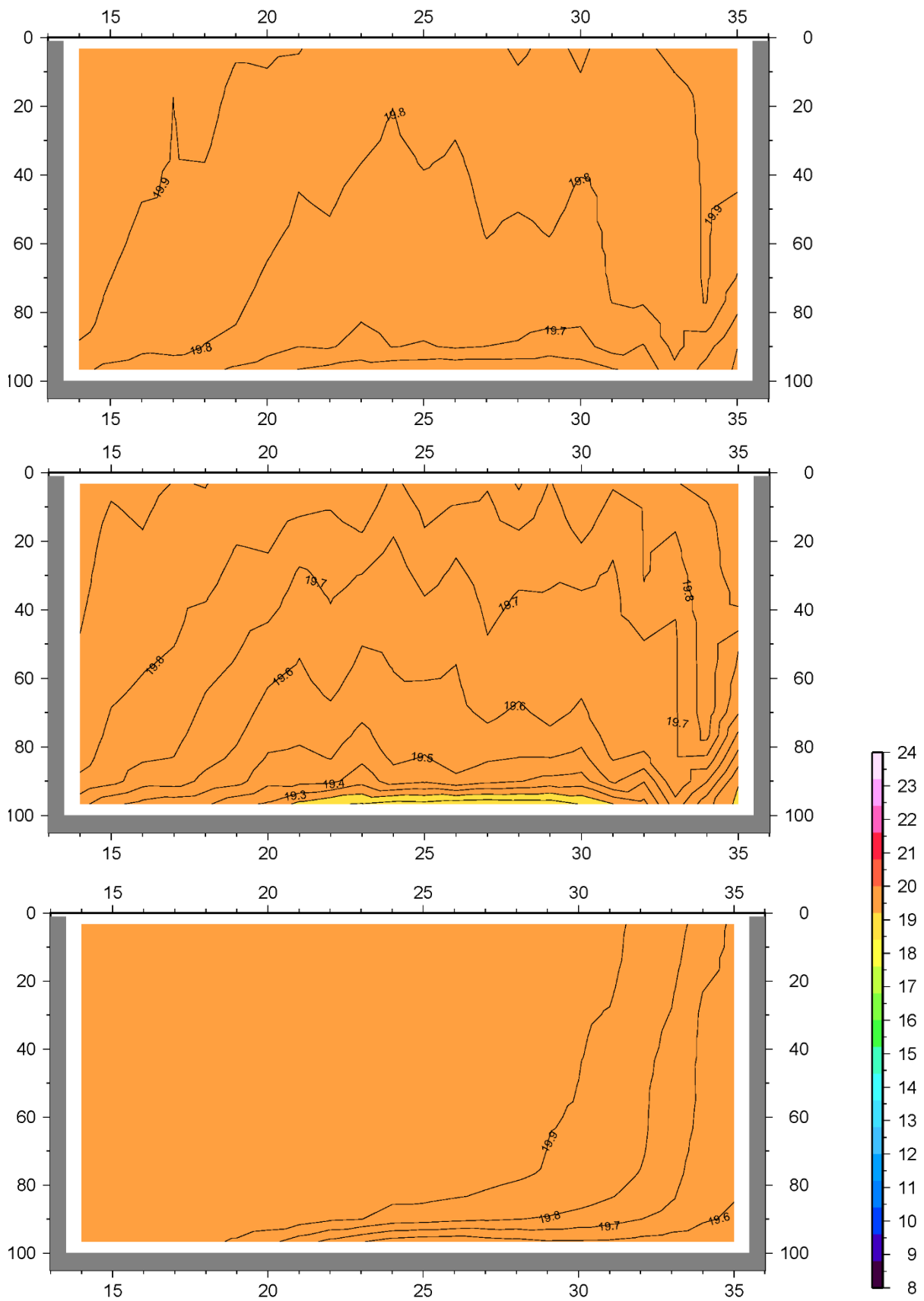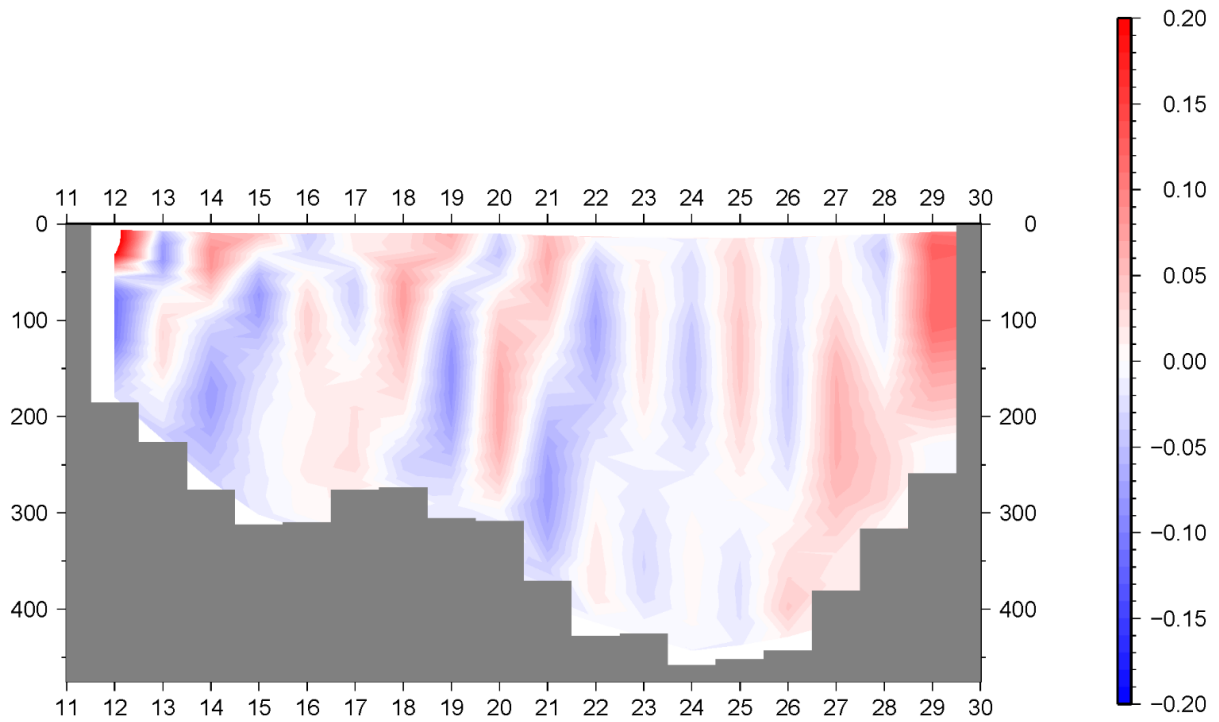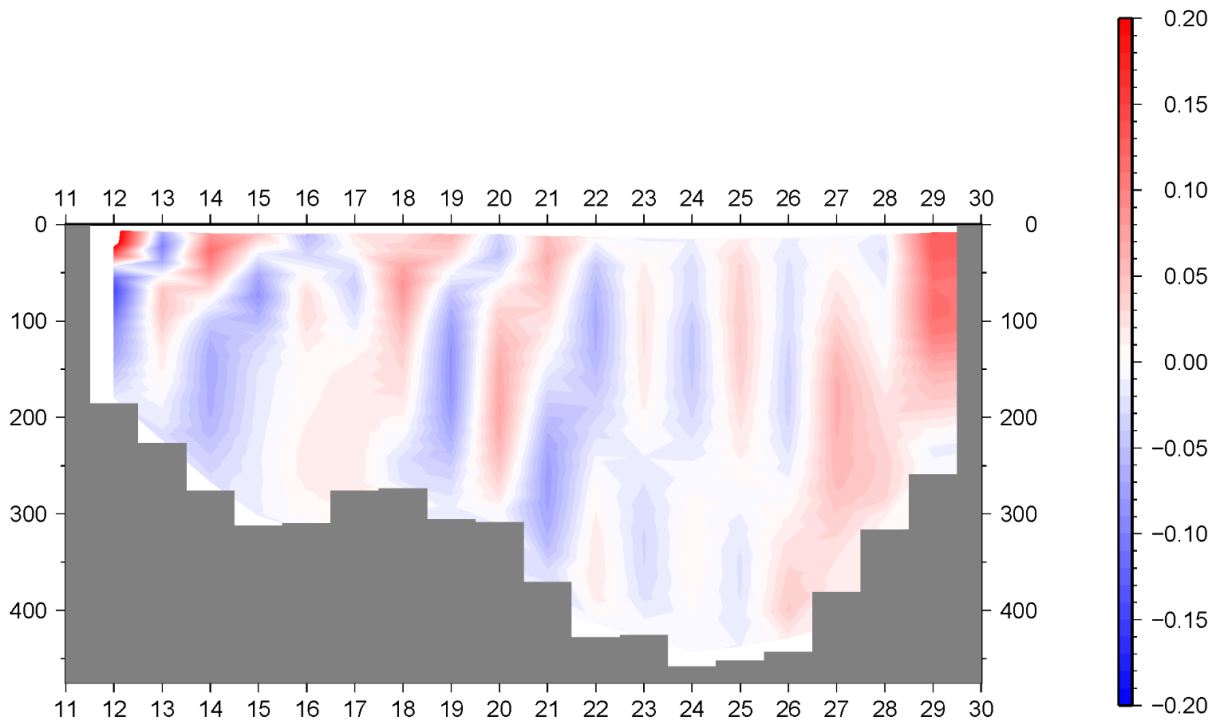
Panel J1: Section V_3 temperature in °C of exp. 2041 (top)), exp. 2031 (middle) and exp. 2042 (bottom). The y axis represents the depth of the section while the x axis represents the jth grid cell.
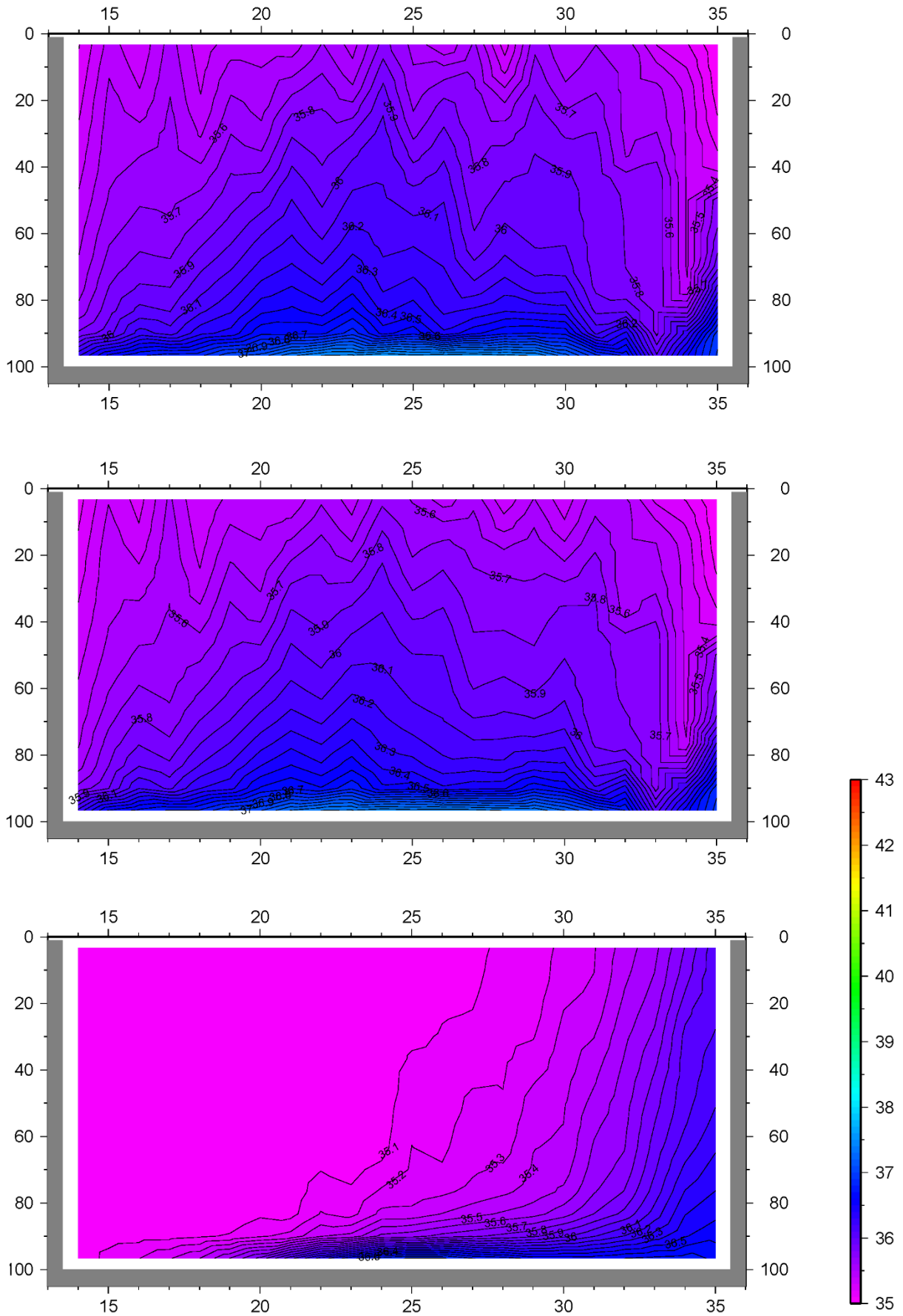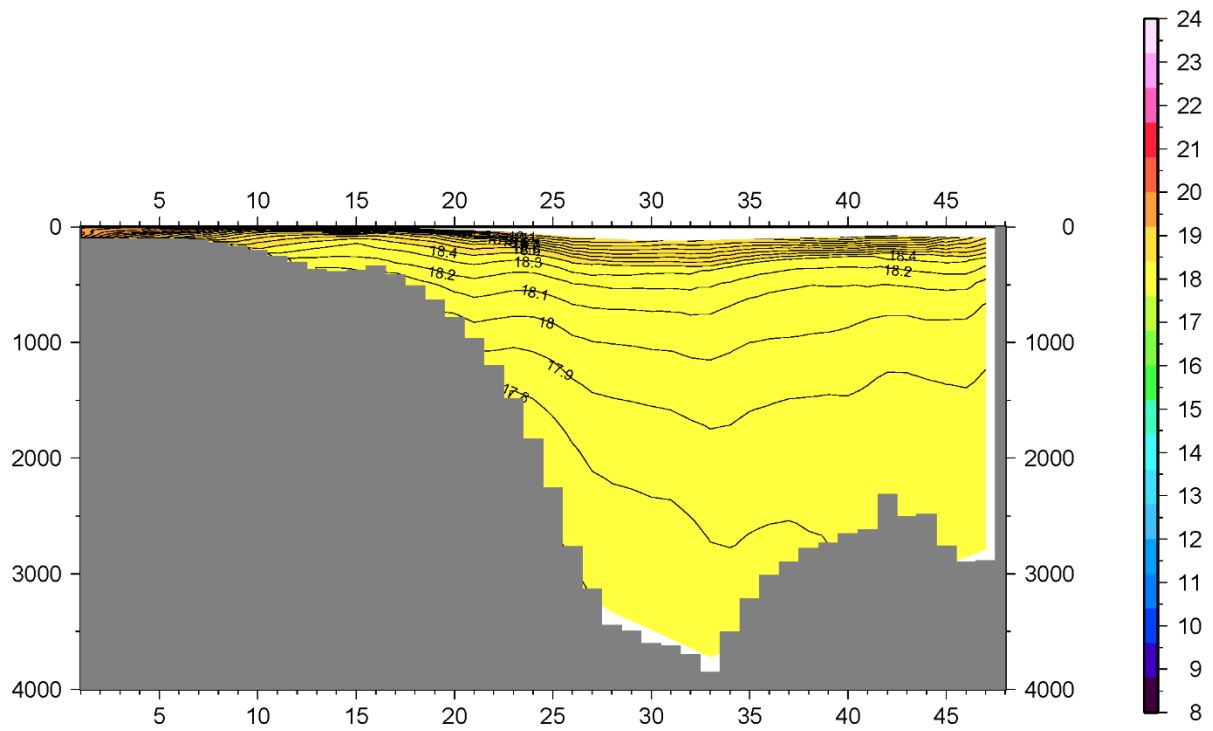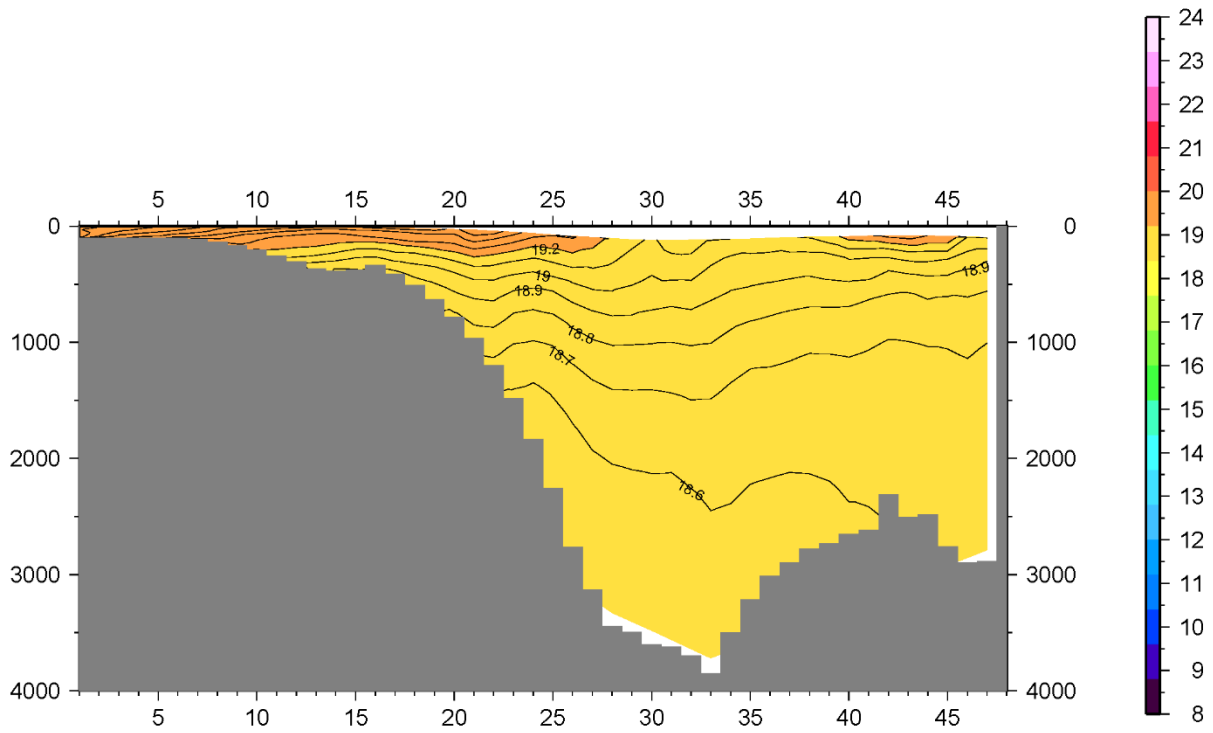
Panel J2: Section V_3 salinity in ppt of exp. 2020 (top), exp. 2041 (middle) and exp. 2042 (bottom). The y axis represents the depth of the section while the x axis represents the jth grid cell.

*Panel J3: Section V_3 velocity of in- and outflow in m/s of exp. 2020 (top), exp. 2041 (middle) and exp. 2042 (bottom). (red=eastward flow, blue=westward flow). The y axis represents the depth of the section while the x axis represents the j*th* grid cell.*
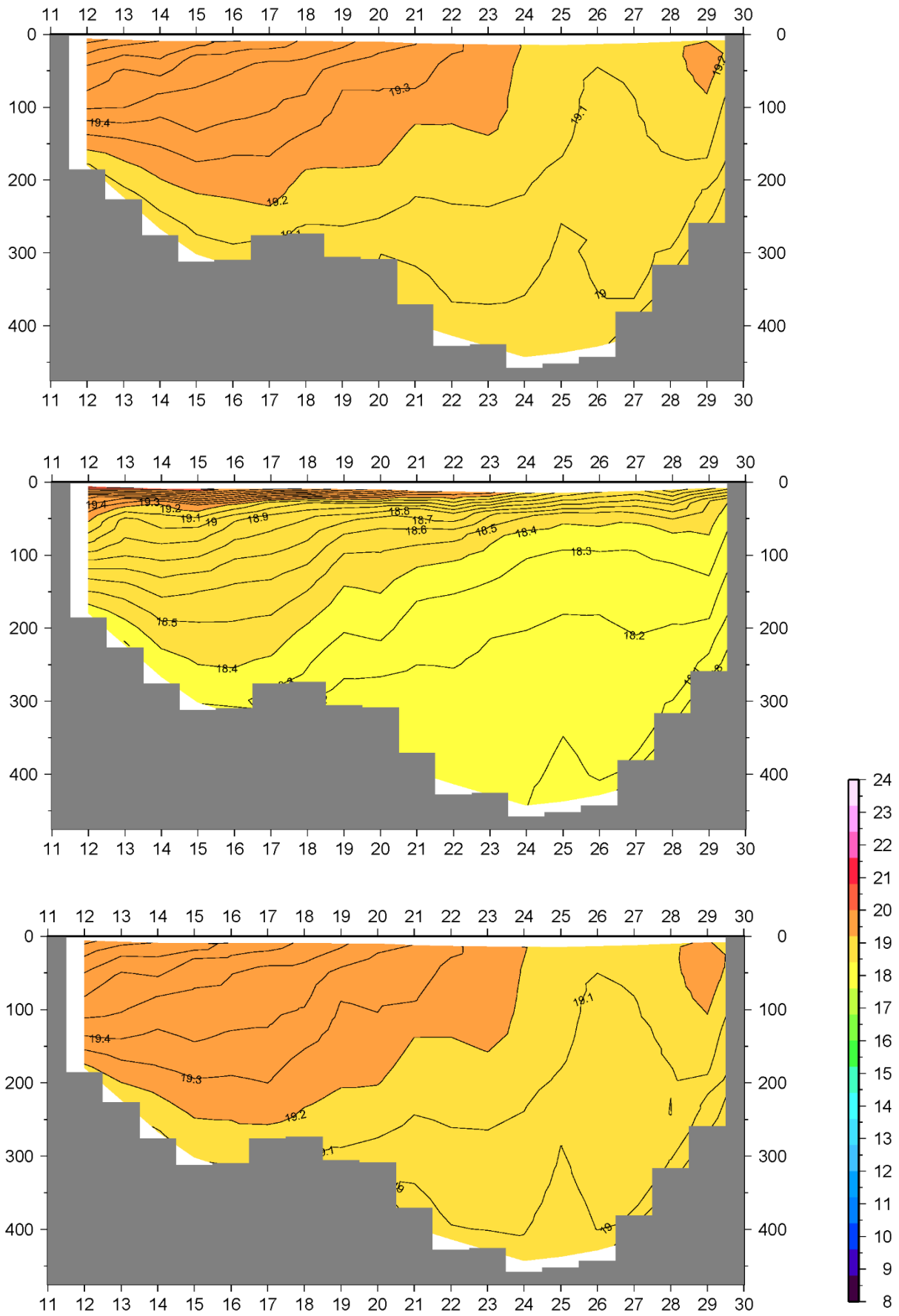
Panel J4: Section V_2 temperature in °C of exp. 2041 (top), exp. 2031(middle and exp. 2042 (bottom). The y axis represents the depth of the section while the x axis represents the jth grid cell.
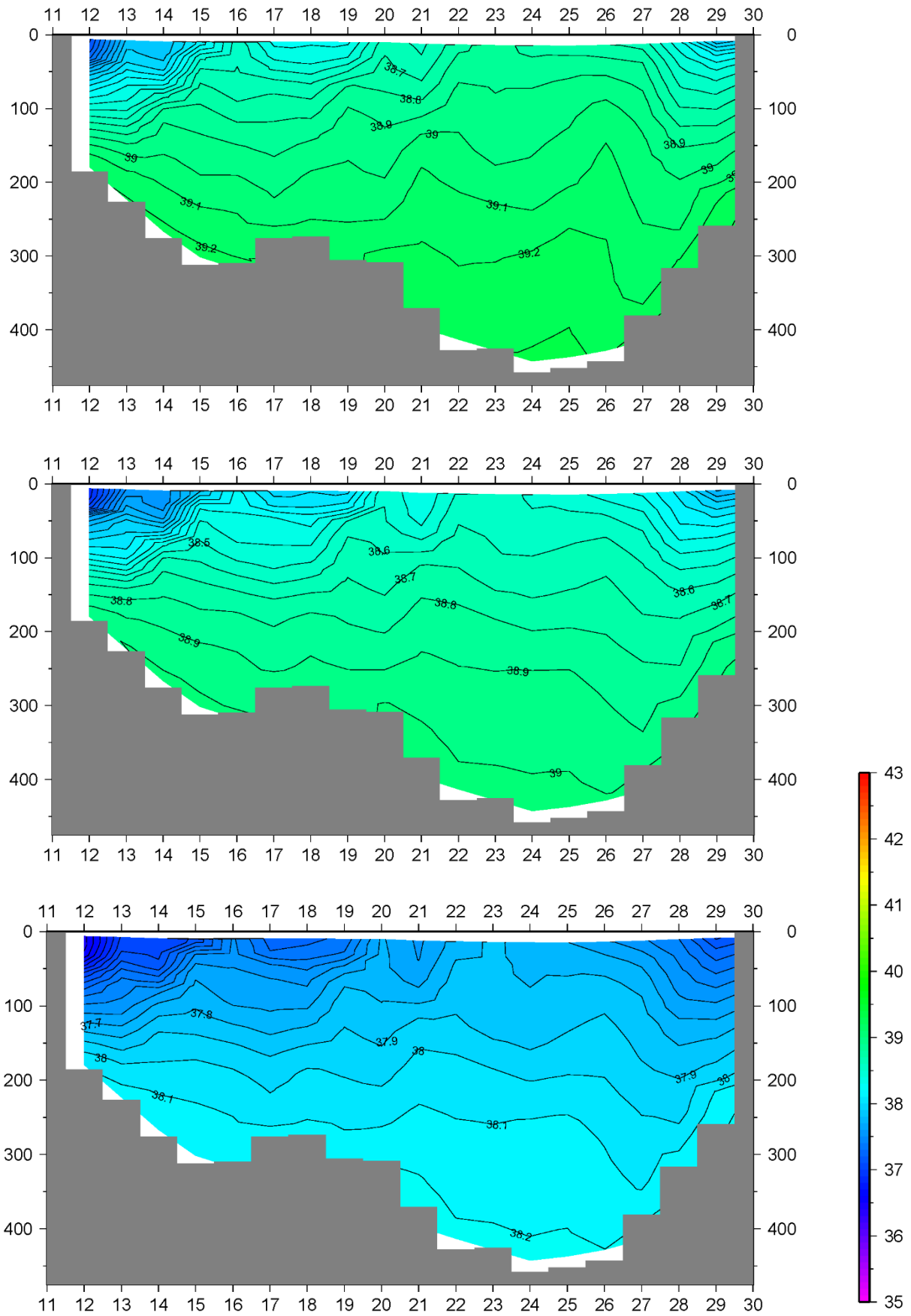
Panel J5: Section V_2 salinity in ppt of exp. 2020 (top), exp. 2041 (middle) and exp. 2042 (bottom). The y axis represents the depth of the section while the x axis represents the jth grid cell.
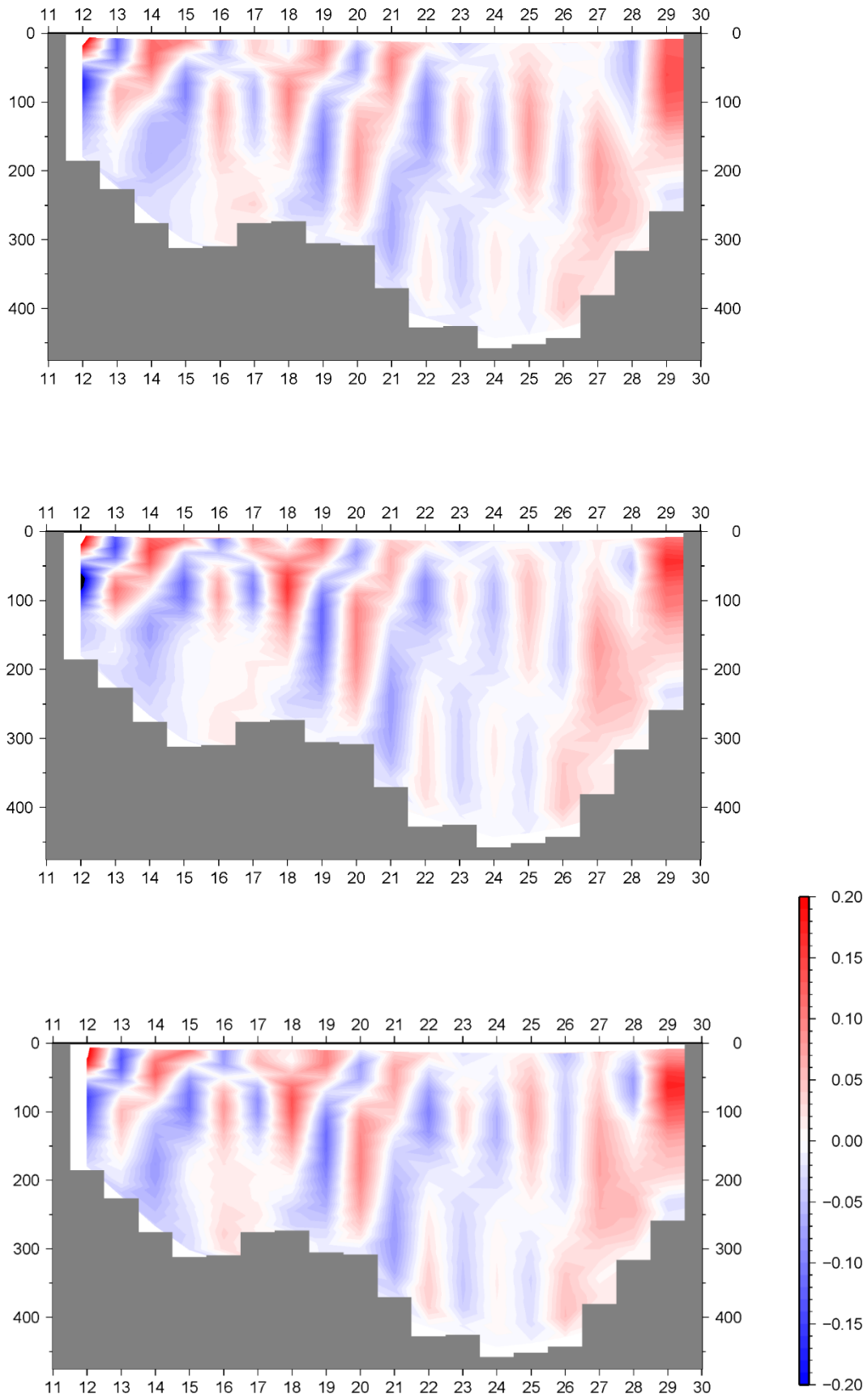
Panel J6: Section V_2 velocity of in- and outflow in m/s of exp. 2020 (top), exp. 2041 (middle) and exp. 2042 (bottom). (red=eastward flow, blue=westward flow). The y axis represents the depth of the section while the x axis represents the jth* grid cell.*

Panel J7: Section V_2 velocity of in- and outflow in m/s of exp. 2031 (top) and exp. 2044 (bottom). (red=eastward flow, blue=westward flow). The y axis represents the depth of the section while the x axis represents the jth grid cell.
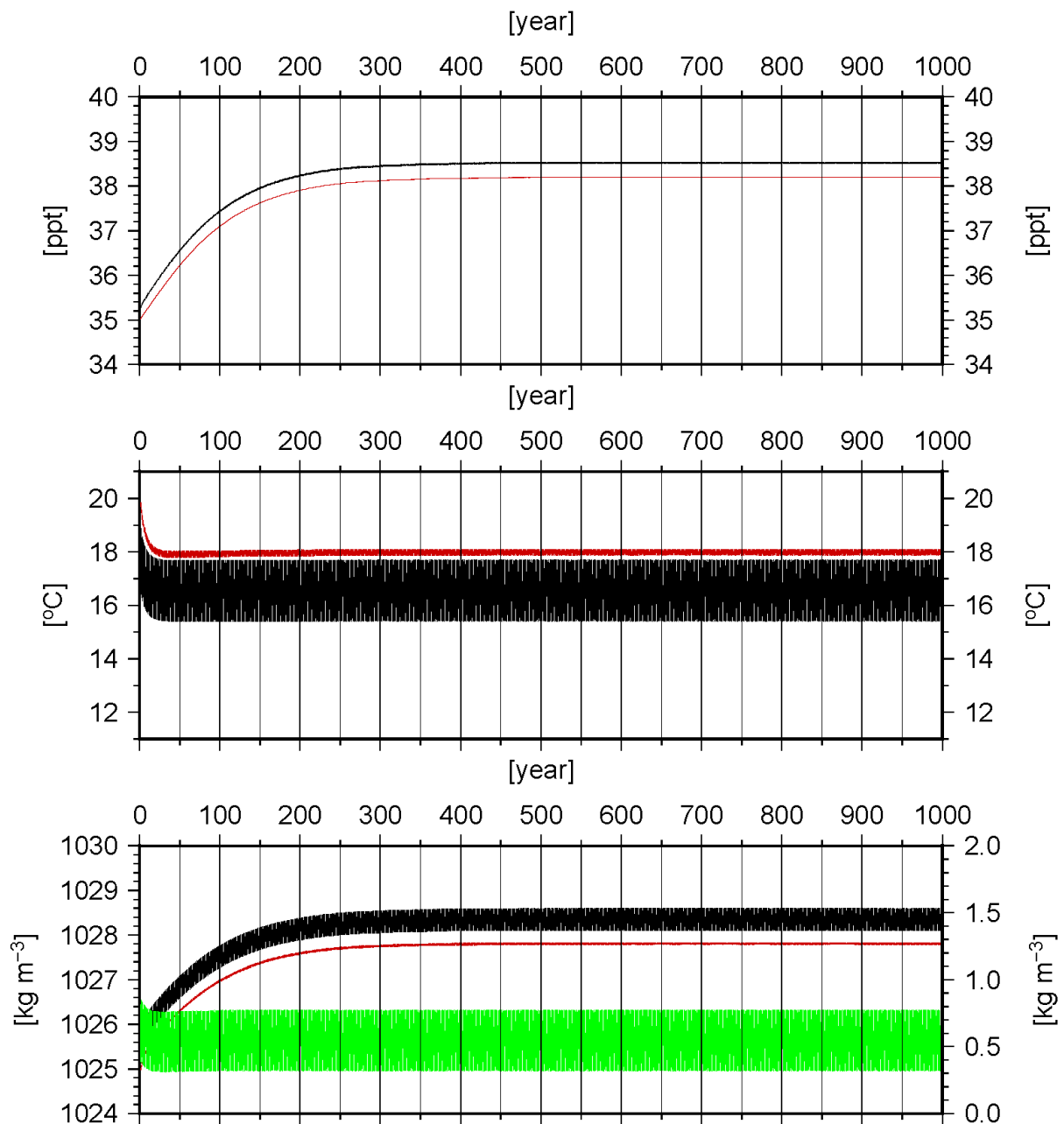
Panel J8: Section H temperature in °C of exp. 2041 (top) and exp. 2031 (bottom). The y axis represents the depth of the section while the x axis represents the ith grid cell.
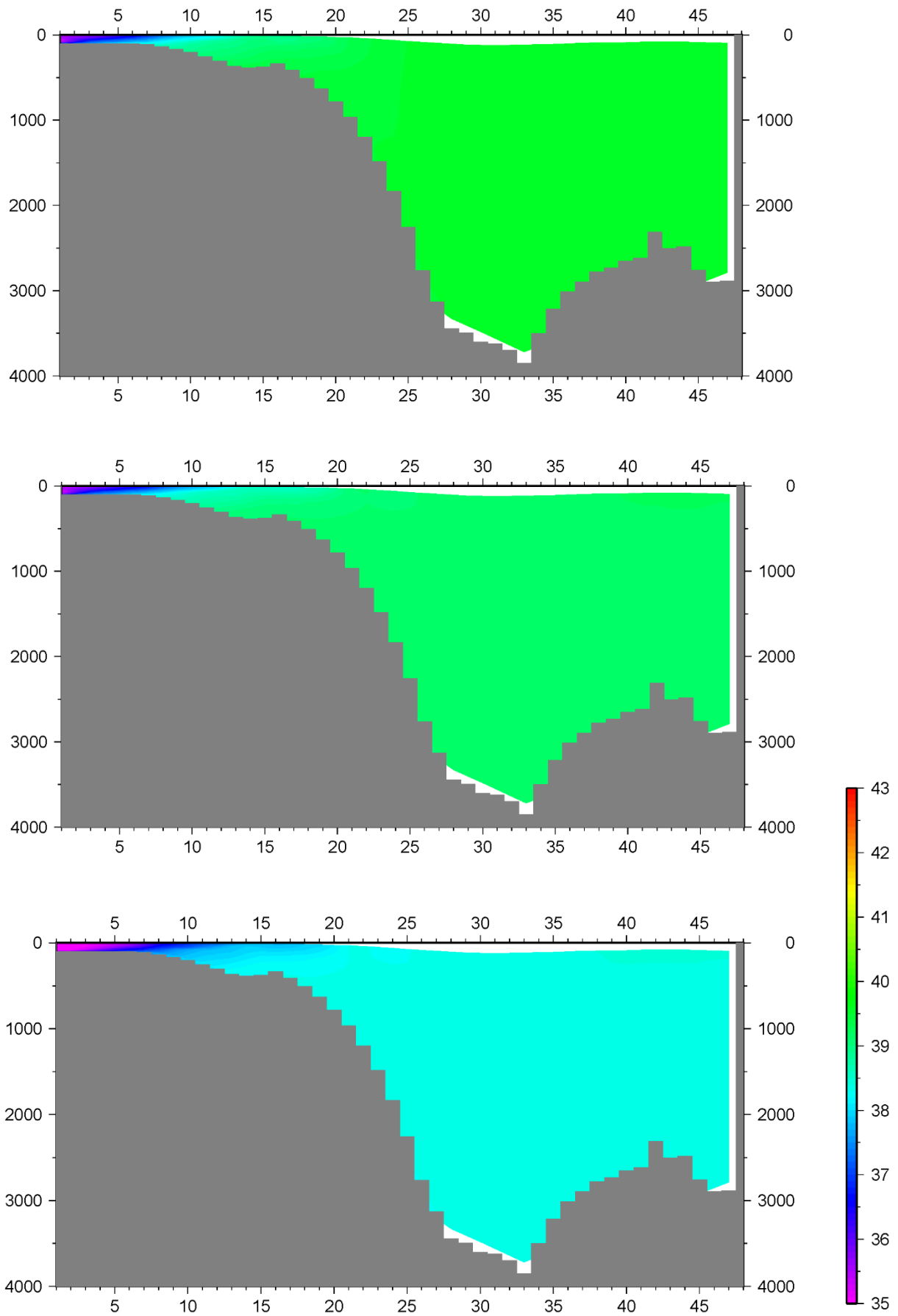
Panel J9: Section H salinity in ppt of exp. 2020 (top), exp. 2041 (middle) and exp. 2042 (bottom). The y axis represents the depth of the section while the x axis represents the ith grid cell.

Appendix K

Panel K1: Volume average salinity [ppt], volume average temperature [°C] and calculated volume average density [kg m-3] of the Adriatic box (black) and the Ionian box (red) and the density difference (green). The y axis on the right in the 3rd image corresponds to the density difference (green) in kg m-3. All data is recorded over the 1000 year run time of experiment 2044.
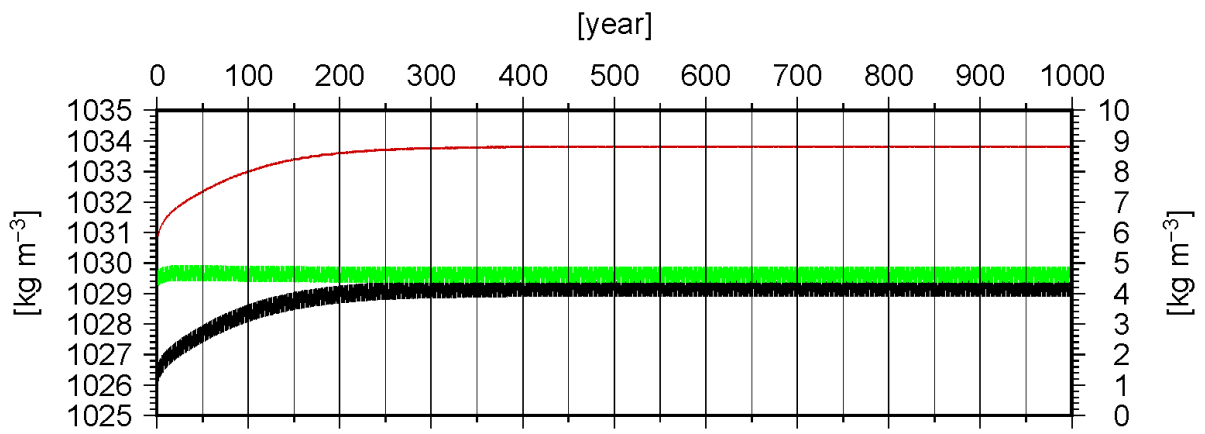
Figure K2: Volume average density [kg m⁻³] of the Adriatic box (black) and the Ionian box (red) and the density difference (green). The y axis on the right corresponds to the density difference (green) in kg m⁻³. All data is recorded over the 1000 year run time of experiment 2044.
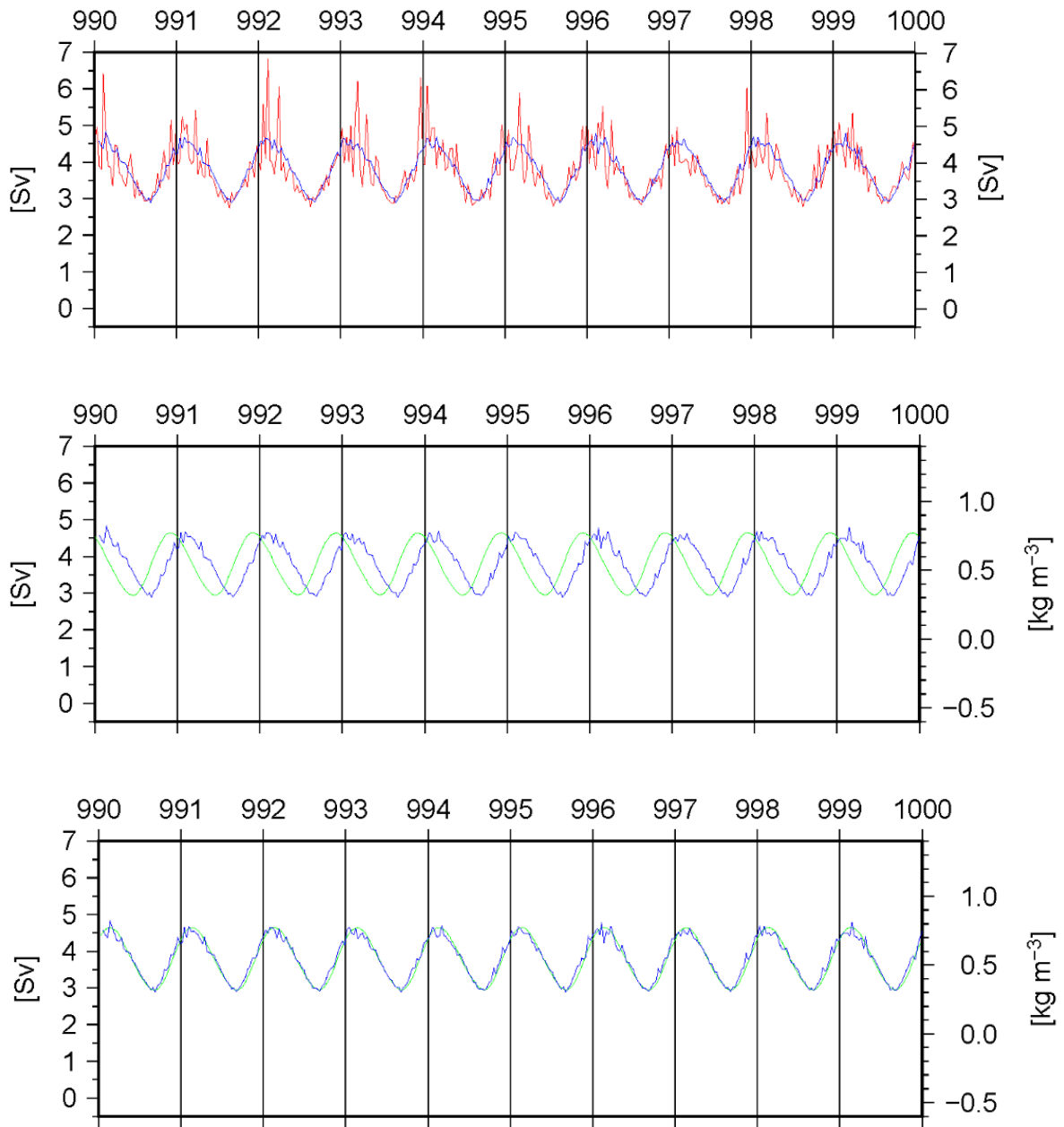
Appendix L

Figure L1(a-b-c):

a (top): Southward flow [Sv] through the strait of Otranto (red) and the calculated southward flow average for a 10 year moving window [Sv] (blue). All data was taken from the run of experiment 2044.

b (middle): The calculated southward flow average [Sv] (blue) and the density difference between the Adriatic and Ionian box [kg m^{-3}] (green). All data was taken from the run of experiment 2044.

c (bottom): The calculated southward flow average [Sv] (blue) and the shifted density difference between the Adriatic and Ionian box [kg m^{-3}] (green). All data was taken from the run of experiment 2044.
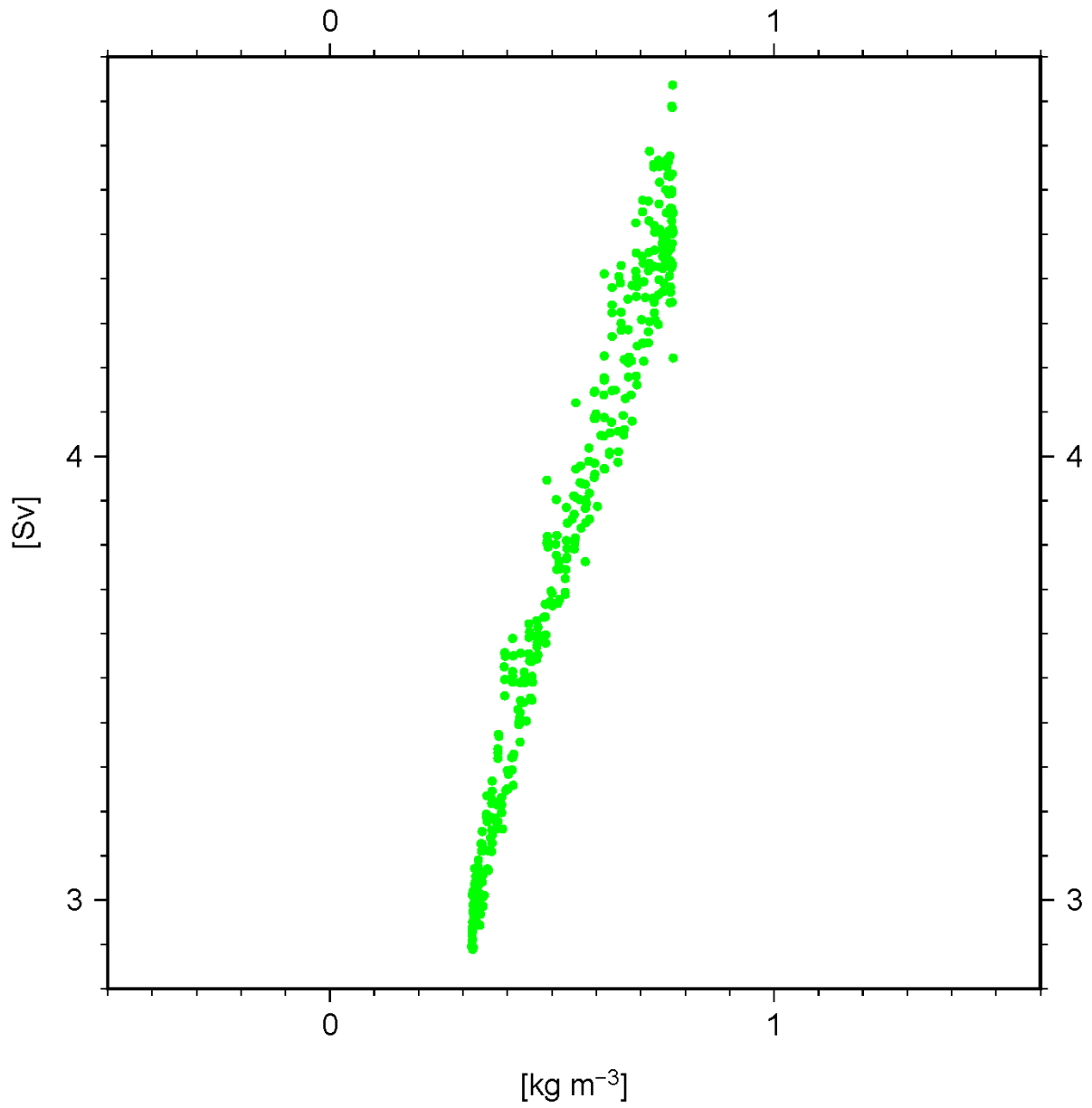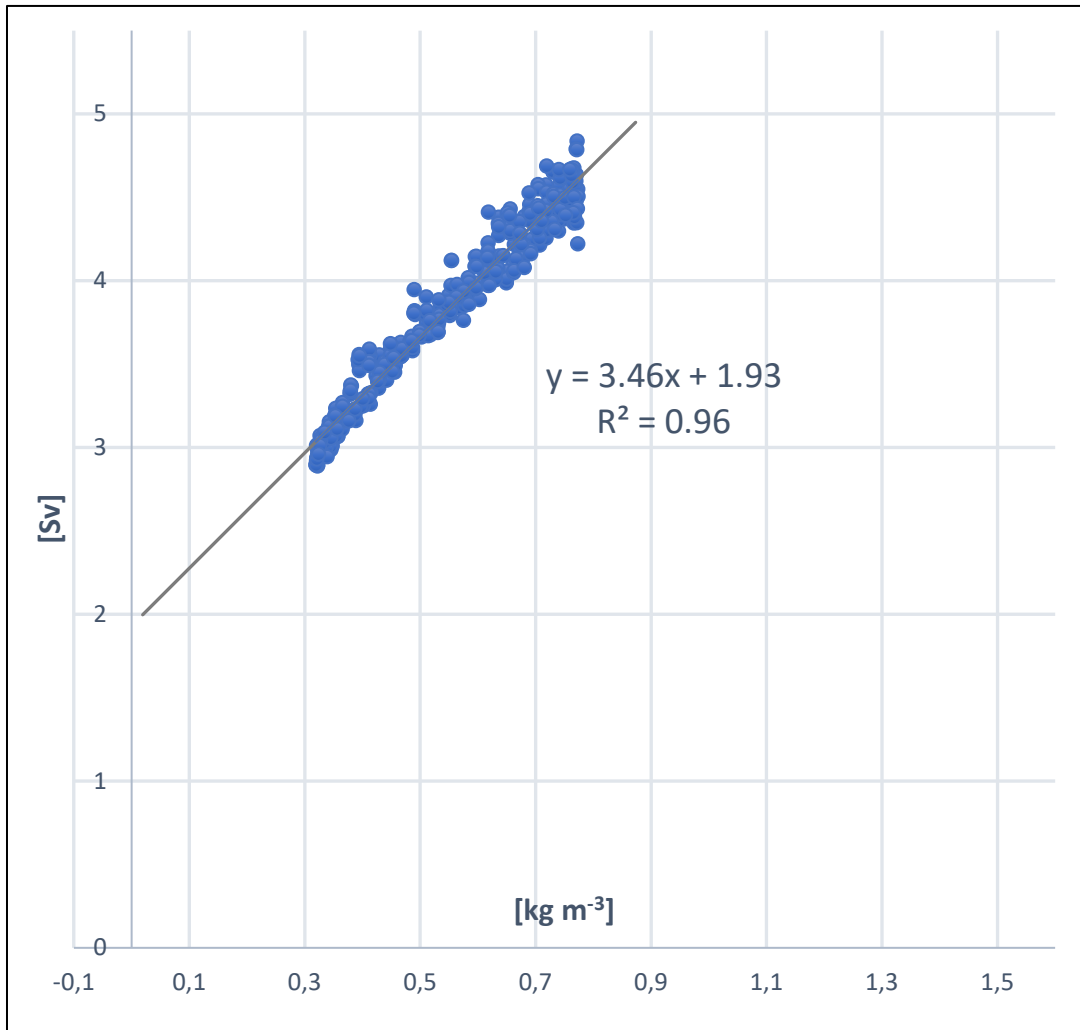
Figure L2: The shifted density difference between the Adriatic and Ionian box [kg m-3] (x-axis) versus the calculated southward flow average [Sv] (y-axis). All data was taken from the run of experiment 2044.

$y = 3.46x + 1.93$
$R^2 = 0.96$

Figure L3a: The shifted density difference between the Adriatic and Ionian box [kg m^{-3}] (x-axis) versus the calculated southward flow average [Sv] (y-axis). A linear relation is shown. All data was taken from the run of experiment 2044.
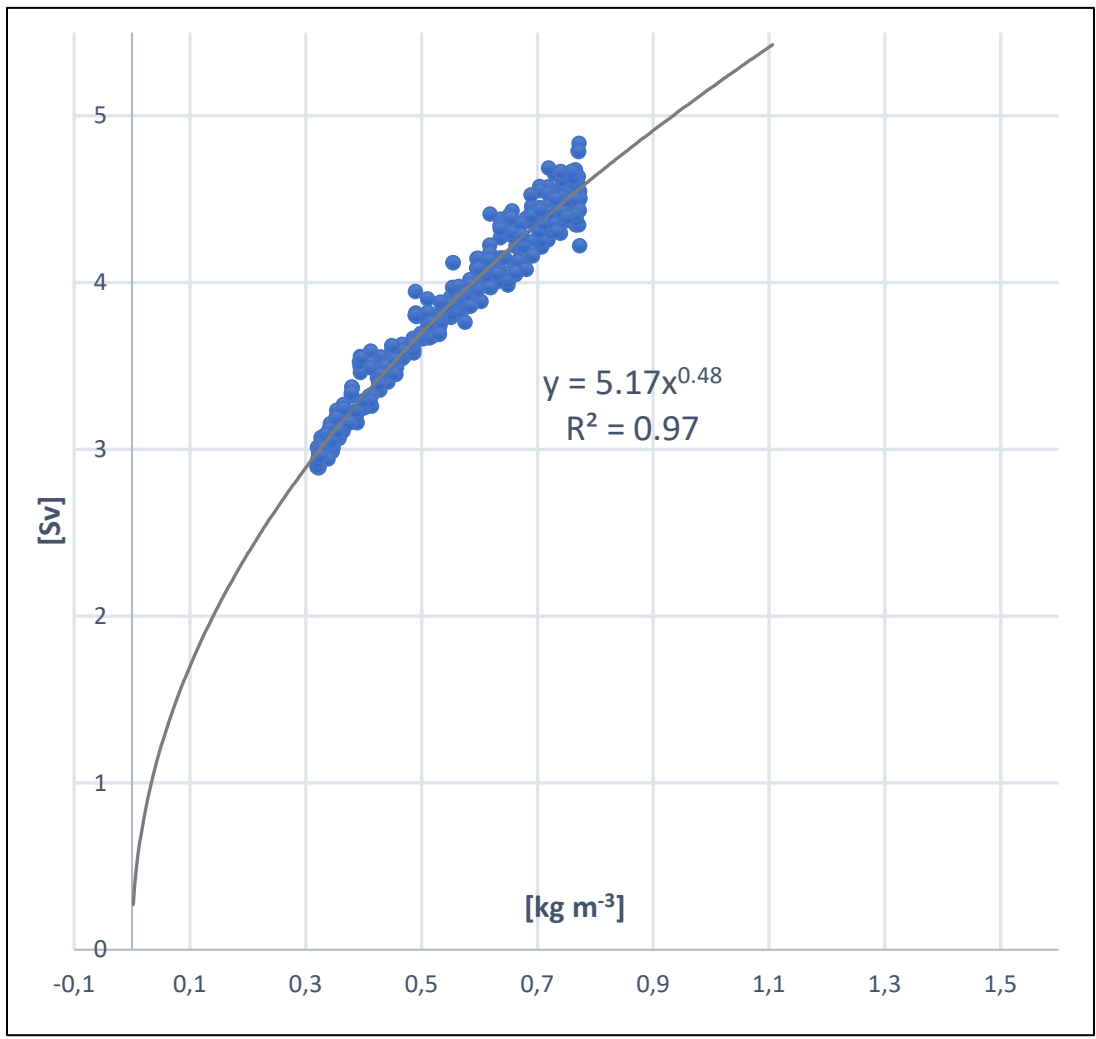
Figure L3b: The shifted density difference between the Adriatic and Ionian box [kg m⁻³] (x-axis) versus the calculated southward flow average [Sv] (y-axis). A power law relation is shown. All data was taken from the run of experiment 2044.